UTILITY OF PHOTOACOUSTIC IMAGING, AN ADVANCED DRUG DELIVERY APPROACH AND DRUG DISCOVERY FOR CORNEAL NEOVASCULARISATION DIAGNOSIS AND TREATMENT

LUI KWOK HO

PhD

The Hong Kong Polytechnic University

2023

The Hong Kong Polytechnic University

Department of Applied Biology and Chemical Technology

Utility of Photoacoustic Imaging, an Advanced Drug Delivery Approach and Drug Discovery for Corneal Neovascularisation Diagnosis and Treatment

LUI KWOK HO

A thesis submitted in partial fulfilment of the requirements for the degree of Doctor of Philosophy

August 2022

CERTIFICATE OF ORIGINALITY

I hereby declare that this thesis is my own work and that, to the best of my knowledge and belief, it reproduces no material previously published or written, nor material that has been accepted for the award of any other degree or diploma, except where due acknowledgement has been made in the text.

_____ (Signed)

LUI KWOK HO (Name of Student)

What is wanted is not the will to believe, but the will to find out, which is the exact opposite.

Bertrand AW Russel
British Philosopher

Abstract

The ever-evolving photoacoustic imaging (PAI) technique and nanotechnology have shown tremendous opportunities for improving various biomedical applications such as cancer diagnosis, molecular imaging, and advanced drug delivery strategy. The utilisation of these techniques drives the biomedical field into the next era by providing precise diagnosis and drug delivery strategies in different biomedical applications. This thesis aims to address and tackle issues associated with corneal neovascularisation (CNV) using PAI and nanotechnology to provide objective analysis and enhance ocular drug absorption. Furthermore, a newly developed focal adhesion kinase (FAK) inhibitor was investigated for its feasibility as a CNV treatment. This serves as a first attempt to lay a foundation for its future application in ocular disease treatment.

In chapter three, the PAI technique was applied with *in vivo* alkali-induced CNV model to examine its potential in identifying and quantifying haemoglobin species within the diseased cornea. *In vivo* results demonstrated that the PAI could identify and quantify haemoglobin species based on their corresponding wavelengths. Furthermore, the PA signal quantification revealed an increase across different PA signal parameters, which matches the severity observed in the slit-lamp examination. Thus, this offers an objective and quantitative approach for future ocular disease examination. Furthermore, this study also demonstrated the feasibility of employing metformin eye drops to combat CNV.

Conventional ocular drug delivery approaches often suffer from poor bioavailability due to the natural ocular barrier, which hampers the treatment outcome. In particular, hydrophobic drugs have difficulty penetrating the cornea through topical administration and exert their medicinal effect. The emergence of a polymeric nanoparticle drug delivery system is a potential solution to this problem. In chapter four, we developed a polymeric nanocarrier conjugated with cell-penetrating peptides for enhanced ocular drug delivery. The system employed a hydrophobic drug as a model drug while the surface of the nanoparticle was modified with octa-arginine (R_8) peptide. The optimized nanocarrier showed an overall negative charge (-6.55 ± 0.94 mV) with size of 185.2 ± 4.45 nm. *In vitro* analysis revealed the nanocarrier possessed sustained-release property while enhanced absorption was observed with confocal microscopy. Furthermore, the cell-penetrating peptide assisted in the penetration of the

nanocarrier to human umbilical vein endothelial cells (HUVECs) after incubation. Benefitting from these properties, *in vivo* experiments with the nanocarrier, showed outstanding treatment performance compared to control groups. Overall, the data presented in this work demonstrated the potential of surface-decorated nanocarrier in the ocular drug delivery aspect.

In chapter five, the efficacy of a newly developed focal adhesion kinase (FAK) inhibitor (KX2-4245) was investigated in the CNV model. Disruption of anti-angiogenic and pro-angiogenic factors in the cornea leads to the sprouting of blood vessels, resulting in CNV formation. Several angiogenic contributors, such as VEGF and FAK, have previously been identified. In this work, an MTT assay was conducted to probe the cell viability after KX2-4245 treatment. Quantitative analysis revealed that no cytotoxicity could be observed at a concentration of 2 nM or below. Furthermore, the KX2-4245 showed an anti-angiogenic effect in the experimental CNV model and is well-tolerated through topical administration. The data presented in this work lays a foundation for its future utility in treating ocular diseases associated with angiogenesis.

Overall, these findings provide a solution to tackle existing problems associated with ocular imaging and administration methods.

List of Publications

1. **Lui K-H**, Li S, Lo W, Gu Y, Wong W-T. In vivo photoacoustic imaging for monitoring treatment outcome of corneal neovascularization with metformin eye drops. *Biomed Opt Express.* 2021;12(6):3597-3606. doi:10.1364/BOE.423982.

2. Li S, **Lui K-H (co-first author)**, Li X, Fang XY, Lo W, Gu Y, Wong W-T. pH-Triggered poly(ethylene glycol)-poly(lactic acid/glycolic acid)/croconaine nanoparticles-assisted multiplexed photoacoustic imaging and enhanced photothermal cancer therapy. *ACS Appl Bio Mater*. 2021;4(5):4152-4164. doi:10.1021/acsabm.0c01578.

3. Li S, **Lui K-H (co-first author)**, Tsoi TH, Lo W, Li X, Hu X, Tai W C S, Hung C H L, Gu Y, Wong W-T. pH-responsive targeted gold nanoparticles for in vivo photoacoustic imaging of tumor microenvironments. *Nanoscale Adv*. 2019;1(2):554-564. doi:10.1039/c8na00190a.

Acknowledgements

My heartfelt thanks to the following persons, without whom I would not have been able to complete this PhD degree. Without these amazing people, I would not have the strength to make this journey possible.

First and foremost, I would like to express my deepest gratitude to my chief supervisor Prof. Wing-Tak Wong and co-supervisor, Prof. Dennis Shun Chiu Lam, for their generous support, guidance, and encouragement during my PhD study. This life-changing opportunity has granted me precious experience that would be beneficial for the rest of my life. Needless to say, their vision and mentorships expanded my horizon beyond the level of scientific research. Therefore, I dedicate this thesis to my forever mentors and wish them and their families the best.

Second, I would like to thank all the former and current Wong's group members: Dr. YanJuan Gu, Dr. Wai-Sum Lo, Prof. Ga Lai Law, Dr. Chi-Tung Yeung, Dr. Shiying Li, Dr. Xueyang Fang, Dr. King-Him Yim, Ms. Daisy Yuen Ting Wong, Mr. Xin Li and Mr. Hugo Tse for their indispensable and valuable support during this unforgettable journey.

Third, I would like to express my greatest appreciation to Mr. Ryan Christopher Mellor, a true friend who has guided and supported me during my darkest hour. I would also like to thank Dr. Doris Mei Ho So and Ms. Temy Leung for their help.

All staff members in Centralized Animal Facilities (CAF) and University Research Facility in Life Science (ULS) are equally important. I would like to express my greatest appreciation for their grateful support in facilitating the smooth running of my projects.

My special thanks also go to Prof. Johnson Lau, Athenex, Inc. and C-MER Eye Centre Hong Kong for providing a precious collaboration opportunity and technical support for my study.

Last but not least, I am eternally grateful to my parents, my brother, my sister and Mr. Keith Lui for their unconditional love, care and support during my study. I would also like to express my deepest gratitude to my grandfather for his generosity and guidance. His wisdom, patience and life

experiences are worthy of my respect. Without my family, I could not have had the strength to complete my study.

I sincerely wish the above-mentioned persons a healthy and joyful life.

Table of Contents

List of Figures and Tables

List of Abbreviations

AL	argon laser
ALK-1	activin receptor-like kinase 1
AMD	age-related macular degeneration
ANSI	american national standard for safe use of lasers
ARPE19	spontaneously arising retinal pigment epithelial cell
ATCC	American Type Culture Collection
ATP	adenosine triphosphate
BSA	bovine serum albumin
CNV	corneal neovascularisation
CO2	carbon dioxide
COX	cyclooxygenase
CPP	cell penetrating peptide
CR-sO2	chorioretinal oxygen saturation
CS	chondroitin sulfate
CW	continuous-wave
DAMP	danger-associated molecular pattern
DAPI	4’,6-diamidino-2-phenylindole
DCM	dichloromethane
DL	drug loading
DLS	dynamic light scattering
DMEM/F12	dulbecco's modified eagle medium/nutrient mixture F-12
DMSO	dimethyl sulfoxide
DR	diabetic retinopathy
DS	dermatan sulfate
ECM	extracellular matrix

EE	encapsulation efficiency
EGFR	epidermal growth factor receptor
EPR	enhanced permeability and retention
ERK	extracellular signal-regulated kinase
FAK	focal adhesion kinase
FBS	fetal bovine serum
FDA	united states food and drug administration
FGF	fibroblast growth factor
FGFR	fibroblast growth factor receptor
FK506	tacrolimus
FND	fine needle diathermy
FTIR	fourier-transform infrared
GAG	glycosaminoglycan
Grb2	growth factor receptor bound protein 2
HA	hyaluronan
HDA	hemispherical
HER-2	human epidermal growth factor receptor 2
HIV-1	human deficiency virus type 1
HS	heparan sulfate
HSPG	heparan sulfate proteoglycan
HUVEC	human umbilical vein endothelial cell
IC50	half maximal inhibitory concentration
ICG	indocyanine green
ICNIRP	international commission on non-ionising radiation protection
IL	Interleukin
IOP	intraocular pressure
IR	infrared

IS	internal standard
KBr	potassium bromide
KS	karatan sulfate
KSPG	karatan sulfate proteoglycan
LK	lipid keratopathy
LTC	laser thermal cauterisation
MAPK	mitogen-activated protein kinase
MCP-1	monocyte chemotactic protein-1
MMP	matrix metalloproteinases
MOM	mathematical optical model
MRI	magnetic resonance imaging
mRNA	messenger RNA
MTT	3-(4,5-dimethylthiazol-2-yl)-2,5-diphenyltetrazolium bromide
Nd:YAG	neodymium-doped yttrium aluminium garnet
NIR	near-infrared
NIR-AF	near-infrared autofluorescence
NF-κB	nuclear factor-kB
NLR	nucleotide-binding domain
NLRP	NLR family pyrin domain containing 3
NP	nanoparticle
NSAID	nonsteroidal anti-inflammatory agent
OCT	optical coherence tomography
OIR	oxygen-induced retinopathy
OR-PAM	optical-resolution photoacoustic microscopy
PA	photoacoustic
PAI	photoacoustic imaging
PAOM	photoacoustic ophthalmoscope

PASI	psoriasis area severity index
PBS	phosphate-buffered saline
PDGF	platelet-derived growth factor
PDGFR-β	platelet-derived growth factor receptor-β
PDI	polydispersity
PEG	polyethylene glycol
PG	proteoglycan
PI3K	phosphoinositide 3 kinase
PK	penetrating keratoplasty
PKC	protein kinase C
PLCγ	phospholipase Cγ
PLGA	poly lactide-coglycolide
PTT	photothermal therapy
PVA	polyvinyl alcohol
ROCK	Rho-associated protein kinase
RPE	retinal pigment epithelium
RSOM	raster-scanning optoacoustic mesoscopy
RTK	receptor tyrosine kinase
RTK-i	receptor tyrosine kinase inhibitor
RT-PCR	reverse transcription polymerase chain reaction
SFP	spectroscopic fundus photography
SH2	src homology 2
SLRPG	small leucine-rich proteoglycan
SNR	signal-to-noise ratio
sO2	oxygen saturation
STAT	signal transducer and activator of transcription 3
TEM	transmission electron microscopy

TGF-β	transforming growth factor beta
TNF-α	tumour necrosis factor alpha
TSAd	T-cell specific adaptor protein
UPLC-MS	ultra-performance liquid chromatography-tandem mass spectrometry
US	ultrasound
VEGF	vascular endothelial growth factor
VEGFR	vascular endothelial growth factor receptor
Vis-OCT	visible-light optical coherence tomography

1 Introduction

1.1 General Overview of Ocular Structure

In general, the eye can be broadly divided into anterior and posterior segments. The front section, which occupies one-third of the eye, is known as the anterior segment, whereas the poster segment is the remaining two-thirds of the globe. The anterior segment consists of various tissues such as the cornea, conjunctiva, iris, ciliary body, aqueous humour and lens. The cavity between the cornea and lens is the known as anterior chamber. The function of the anterior segment is to serve as a mechanical barrier and allow light ray passes through into the posterior segment of the eye. The poster segment, located back at the eye, comprises of sclera, choroid, vitreous, retina and optic nerve. The primary function of this part of the eye is to detect light and transmit electronic signals to the brain through the photoreceptor cells on the retina. Figure 1.1 illustrates the anatomy of ocular tissue including drug administration pathway and their respected elimination routes.[1]

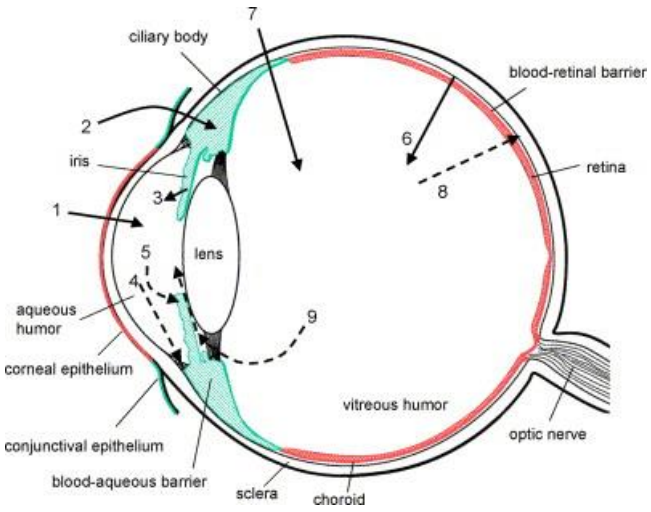

Figure 1.1 Schematic illustration of ocular anatomy and drug delivery barriers

Drug(s) penetrate the cornea via a topical route (1). Conjunctival and sclera act as alternative paths for absorption, which diffuses into the ciliary body (2). Systemic administered drug(s) diffuse from the iris blood vessels into the anterior segment (3), which eliminates via aqueous humour outflow (4) or iris venous blood flow by diffusion (5). Systemic drug(s) need to penetrate retinal pigment epithelium and retinal capillary endothelium to reach vitreous humour and retina (6). Intravitreal injection effectively delivery drug(s) into the posterior segment (7) which eliminates through blood-retinal barrier (8) or by diffusion (9). (red: diffusion pathway; green: elimination route) Reprinted with permission from ref. 1. Copyright 2005, Elsevier

1.2 Anatomical Structure of Cornea

The detailed anatomical structure of the cornea has been well-documented with histological analysis in which the cornea exists as a multi-layer tissue. As the outermost layer of the eye, the cornea constantly unveils itself to the external environment to face various foreign materials and pathogens during our lifetime. It can be generally divided into three separate regions: central cornea, peripheral cornea, and limbus. The cornea is a transparent, smooth, and avascular tissue with a convex and spherical shape. The ocular transparency, smoothness and architecture are crucial for optimal vision. Despite being a transparent tissue, the cornea consists of five different layers. These are epithelium, bowman's layer, stroma, Descemet's membrane and endothelium. They stack on top of each other and join together to form an intact cornea, as shown in Figure 1.2. The following sections will address the detail of the individual layer and their corresponding function within the cornea.

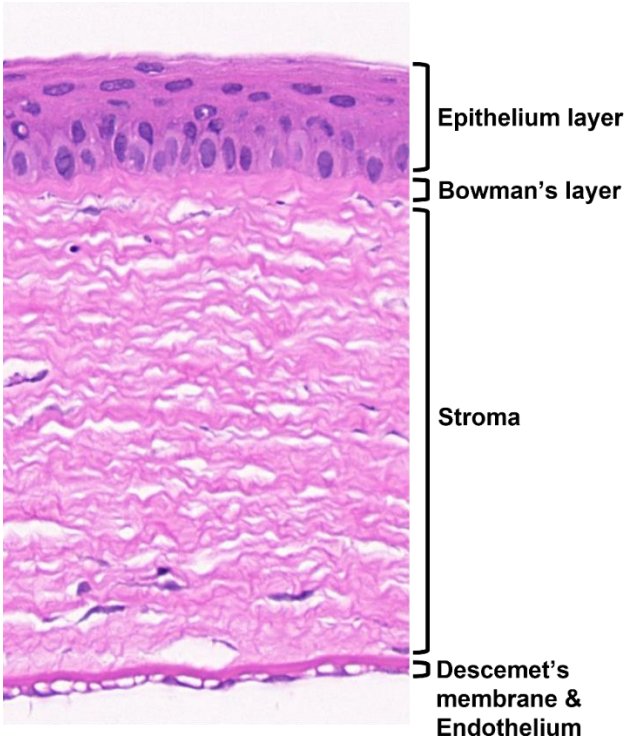

Figure 1.2 H&E image of rat's cornea

Intact rat's cornea showing epithelium, bowman's layer, stroma, Descemet's membrane, and endothelium.

1.2.1 Epithelium Layer

As the cornea's outermost layer, cells within the epithelial layer can be divided into three types: superficial cells, wing cells and basal cells. Histological section revealed that the epithelial cells possess a non-keratinized and squamous nature while closely packed next to one and other. An intact corneal epithelial layer generally contains two to three layers of superficial cells, two to three layers of wings cells and finally, a monolayer of basal cells.[2] The appearance of the superficial cells gradually turns flat and exhibits irregular shape as they move toward the superficial surface of the cornea, as illustrated in Figure 1.3.

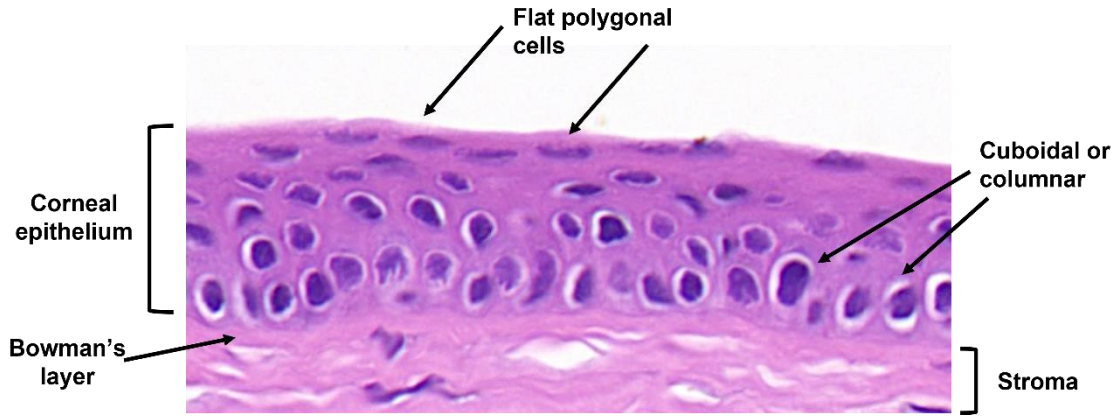

Figure 1.3 H&E image of rat's corneal epithelium

H&E image reveals the structure of rat's corneal epithelium

The irregular nature of superficial cells is mainly related to the presence of microplica on the surface.[3] Furthermore, a charged and delicate glycocalyceal layer cover on top of the microplica enhances the surface area and allows better interaction with the tear film on the surface of the cornea. The presence of desmosomes between cell membranes also facilitates the epithelium cells to adhere to each other and assist in forming a tight junction complex.[4] Therefore, the desmosomes and tight-packing nature make the cornea nearly impermeable for tears or foreign material to enter intracellular space. Underneath the superficial cells is location of wing cells; their function is to maintain the tight junction property after the renewal of superficial epithelial cells every 7 – 10 days.[5] The final epithelial cells

within the epithelium layer are the basal cells which exhibit a columnar or cuboidal shape depending on the location of the basal cells.[4] In this context, the basal cells within the central cornea are columnar, whereas peripheral basal cells are in cuboidal shape. Moreover, these basal cells are the only epithelium layer component that possesses cell mitosis capability.[6] Although the cornea is highly impermeable, the gap channels between these tight junctions provide a pathway for the entrance of small molecules through diffusion.[4] As a results, this tight junction complex hinders ocular drug absorption and will be discussed later.

1.2.2 Bowman's Layer

The Bowman's layer is a smooth and fine layer which assists the cornea in maintaining its overall shape. The type I collagen, type V collagen and proteoglycan condensed together to assemble the Bowman's layer, which lies between the epithelium layer and stroma. This layer does not possess regenerative property; thus, scar formation may occur if it is injured.[4] The presence of scaring may result in compromised vision.

1.2.3 Stroma

Stroma, a transparent and bulky structural framework, accounts for approximately 90% of the whole corneal thickness. This thick structural framework occupies the space between the Bowman's layer and Descemet's membrane.[7] This space composes of many diverse cells, such as glycosaminoglycans (GAGs) and proteoglycans (PGs). These essential components join together to form a unique extracellular matrix (ECM) that is required to work synergistically for optimal vision. Different types of cells and tissue can be found in this layer, such as fibroblastic cells, Schwann cells, keratocytes and neural tissue. Despite the wide varieties of cells within the stroma, the predominant composition is type I collagen.[8] However, other types of collagens, such as type VI and type XII, are present within the stroma. Although it is the bulkiest layer of the cornea, it retains a transparency nature which is vital for visual acuity. The transparency is primarily due to the precise arrangement and organisation of the ECM and fibres within the stroma layer.

The ECM is made up of GAGs and different types of collagens such as type I, III, V and VI.[4] PGs are compounds with a protein as their core structure and are covalently coupled with one or more side chains of GAG. GAGs are a family of unbranched polysaccharides which sub-divides into different sulfated components depending on the repetition of the disaccharide units involved. These GAGs are Karatan sulfate (KS), Chondroitin sulfate (CS), Dermatan sulfate (DS), Heparan sulfate (HS) and, Heparin and Hyaluronan (HA), where sulfotransferase and epimerase participate during their biosynthesis.[9,10]

The primary type of PG present in stroma is KS. It is predominantly in the central cornea region and gradually becomes less towards the limbus region.[11] Other types of PG, such as DS and CS, account for a small portion. The KSPG is made up of galactose and N-acetylglucosamine, where the disaccharides are repeatedly linked with each other and are sulfated at position six-carbon. Depending on the linkage with the amino acid on the PG, this could result in different types of KS. The amino acid that can be sulfated on the core protein includes asparagines, serine/threonine and serine, which gives rise to type I, type II and type III KS, respectively.[12] Furthermore, the linkage among the KS also differs between the species such that N-linked branched oligosaccharide, O-linked glycan and mannose-serine linkages are observed in type I, type II and type III KS.

Nemours studies have demonstrated that the cornea possesses a high amount of KSPGs, particularly type I KSPG. In the cornea, these KSPGs exert their properties through bounding to a group of molecules known as small leucine-rich proteoglycans (SLRPGs). These SLRPGs include keratocan, mimecan, lumican, fibromodulin and osteoglycin. Upon bounding, the KS-SLRPG complexes regulate various biological functions such as corneal wound healing and corneal development.[13] Therefore, KS deficiency would lead to corneal thinning. Furthermore, a study by Littlechild et al. revealed that CS up-regulation was significantly enhanced as compensation for KS deficiency in an experimental mice model.[14] Therefore, these have shown the importance of KS in a healthy cornea. Nevertheless, the SLRPGs also indicated a role in organising corneal collagen fibres, which it is necessary for corneal transparency.

Furthermore, corneal collagen fibres arrange themselves in a parallel bundle fashion and pack in either layer or lamellae style. These collagen fibres are known as fibrils, and the density of these fibrils vary across the cornea.[4] Throughout the whole cornea, the prepuillary corneal region contains a higher density of collagen fibrils compared to the peripheral region.[15] This precise arrangement of corneal fibrils notably contributes to structural integrity, mechanical strength, and corneal transparency. Apart from the presence of PG and collagen fibrils, keratocytes are the predominant cell type within the corneal stroma. These cells are the foundation of overall cornea function and are responsible for collagen and PG secretion. In addition, they are also crucial in maintaining the hydration level of stroma and ECM environment.

1.2.4 Descemet's Membrane

Descemet's membrane is a membrane that lays between the stroma and endothelium layer. Studies have revealed that Descemet's membrane contains four components within their overall structure: collagen type IV, nidogens, laminins and perlecan.[16,17]

In the basement membranes, collagen type IV has been found as the primarily component and comprises of six distinct α-chains.[18] The collagen type IV interacts with the chains on the laminins and thus, establishes a network and stabilises the membrane structure.

The structure of laminins, also known as heterotrimeric glycoproteins, has been well documented.[19] The laminins possess three distinctive chains, namely α, β, and γ chain, and a wide variety of trimer combinations has been identified in the past.[20] The role of laminins in Descemet's membrane has been thought to associate with corneal development, repair process and regeneration.[19]

The nidogens consist of two species, namely nidogen-1 and nidogen-2. The difference between these two sulfated monomeric glycoproteins is their molecular weight, where nidogen-1 is 150 kD and nidogen-2 is 200 kD.[21] In the basement membrane, the nidogens interact with diverse species such as collagen type IV, laminins and perlecan. These interactions are essential in preserving the structural integrity of the basement membrane, which is responsible for its organisation and stabilisation.

Perclecan, heparan sulfate proteoglycan (HSPG), contributes to the basement membrane stability and fabrication through binding with other molecules such as collagen type IV and laminins.[22] The HSPG is specific to the basement membrane, with its structure containing one single chain and five domains.

Other notable components within Descemet's membrane include, but are not limited to collagen type VIII, keratan, DS and fibronectin. Among these components, fibronectin is particularly important for maintaining the architecture of Descemet's membrane. Fibronectin has been shown to situate on both interfaces of the Decrement's membrane, where it comes into contact with the stroma and endothelium. This acts as an adhesive to link up both layers and maintain the corneal structure.[23] Besides, the Descemet's membrane is also responsible for corneal homeostasis and transparency. The supply of nutrients and macromolecules is vital for the function of a healthy cornea. As an avascular tissue, Descemet's membrane's porous hexagonal lattice configuration modulates the entry of crucial molecules into the stroma. Therefore, the Descemet's membrane and endothelial layer manage the corneal transparency, hydration, and structural integrity under normal physiological conditions.[24]

1.2.5 Endothelium Layer

The endothelium layer is the cornea's innermost layer, and it is constantly in direct contact with the aqueous humour. Underneath the cornea is the anterior chamber; it is filled with aqueous humour, which serves as a critical ocular structural support and a nutrient reservoir for ocular tissues.[25] The endothelium layer is a monolayer with a leaky arrangement and possesses metabolically active cells that exhibit hexagonal morphology (Figure 1.4).[26] Due to their high metabolism, these cells are abundant with mitochondria to serve their purpose. Studies suggested that the endothelium cell has limited self-regenerative ability and is arrested in the G1 phase through cell cycle analysis.[27] The underlying mechanism is currently unknown. However, endothelium division can be demonstrated under culture conditions. Nevertheless, the existence of this layer is essential for corneal development as it secretes collagen to form the Descemet's membrane at the early stage of birth. Once the Descemet's membrane is mature, the newly secreted collagen by endothelium cells is not banded.[25]

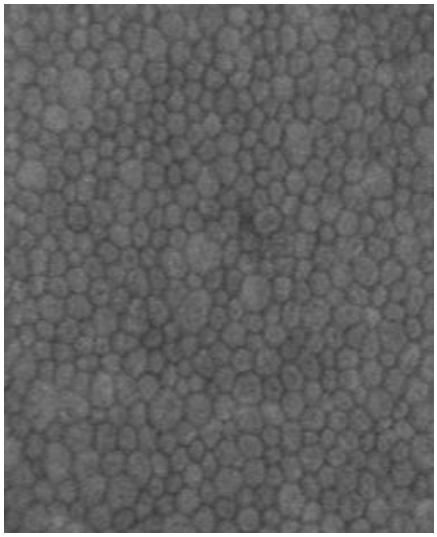

Figure 1.4 Image of human corneal endothelium

A confocal image of endothelium shows hexagonal morphology. Reprinted with permission from ref. 26. Copyright 2015 Elsevier

In addition to corneal development, the endothelial layer is also responsible for maintenance of stroma conditions through a process called deturgescence. The endothelium acts as a permeable barrier and an efficacious pump simultaneously to osmotically remove excess water as well as modulate the uptake of essential substrates from the aqueous humour. The deturgescence relies on the Na^+K^+ ATPase bounded on membrane and intracellular carbonic anhydrase pathway ion transport systems to control the hydration level of the stroma.[4] The systems generate an osmotic gradient which develops a net flux from the hypo-osmotic compartment to hypertonic aqueous humour. This process is crucial for corneal transparency as it maintains a constant water content within the stroma.[2] Disruption of this process will result in corneal oedema, which leads to compromised vision. Thus, the property of the endothelium layer is also referred to as pump-leak-mechanism.[25] Overall, it has a profound effect on corneal development and integrity owing to its contribution.

1.3 Corneal Neovascularisation Etiology

The function and health status of the cornea are undoubtedly vital for our vision. Any impairment of a specific tissue part could lead to a significant decline in an individual's visual acuity. In this thesis,

we will focus on one corneal disease, namely corneal neovascularisation (CNV). This section of the thesis will explore the etiologies of CNV.

The nature of corneal avascularity and clarity is fundamental for optimal vision. Compromise of this nature would lead to blurry vision or vision loss in severe case. Among different types of ocular complications, corneal diseases are one of the most common causes of blindness worldwide, with most cases presented with CNV. Under normal physiological conditions, the capillaries and venules stay at the corneal limbus to supply essential nutrients to the cornea. However, new blood vessels sprout from the pericorneal plexus and compromise the transparent nature of the cornea under CNV. Statistics estimated that 1.4 million people develop CNV each year, with 12% losing their vision due to CNV.[28] CNV can result from the following pathological events: infection, use of contact lenses, chemical injury, and inflammation. For example, the chlamydial infection blinded approximately 6 million people, whereas onchocerciasis infection account for 270,000 blindness cases with 120 million people worldwide at risk.[29] Herpetic keratitis, a viral infection, causes 500,000 incidents in the USA.[28] Prolonged usage of soft hydrogel contact lenses also reported having CNV features in 1.3% of 9 million contact lens users.[30] These etiologies lead to corneal opacification, blood vessel invasion, and surface irregularity. Among these conditions, the surface irregularity causes higher severity as fluid and lipids extravasation could further damage the corneal stroma architecture, thus decreasing corneal transparency and visual acuity.

The cornea is avascular and immunological privileged under normal physiological conditions.[31–33] Corneal avascularity relies on the equilibrium state of angiogenic and anti-angiogenic factors. The disruption of this balance would lead to the growth of new corneal vessels, which subsequently invades or compromises the corneal homeostasis.[34] Furthermore, downregulation of certain anti-angiogenic factors also accompanies CNV pathogenesis.[35] Despite the unfavourable outcome, CNV can be a physiologically healing reaction to traumatic, immunologic, infectious, allergic, anoxic, and degenerative stimuli.[33,36–38] It is the chronic and sustained angiogenic response that would lead to pathological CNV condition.[39] Therefore, the CNV status must be well controlled and resolved to prevent progression of pathological CNV condition.

With the technological advancement in molecular biology, several key pathogenic factors in CNV have been well explored in the past decade. These include, but are not limited to, vascular endothelial growth factor (VEGF), matrix metalloproteinases (MMPs), fibroblast growth factor (bFGF), and cytokines.

1.3.1 Vascular Endothelial Growth Factor

The vascular endothelial growth factor (VEGF) is a crucial biological molecule that provides essential biological effect in various biological settings. The VEGF is a family consisting of five different forms: VEGF-A, VEGF-B, VEGF-C, VEGF-D, and placental growth factors among mammalian species.[40] However, the poxvirus orf virus secretes and encodes only VEGF-E, which is absent in human. The VEGF has been extensively investigated in the past to understand its role in angiogenesis. Despite the different types of VEGF, VEGF-A has been identified and recognised as the primary contributor to pathological angiogenesis. A wide variety of ocular cells could secrete VEGF, such as corneal epithelium, corneal endothelium, keratocytes and retinal pigment epithelial cells.[41] In addition, under injury or inflammatory settings, VEGF-C and VEGF-D can be secreted by macrophages, contributing to angiogenesis.[42] The VEGF exerts its biological effects through its interaction with tyrosine kinase receptors, namely the VEGF receptor (VEGFR). The pathological angiogenesis involvement of three distinct tyrosine kinase receptors has been identified and well-documented in the past. It was found that VEGF-A binds to VEGFR1 and VEGFR2 to propagate its angiogenic effects.[42–44] Despite having a higher affinity towards VEGFR1, the kinase activity between the combination of VEGF-A and VEGFR1 is considerably lower compared with the binding with VEGFR2. Upon binding with VEGFR2, it induces dimerization and auto-phosphorylation which leads to the activation of phospholipase C and gamma 1. This results in stimulating the PKC-Ca^{++}-c-Raf-MEK-MAPK pathway,[45] which facilitates and elicits numerous cellular responses such as endothelial cell proliferation, migration, tube formation and blood vessel maturation. Various *in vivo* studies have also demonstrated that upregulation of VEGF-A and VEGFR2 can be observed in cornea under vascularised or

inflammatory state.[46–50] Therefore, VEGFR2 is considered as the fundamental signalling receptor which drives angiogenesis through its interaction with VEGF-A.

The VEGF-B and placental growth factor only specifically bind with VEGFR1, whereas VEGF-C and VEGF-D bind to VEGFR2 and VEGFR3. Despite the major pathological angiogenic effect originating from the binding between VEGF-A and VEGFR2, other types of receptor binding also contribute certain significance towards angiogenesis. A study by Tammela et al.[51] demonstrated that inhibition of VEGFR3 results in diminishing blood vessels density, branching and proliferation. Moreover, they also discovered that VEGFR3 could induce and sustain angiogenesis even under settings of inhibiting biological activities of VEGFR2. In addition, the group also revealed that simultaneously inhibiting both VEGFR2 and VEGFR3 could result in a synergistic anti-angiogenic effect.[51] Thus, this indicates that angiogenesis is a multi-pathway driven status, and combined blockade of different VEGF members may serve as an anti-angiogenic treatment strategy.

1.3.2 Matrix Metalloproteinases

The matrix metalloproteinases (MMPs) are a class of critical zinc-dependent enzymes that play a crucial role in a wide variety of biological processes such as body growth (physiological process) and CNV (pathological process).[52] The MMPs are a large family of proteolytic enzymes that can be generally divided into three different types: collagenase, gelatinase and stromelysin. In humans, eight types of MMPs have been identified in the cornea: MMP-1, MMP-13, MMP-2, MMP-9, MMP-3, MMP-10, MMP-7, and MMP-14.[53] The proteolytic activity of MMPs is a vital contributor to facilitating the progression of CNV, where it degrades the ECM and generates spatial area for the endothelial cell migration.[54] Under ischemia condition, the Rho-associated protein kinase (ROCK) pathway is upregulated through sonic hedgehog (Shh) protein. The Rho/ROCK pathway has a relationship with angiogenesis as it affects various cellular activities such as endothelial cell migration and tube formation.[55] Studies have demonstrated that the Shh protein could upregulate the expression of MMP-9, angiopoietin 1 (Ang 1) and VEGF. Thus, these angiogenic factors participate and contribute to

angiogenesis.[56–58] Among the different types of MMPs, the MMP-2 (gelatinase A) and MMP-9 (gelatinase B) are frequently investigated for their roles in corneal angiogenesis.

1.3.3 Structure of MMPs and Roles of MMPs in CNV

The MMP family members share some common structural features. They compose of a signal N-terminal peptide, a catalytic domain, a pro-domain, a hemopexin domain and a linker. A schematic MMP structural illustration is shown in Figure 1.5.[59] The role of the signal N-terminal peptide is to assist with peptide secretion. The catalytic domain is made up of β-sheets, α-helixes, calcium and zinc ions. The pro-domain is an important part of the structure as it retains the MMP in an inactive status and is removed upon enzyme activation. Finally, the hemopexin domain consists of a β-propeller, and the linker is responsible for connecting the catalytic and hemopexin domain.[52,60–66]

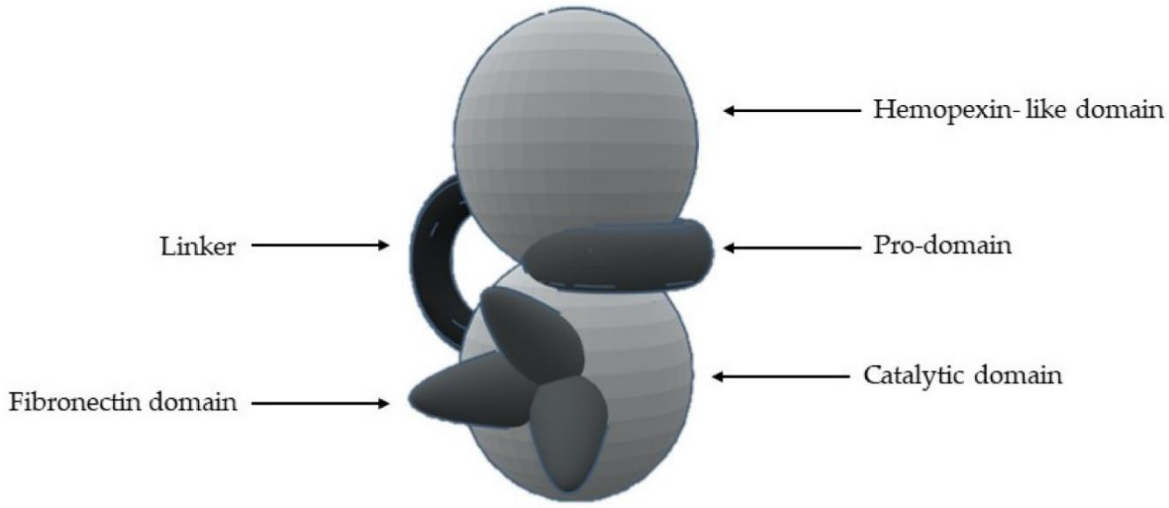

Figure 1.5 Schematic illustration of MMP general structure

General structure of MMP contains hemopexin-like domain, pro-domain, catalytic domain, fibronectin domain and linker. This work by Laronha et al.[59] is licensed under copyright 2020 MDPI Creative Commons Attribution 4.0 International License

A three-dimensional structure of MMP-2 is shown in Figure 1.6.[59] Despite similar structural features, the MMP-2 and MMP-9 slightly differ in their molecular structure. Studies have revealed that MMP-2 and MMP-9 contain fibronectin type II domains in their catalytic domain.[59] The incorporation of the fibronectin domains allows these MMPs to bind to collagen (type I and type IV), gelatin and

elastin in both pro- and active forms,[52,61] thus fulfilling their roles in degrading the ECM and assisting in pathological CNV progression. Apart from generating spatial distribution, these MMPs are also capable of releasing angiogenic factors that modulates CNV progression.

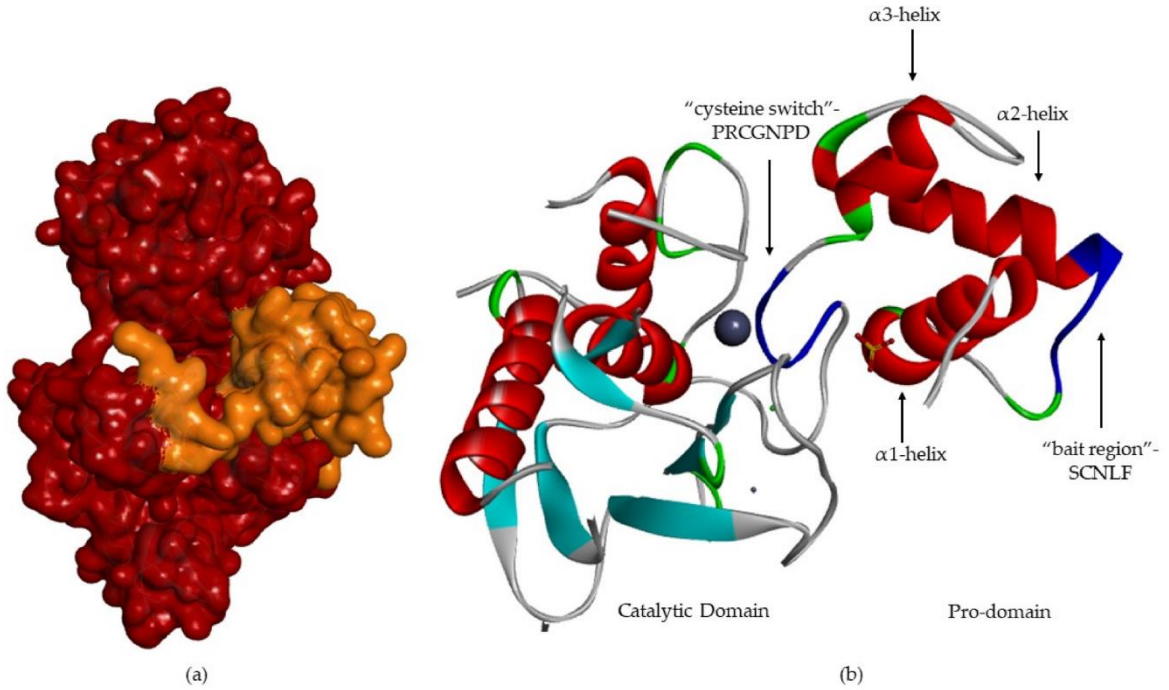

Figure 1.6 Structure of MMP-2

(a) MMP-2 structure where orange colour represents pro-domain; (b) 3D structure of MMP-2. The figure is adapted and reprinted from Laronha and Caldeira's work[59] under the permission of copyright 2020 MDPI Creative Commons Attribution 4.0 International License

However, studies have suggested that MMP-2 requires the presence of MMP-14 to modulate CNV such that MMP-14 null mice result in CNV inhibition. It is suggested that the MMP-14 activates the pro-MMP-2 (the inactive form of MMP-2) through a series of actions.[52,67] The MMP-14 acts as a receptor for MMP-2, followed by the cleavage of the pro-domain from the MMP-2. Hence, this indicates the importance of MMP-14 in modulating CNV. Moreover, the cleavage of inhibitory cytokines (heparin affin regulatory peptide and connective tissue growth factor) by the MMP-2 also assist in releasing active VEGFs, which contribute to angiogenesis.[68] Furthermore, the MMP-9 are also closely related to VEGF molecules. Research has suggested that the VEGF promotes MMP-9

expression while MMP-9 increases VEGFs expression in epithelial cells.[69] Therefore, these results indicate that angiogenic factors could influence each other in CNV.

1.3.4 Fibroblast Growth Factor Overview

The fibroblast growth factor (FGF), a class of angiogenic factors, has been investigated thoroughly since the 1980s. The FGF is important in normal physiological activities such as tissue repair, cell proliferation and migration. Studies have identified more than 22 FGF family members in this class of angiogenic factors, particularly the FGF-1, 2, 4, 5 and 8, that exhibit excellent capability in driving angiogenesis.[70–72] Among these five FGF members, the FGF-1 (acidic FGF) and FGF-2 (basic FGF/bFGF) are more potent angiogenic factors and have revealed its angiogenic influence on endothelial cells through *in vivo* experiments. The FGF-1 and FGF-2 express their effect on the endothelial cell proliferation and are capable of arranging the cells into tube-like architecture, therefore promoting angiogenesis. The FGF interacts with the four different tyrosine kinase receptors which activate biological proteinases such as mitogen-activated protein kinase (MAPK), phosphoinositide 3 kinase (PI3K) and the phospholipase Cγ (PLCγ) pathway.[73–76] Multiple subgroups of MAPK, ERK1/2, JNK1/2 and p38 alpha/beta have been identified in the past.[74] The binding of FGF with the FGF receptors (FGFRs) release biological signals to phospholipase C, which leads to the activation of PLC γ1. This activation results in vascular smooth muscle cell proliferation and migration through cleavage of phospholipid phosphatidylinositol 4,5-bisphosphate.[77] Consequently, these interactions stimulate various cellular activities in angiogenesis. In addition, the FGF works with the HSPGs, where these HSPGs protect and prevent the FGF from degradation.[78] Therefore, FGFs act as a substantial stimulator for the angiogenic process.

However, the precise mechanism of FGF in angiogenesis remains unclear. It is thought that the FGFs induce other pro-angiogenic factors, provoking the proliferation and migration of endothelial cells.[79] Moreover, the FGF also has the ability to express pro-angiogenic MMP, contributing to CNV progression. Furthermore, the FGF may have an interdependent relationship with VEGF and function in either one or combined mode: intracrine, autocrine or paracine.[80] A study conducted by Chung's

group demonstrated the relationship between FGF and VEGF through the implantation of bFGF into the corneal stroma.[81] Their result indicated that the implantation resulted in an aggressive angiogenic response. Moreover, they also treated the animals with either anti-VEGFR-2 or anti-VEGFR-3. The animal that received anti-VEGFR-2 treatment revealed a significant reduction of angiogenesis, whereas the group with anti-VEGFR-3 exhibited angiogenesis. Thus, the VEGF inhibition treatment indirectly revealed the underlying association between FGF and VEGF.

1.3.5 Fibroblast Growth Factor(s) in Ocular Tissue

Among the ocular tissue, the epithelial cells, stromal fibroblasts, and endothelial cells can produce mRNAs that encode bFGFs. These FGFs show a distinct function in their corresponding anterior components. In the case of corneal epithelial cells, the FGF-2 acts in autocrine and paracrine mode to stimulate the proliferation and wound healing processes.[82] The FGF-2, however, promotes stromal wound healing with the enhancement of cellular proliferation through the paracrine effect.[83] On top of that, animal experiments also demonstrated that FGF increases the stromal fibroblast motility.[84] Furthermore, FGF also plays a role in the endothelial mesenchymal transformation and wound healing of corneal endothelial cells.[85] In addition, other FGF members also express their influences in the posterior ocular segment. For instance, the regeneration and proliferation of lenses involve FGF-1 and FGF-2,[86] while FGF-2, FGF-5 and FGF-9 have been shown to have a role in the proliferation and regeneration of retina cells.[87]

1.3.6 Role of Fibroblast Growth Factor(s) in Corneal Angiogenesis

Despite the large family of FGFs, the FGF-2 has been identified as the most common member to motivate the progression of corneal angiogenesis.[77] Chemical burn (i.e. alkali burn) is one of the causes of CNV, and FGF-2 may have a role. Experimental data indicated that the presence of FGF-2 (in the epithelium, endothelium as well as substantia propria layer) manifests on the second day after the injury.[88] Correspondingly, the mRNA-296 upregulates the expression of FGF-23 following the alkaline injury where the FGF-23 interacts with the cytokine-cytokine receptor.[77] As a result, this interaction induces inflammatory responses. Keratitis, an inflammatory condition, is another major

cause of CNV, and it's commonly related to either bacterial or viral infection in the eye. During viral infection, the presence of immune cells and pathogens leads to the permeation of cytokines and pro-angiogenic factors (i.e FGF-2) to the cornea.[89] These contribute to further inflammation on the surface of the cornea. Despite the removal of the virus in the late stage, the FGF-2 continues to mediate cytokines (e.g. VEGF-1, IL-6) expression, which associates with and induces CNV.[73] The role of FGF-2 in CNV is illustrated in Figure 1.7.[77]

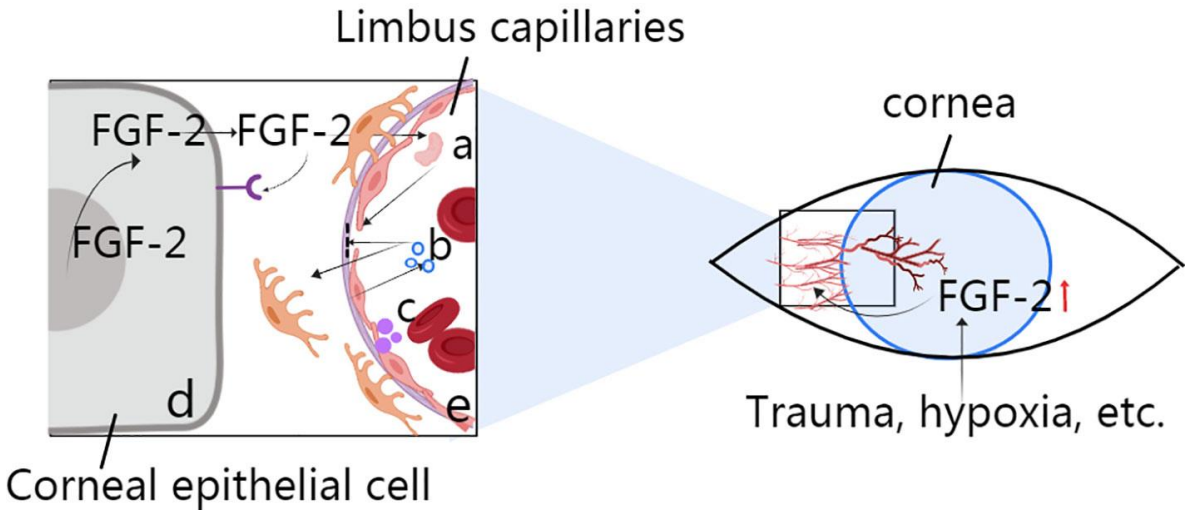

Figure 1.7 Role and biological activity of FGF-2 in CNV

(a) Secretion of FGF-2 destabilise endothelial cell junctions. (b) Basal membrane and pericytes disruptions. (c) Induction of blood vessel destabilisation. (d) Production of corneal epithelial cells through autocrine or nuclear actions. (e) Src kinase activation. The figure by Chen et al.[77] is licensed under copyright 2020 Frontiers Creative Commons Attribution 4.0 International License

The increased level of FGF and other angiogenic factors shifted the dynamic state towards angiogenic factors within the cornea. This imbalance state often leads to cornea angiogenesis and affect the cornea's clarity. Factors such as VEGF, FGF and chemokines lead to several undesirable events in the cornea. In addition, these angiogenic factors trigger cascade events and signalling pathways upon binding to the receptor of the corresponding vascular endothelial cells.[77] This binding result in the activation of Src kinase and enhances integrins expression through injury of endothelial cell junction. Moreover, the complementary binding influences the behaviours of MAPK and phosphoinositide 3 kinase (PI3K), which promote endothelial cell proliferation. Additionally, the binding induces

endothelial cells to secrete MMPs, disrupting basal membrane and promote pericyte detachment. Furthermore, the endothelial cell releases Ang 2 and destabilizes blood vessels. This leads to the formation of new blood vessels and causes unfavourable conditions on the surface of the cornea.

1.3.7 Cytokine in CNV

Inflammatory cytokines such as TNF-α, IL-1 and IL-6 have been shown to have significant effects and role in chemical-induced CNV. These inflammatory molecules can result in a series of biological events leading to corneal opacification and stromal scarring. Moreover, the inflammatory reaction further damages the corneal structure by amplifying leucocyte recruitment to the damaged cornea. Thus, the role of inflammatory molecules in CNV progression must not be underrated.

1.3.8 Role of Tumour Necrosis Factor Cytokine

The tumour necrosis factor cytokine (TNF-α), a 51 kDa soluble homotrimers, is a mediator that causes tumour necrosis. However, it is the first mediator produced due to oxidative stress after chemical injury at that ocular surface.[90] The TNF-α initiates the acute phase of inflammatory response in the ocular tissue by binding to tumour necrosis factor receptors (TNF-RI and TNF-RII). The binding resulted in the stimulation of both innate and adaptive immune cells infiltrating the corneal injured site, thus inducing CNV progression. Infliximab, an antibody against TNF- α, has been shown to alleviate the CNV progression with a single intraperitoneal injection of 6.25 mg/kg.[91] The drug reduces the immune cell infiltration after alkali injury on the corneal surface.

1.3.9 Role of Nuclear Factor-kB

The nuclear factor-kB (NF-κB) is a crucial transcription factor for the fabricating of other pro-inflammatory cytokines. Its origin can be related to the superoxide generated during the ocular alkali injury.[92] The NF-κB consists of two forms (heterodimer and homodimer) which they bind to DNA to induce cytokine upregulation (i.e. IL-1,6 and 8).[93,94] Thus, the NF-κB assists in provoking the cytokine and play a role in angiogenesis, inflammation, and immune cell activation.

1.3.10 Role of Interleukin-1β

In the early stage of ocular alkali injury, the activated NF-κB is responsible for the upregulation of pro- IL-1β (17.5 kDa). The NLR family pyrin domain containing 3 (NLRP3) within neutrophils is activated, which leads to caspase-1 initiating proteolytic cleavage of pro-IL-1β.[95] Subsequently, this releases the active IL-1β to exert its inflammatory effect in damaged ocular tissues. Studies have revealed that treatment with blockage of NLRP3 and NLRP3 antagonist (IL-1β-ra) improved corneal clarity and transparency. These work by hindering the critical steps of NLRP3 and seizing the inflammatory effect of IL-1β, respectively.[96,97] However, the antagonist does not significantly inhibit CNV progression if applied after the angiogenesis had initiated for a while.[98] This suggested that the IL-1β is not necessarily required for sustaining the angiogenesis. Furthermore, it has been demonstrated that the IL-1β causes CNV through induction of angiogenic factors such as VEGF-A.[99]

1.3.11 Role of Interleukin-6

Corneal epithelial damages induce the release of IL-1α, which acts as an inflammatory regulator and facilitates Interleukin-6 (IL-6) production. It is suggested that IL-6 intracellular signalling might relate to the epithelial cell migration in CNV progression. IL-6 initiates signal transducer phosphorylation and plays a role in activating signal transducer and activator of transcription 3 (STAT3). Consequently, it drives the corneal epithelial cells migration.[100] Investigation demonstrated that the presence of IL-6 membrane receptor (mIL-6-R) and soluble receptor (sIL-6-R mRNAs) were recognized in both epithelial and fibroblast cells. Blockage of sIL-6-R with MR16-1, an antibody of IL-6, resulted in a reduced vascularised area in CNV.[101] Therefore, IL-6 may serve as a future therapeutical target for corneal angiogenesis.

1.3.12 Role of Interleukin-8

In alkali-induced corneal injury, the damaged cells release extracellular RNA, DNA and ATP to the surrounding. These extracellular substances are known as danger-associated molecular patterns (DAMPs) and are recognized by immune cells (i.e. neutrophils, mast cells and macrophages).[90] Subsequently, the immune cells will discharge interleukin-8 (IL-8). Before the IL-8 interacts with

another receptor, its N-terminal domain must be cleaved by MMP-9 and transformed into the active form.[102] After corneal alkali-injury, the IL-8 in epithelial cells and stromal cells recruit neutrophiles and expresses inflammatory effect through chemotaxis of immune cells (i.e. T lymphocyte, neutrophils and basophils). The IL-8 is s a pleiotropic cytokine as it has different roles in inflammation and angiogenesis. The presence of IL-8 inhibits apoptosis factors and thus, enhances the survival of endothelial cells.[103] In addition, it is also capable of amplifying endothelial cell proliferation and capillary tube formation which are all vital for angiogenesis. Thus, the IL-8 presents a vast challenge for CNV treatment.

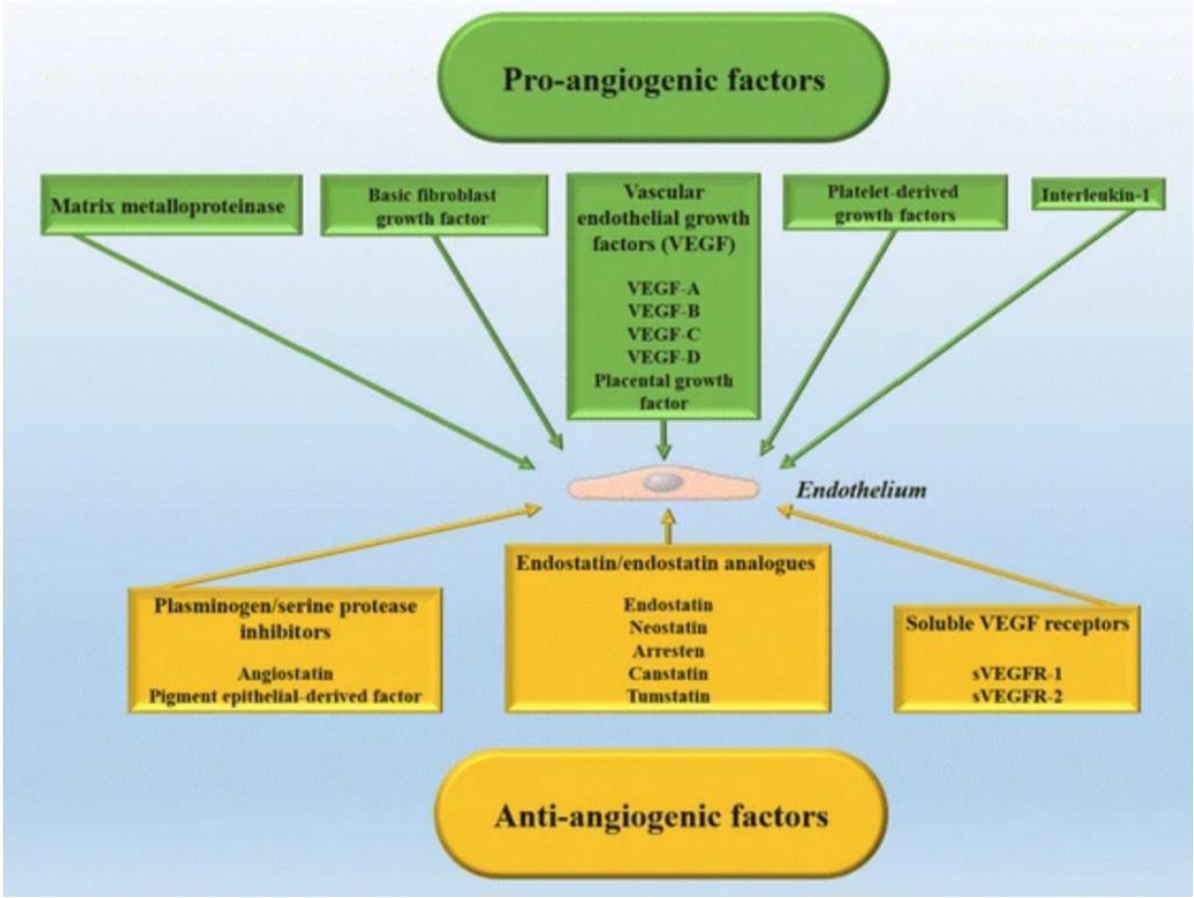

Figure 1.8 Pro-angiogenic and anti-angiogenic factors in CNV

Summary of pro-angiogenic and anti-angiogenic factors acting on endothelium cells. The figure is adopted from Feizi et al.[30] under the permission of copyright 2017 Frontiers Creative Commons Attribution 4.0 International License

1.4 Clinical Evaluation of Corneal Neovascularisation

The negative impact of CNV on the ocular surface could be devastating to an individual's visual acuity. Thus, a reliable and accurate clinical investigative method is warranted to document and monitor CNV. Common clinical instruments or methods employed for CNV investigation include slit-lamp biomicroscopy, corneal angiography and so on. These methods have been employed clinically to examine and assess the progression and treatment outcome of CNV.

1.4.1 Utility of Slit-Lamp Biomicroscopy

Slit-lamp biomicroscopy is a standard tool for ophthalmologists to examine a patient's ocular tissue such as eyelid, cornea, conjunctiva, lens and sclera. It can also magnify the view of eye tissues and provide a detailed anatomical diagnosis of individual eye conditions. With the aid of slit-lamp biomicroscopy, clinicians can obtain a better view of the cornea and examine its thickness. It is, therefore, helpful for determining and investigating the cornea condition through various illumination techniques.[104] Illumination techniques such as diffuse illumination, indirect illumination and retro-illumination have been widely employed to obtain and investigate anterior segment diseases. The diffuse illumination technique allows an overall assessment of corneal condition, whereas the latter two techniques allow clinician to detect lesions (e.g. neovascularisation) on the cornea. Slit-lamp biomicroscopy equipped with a digital camera allows documentation of CNV through pixel measurement, contrast enhancement and density threshold identification.[105] Moreover, image processing software (e.g. ImageJ) can further assist CNV evaluation. A semi-automated or manual approach with image processing software can quantify vascularised areas.[106] However, the semi-automated approach is preferred as it avoids potential inter- and intra-observer variability. In addition, it might not be able to provide details on other vital information (e.g. localisation, origin and leakage), which serves as necessary guidance for clinical judgement and decisions.[107]

1.4.2 Evaluation of CNV with Corneal Angiography

Corneal angiography is a technique to visualize blood vessels and is particularly useful in revealing details of CNV. This technique utilizes either or both fluorescein and indocyanine green (ICG)

dye. To conduct corneal angiography, the patient receives an intravenous injection of the dye(s) followed by an examination with scanning laser ophthalmoscopy.[107] ICG is an aqueous soluble tricarbocyanine dye with 800 to 810 nm as its peak spectral absorption, which is beneficial for choroidal and retinal vasculature imaging.[108] Fluorescein allows visualisation of vessel maturity and leakage behaviour, whereas ICG enables superior delineation of blood capillaries and detects deeper CNV. This is particularly advantageous as it can overcome corneal scarring or haze that obscures the presence of blood vessels.[105] Several past investigation have proven its usefulness in identifying and assessing CNV with a relatively safe profile in ophthalmic settings.[109] [110] [111] Therefore, these dyes and techniques empower clinicians to closely monitor and quantify CNV progression as well as treatment outcome.

1.5 Clinical Treatment Option for CNV

With the rapid development nature of CNV and difficulties in ocular drug delivery, CNV treatment can be problematic. In general, CNV treatment aims to occlude blood vessel formation in the cornea through either anti-angiogenesis or angioregression approach.[112] The anti-angiogenesis approach focuses on ceasing neoangiogenesis at the beginning of CNV development, while the angioregression therapy targets and induces reversion of immature or old blood vessels. Though many clinical treatments are available, they all have different degrees of accomplishment in CNV treatment. Therefore, the CNV treatment can be classified as either medical or surgical.

1.5.1 Medical Treatments

Medical treatment of CNV employs different types of medicine to achieve anti-angiogenesis. This can be achieved through either topical administration or subconjunctival injection. Examples of medical treatments include corticosteroids, nonsteroidal anti-inflammatory agents, anti-VEGF agents, tyrosine kinase inhibitors and immunosuppressive agents.

1.5.1.1 Corticosteroids

Corneal angiogenesis could result from inflammation where inflammatory cells infiltrate the cornea and act as potent angiogenic mediators. In this regard, anti-inflammatory medication would be an adequate treatment option for CNV treatment. Corticosteroids are often considered as a first-line

option for CNV treatment owing to their potent anti-inflammatory properties and ability to suppress proliferation of corneal vessels. Several studies investigated the treatment efficacy in CNV with different corticosteroids such as dexamethasone,[99,113,114] cortisone,[115–117] prednisolone,[114,118,119] and hydrocortisone.[116] Despite their potent anti-inflammatory properties, steroids must be applied at certain time point to maximize their effects. It is suggested that administrating steroids before or immediately after corneal insults would improve treatment efficacy.[34] The underlying anti-angiogenic effect of steroids is thought to relate to their capabilities in inhibiting cell chemotaxis[119–123] and pro-inflammatory cytokines inhibition such as TNF-α, IL-1 and IL-6.[124–129] Interestingly, an enhanced anti-angiogenic effect was observed when cortisone was co-administered with heparin and cyclodextrins.[130–134] The combination of cortisone and heparin acts as a new class of compounds known as angiostatic steroids. This synergistic effect comes from a combination of modulating collagen metabolism, inducing basement membrane dissolution, and promoting inhibition of plasminogen activator.[135,136] However, the corticosteroids accompany some undesired side effects with prolonged usage. These side effects include increased risk of superinfection, cataract and glaucoma.[137]

1.5.1.2 Nonsteroidal Anti-inflammatory Agents

Nonsteroidal Anti-inflammatory Agents (NSAIDs) are another class of medication that exhibit similar or better therapeutic effects against CNV without the common side effects of corticosteroids. An enzyme, cyclooxygenase (COX), which expresses in normal blood vessels (COX-1) and new endothelial cells (COX-2 isoform), has a role in angiogenesis.[138,139] The COX-2 isoform can produce eicosanoids that can modulate the expression of VEGF.[140] The COX transforms arachidonic acid into prostaglandin (PG), which possesses pro-angiogenic properties.[141,142] PG can be found in the cornea during inflammation and wound healing process and thus, may serve as a target for anti-angiogenesis.[36 143 144 145] The NSAIDs prevent the conversion of arachidonic acid to PG through COX inhibition. Examples of NSAIDs that have shown anti-angiogenic properties include indomethacin, ketorolac and flurbiprofen.[114,120,141,144,146,147] However, ocular side effects such as corneal ulceration and full-thickness corneal melts have been reported, and the clinical efficacy of NSAIDs varied.[148–151] Thus, NSAIDs are

not generally considered as a first-line treatment option for CNV and requires close monitoring when prescribed.

1.5.1.3 Anti-VEGF Agents

The advanced molecular understanding of CNV pathogenesis has led to the development of anti-VEGF strategies. Studies have demonstrated that VEGF is one of the key mediators in the angiogenic process. Several strategies have been employed to tackle the role of VEGF in the angiogenic process, such as VEGF neutralizing antibodies, recombinant soluble VEGF receptor protein, and soluble receptor antibodies.[152–154] Despite various strategies, the present clinical option utilises VEGF antibodies for anti-angiogenic treatment. Two notable and well-known anti-VEGF agents, bevacizumab and ranibizumab, are often used in the battle against CNV clinically and experimentally. The difference between the two is the molecular size of ranibizumab is smaller than bevacizumab's. Bevacizumab is a full-length antibody (149 kDa), while ranibizumab is the Fab fragment (48 kDa) and exhibits a higher affinity towards the VEGF-A isoform.[155] These agents demonstrate higher treatment efficacy towards blood vessels that are actively growing rather than established blood vessels.

Bevacizumab, also known as Avastin, is a recombinant humanized murine monoclonal anti-vascular endothelial growth factor antibody developed by Genentech, Roche. It consists of 93% human origin, and the rest are of murine origin. Upon administration, the drug binds to the VEGF-A isoform, inhibiting the biological activities,[156–158] therefore hindering its vital role in angiogenesis. Bevacizumab can be applied through different administration routes such as topical administration and subconjunctival injection.[159–164] Depending on the route of administration, the frequency and concentration may vary from one to another. While most studies demonstrated the anti-angiogenic effect of bevacizumab, some researchers reported Bevacizumab has no effect.[165,166] The diverse etiology of CNV may be the reason behind the anti-VEGF agent treatment outcome. In the cases where angiogenic cytokines are the root cause, administration of anti-VEGF antibodies may not express an excellent treatment effect. [164,167] However, angiogenic stimulus intensity and epithelial barrier also play a role in determining anti-VEGF treatment outcomes.[159] Some researchers suggested that a combined treatment strategy with other anti-angiogenic medication (i.e. platelet-derived growth factor B/PDGF-

β or CD-36 receptor agonists) may further enhance the treatment outcome.[168,169] When Bevacizumab is given systemically for colorectal carcinoma treatment, it exhibits less systemic side effects (e.g. hypertension and thrombosis).[170,171] *In vitro* experimental data revealed that Bevacizumab is non-toxic to human corneal cells.[167] However, corneal epithelial defects have been shown to associate with topical administration of Bevacizumab. It is thought that Bevacizumab disrupts the adhesion between the corneal epithelium and basement membrane. In addition, Bevacizumab may also delay the wound healing process; thus, the use of Bevacizumab may be problematic if applied in a cornea with existing wounds.[155] Therefore, Bevacizumab must be carefully considered prior to administration.

1.5.1.4 Immunosuppressive Agents

Several immunomodulatory medications have shown their capacity as an anti-angiogenic agent, including cyclosporine A, sirolimus, and tocilizumab. These agents can be applied through either topical, injection or systemic administration with promising results in reducing experimental CNV animal models.

Cyclosporine A has shown to be an effective medication for immune disorders in ocular diseases. VEGF-induced angiogenesis was suppressed by systemic administration of cyclosporine A in *in vivo* and *in vitro* experimental angiogenesis model. The mode of the mechanism behind the scene could relate to the inhibition of endothelial cell migration.[172] Furthermore, topical administration of cyclosporine with a concentration of 0.05% even demonstrated a better treatment outcome than Bevacizumab to impede immune-mediated CNV in the rabbit.[173]

Sirolimus, also known as rapamycin, is an immunosuppressive agent capable of arresting cell cycle progression (G1 to S phase), thus achieving T-cell activity inhibition through proliferation arrest. This inhibitory effect was also demonstrated with everolimus, a derivative of sirolimus. Additionally, sirolimus was able to inhibit T-cell proliferation even with co-stimulation under both T-cell receptor activation and CD28 as well as IL-2.[174,175] In mice model of alkali-induced ocular injury, both systemic and topical application of sirolimus reduced the level of IL-6 and transforming growth factor beta (TGF-β). As a result, the sirolimus demonstrated its ability to alleviate corneal opacity and CNV.[176] In another

chemical-induced CNV model in mice employed, everolimus was capable of reducing VEGFR-2 and extracellular signal-regulated kinase 1/2 (ERK 1/2) expression, which are both critical factors for angiogenesis.[177]

Tocilizumab, a fully humanised antibody, is an IL-6 antagonist which possesses the power to reduce CNV in alkali-induced rat CNV models through the topical administration route. The mode of action is to achieve blockage of inflammatory cytokine (IL-6) and thus diminish expression of VEGF.[178]

1.5.2 Surgical Options

Surgical treatment accomplishes angioregression using external energy to occlude blood vessels, thus serving as an approach of CNV treatment. This approach use either laser or heat energy to achieve corneal blood vessel occlusion and subsequently inhibit CNV.

1.5.2.1 Laser Thermal Cauterisation

Laser thermal cauterisation (LTC) uses laser sources to ablate established corneal blood vessels and inhibit CNV inhibition. The LTC has been shown to possess a certain degree of success in both experimental and clinical settings. The laser sources employed in CNV treatment is either an argon laser (AL) or neodymium-doped yttrium aluminium garnet laser (Nd:YAG Laser). The key point of LTC in treating CNV is to provide precise treatment to the affected area and reduce damage to adjacent tissues. These can be controlled through laser power, duration, and timing. The principle behind the LTC relies on light-induced thermal damage to the targeted tissue. The haemoglobin present within the corneal blood vessels under CNV actively absorbs these energies and undergo coagulation, therefore, ablating the corneal vessels.

1.5.2.2 Argon Laser Treatment

The AL clinical application primarily relates to treating lipid keratopathy (LK) and penetrating keratoplasty (PK). The AL can be equipped with a slit-lamp biomicroscopy, which offers high specificity to the targeted treatment area. Marsh et al. investigated the AL treatment efficacy of LK with 63 cases and revealed that the blood vessel density was reduced by 49% and visual acuity improved by 48%.[179] Another study includes 13 patients who underwent post-PK surgery and reported a positive

treatment outcome of AL.[151] Of all patients, 8 out of 13 patients regressed CNV condition and reversed graft rejection. In the same study, three patients received laser treatment before PK surgery, and two patients had nil rejection over the follow-up period. The remaining two patients were reported to benefit from the laser treatment with vessel regression and achieved partial corneal opacification alleviation.

Despite AL treatment's success, certain complications are often associated with AL treatment. First, blood vessels may be difficult to identify solely with slit-lamp during photocoagulation. Thus, the process may require an angiogram to assist.[180] The thermal-induced damage to the blood vessels may also trigger an inflammatory response which leads to VEGF upregulation.[181] Furthermore, the high laser energy may lead to undesired side effects and unwanted damages to adjacent tissues such as peripheral corneal haemorrhage, iris atrophy, corneal thinning and pupillary ectasia.[151,179]

1.5.2.3 Nd:YAG Laser Treatment

Similar to AL treatment, Nd:YAG laser also exhibits corneal blood vessel occlusion capability. A case report by Sharma et al. examined the treatment efficacy of frequency-doubled Nd:YAG laser in quiescent CNV of 30 eyes.[182] The results revealed that 54.15% of vessels were occluded entirely, partially occluded vessels accounted for 9%, while 35.14% were recanalised and two shunt vessels were observed. Among all participants, 14% developed superficial corneal haemorrhage. With these data, the group concluded that Nd:YAG is a safe and effective treatment for CNV. Though another report by Parsa et al. documented a stromal haemorrhage after Nd:YAG treatment.[183]

1.5.2.4 Fine Needle Diathermy

Fine Needle Diathermy (FND) is a surgical technique to occlude corneal blood vessels with an external heat source. Briefly, this technique requires inserting a stainless-steel needle into the cornea where the vessels are to be occluded. A diathermy probe will be brought in contact with the needle to transfer heat energy to the area until a mild blanching of the area is observed.[184] One study examined the treatment efficacy of FND on LK-associated CNV and found that more than 80% were successfully treated. The group concluded that FND is a practical, low-cost, and safe technique for CNV treatment.[33]

However, the cauterisation induced by FND may upregulate the VEGF; thus, combined therapy with topical anti-VEGF medication may further improve treatment outcome.[185]

1.6 Photoacoustic Imaging

The technical advancement of photoacoustic imaging (PAI) in the past decade makes it a promising tool for biomedical research. The PAI modality has been widely employed in various clinical and experimental settings to obtain valuable molecular information where other conventional imaging modalities fail to generate. The capability of PAI technique to achieve high spatial resolution and deeper tissue penetration has gained numerous attention and popularities in the field of biomedical application. Numerous efforts have been devoted to improving its function and properties in biomedical utility over the past decades. Clinical and pre-clinical experimental application of PAI include breast carcinoma imaging, dermatologic imaging, and ocular imaging. These investigations have demonstrated the great ability of PAI in delivering astonishing results not only by providing tissue structural information but also molecular information in relation to the pathological status or therapeutic outcome.

1.6.1 Principle of Photoacoustic Imaging

Photoacoustic imaging (PAI), a hybrid imaging technique, combines optical illumination and ultrasound (US) detection to offer deep penetration into biological tissues and delivery high-resolution contrast images. PAI often employs a nano-second (ns) laser to illuminate biological tissues with a pulse duration less than 10 ns. A continuous-wave (CW) laser can also be used to generate acoustic waves. However, a pulse laser is more common as it provides a higher signal-to-noise ratio than excitation induced by a CW laser.[186] The optical absorption coverts energy into heat in the targeted tissues and subsequently causes a temperature rise. Consequently, the rise of temperature results in a thermoelastic expansion within the illuminated tissues and leads to acoustic wave emission, which is detected by an ultrasonic transducer. The propagation of acoustic pressure waves lingers much longer in biological tissues because sound scatters much lesser than light.[187,188] Thus, acoustic wave detection provides better spatial resolution compared to other traditional optical methods.

The PAI capitalises on the photoacoustic effect from endogenous chromophores in biological tissues or exogenous contrast agents. However, an exogenous contrast agent may be employed to overcome problems where endogenous chromophores exhibit similar absorption spectra.[189–191] Current FDA-approved contrast agents demonstrating strong photoacoustic effects include indocyanine green (ICG) and methylene blue.[192,193] Endogenous chromophores such as melanin, haemoglobin and lipid exhibit their signature absorption spectra at specific wavelengths. These absorption spectra measurement allows individuals to monitor and investigate physiological or pathological states. For example, the change in haemoglobin status has been shown to associate with diseases such as cancer and certain ophthalmic diseases.[194,195] The ability to measure and quantify the haemoglobin content without using an external contrast agent in PAI has drawn much attentions over the past decades.

Haemoglobin, an important molecule, exists in either oxy-haemoglobin (HbO_2) or deoxy-haemoglobin (HbR) in mammal blood with distinct absorption peaks at 750 and 850 nm, respectively. The haemoglobin acts as a strong endogenous chromophore which allows examination of microvasculature and haemodynamic status in biological tissue.[196] Moreover, the quantification of HbO_2 and HbR through PAI allows the calculation of oxygen saturation (sO_2), a significant characteristic of many diseases such as ischemia, hypoxia and hypoxemia. Therefore, the sO_2 acts as an important parameter in assessing physiological status. The sO_2 can be derived from the following equation (Eq. 1), where [HbO2] and [HbR] refer to the concentration of the haemoglobin species.

$$sO_2(\%) = \frac{[HbO_2]}{[HbO_2]+[HbR]} \times 100\% \qquad (1)$$

1.6.2 Advantages of Photoacoustic Imaging

Traditional optical tomography technique such as diffuse optical tomography and fluorescence tomography has limited penetration depth compared with PAI. Moreover, PAI can sustain the high spatial resolution within the entire field of view.[186] These properties make PAI a promising imaging tool for achieving deeper tissue imaging without compromising image quality. Furthermore, PAI utilises a non-ionizing energy source to illuminate and examine target tissues which adds a certain

degree of safety level compared to X-ray computed tomography and positron emission tomography. In addition, the feasibility of PAI to conduct molecular imaging without the use of exogenous contrast agents under specific scenarios makes it stands out as a non-invasive imaging technique. Thus, this imaging technique can derive anatomical and molecular information, which is important for investigating physiological changes under pathological conditions. Finally, the PAI modality is considerably less expensive compared to magnetic resonance imaging (MRI). These merits contribute PAI becoming a next-generation advanced imaging modality.

1.6.3 PAI in Clinical Breast Imaging

With the merits of PAI, breast imaging with PAI has gained tremendous interest in research and clinical translation. Breast cancer is one of the most common types of cancer occuring in women, with new cases exceeding 2 million in 2018.[197] Effective and accurate imaging is utterly vital for diagnosis, staging and therapeutic monitoring. Despite repetitive exposure to ionising radiation, an X-ray mammogram is the most common imaging technique to diagnose breast cancer. It is also worth noting that the precision of an X-ray mammogram depends on the condition of the breast, as denser breast would lead to reduced precision.[198,199] Ultrasonography is another technique to screen breast cancer and distinguish between benign and malignant cysts.[200] Imaging techniques such as MRI and other nuclear imaging modalities are usually employed to a lesser extent than X-ray mammogram and ultrasonography.

It is well documented that angiogenesis and hypoxia are common hallmarks of a malignant tumour.[201] The detection of haemoglobins through optical imaging alongside other imaging modalities makes it an ideal and reliable diagnostic approach for breast cancer screening.[202] However, optical imaging suffers from poor tissue penetration where light only penetrates approximately 1 mm in biological tissues. This limits its clinical translation and utility.

With the emergence of PAI, the penetration depth can reach up to 4 cm and generate high-spatial resolution images as well as provide functional imaging.[203] This imaging technique could strongly influence clinical breast cancer screening.

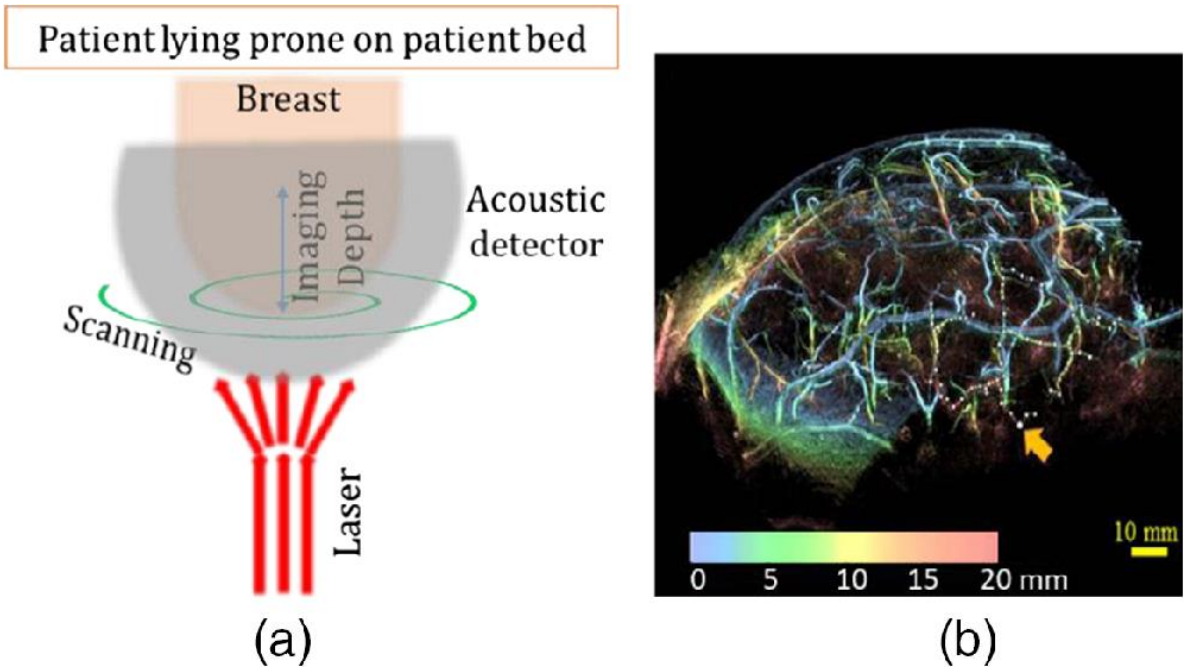

Figure 1.9 Illustration of hemispherical (HDA) breast imaging system

(a) HDA cup covered the breast and scanned in a spiral pattern. (b) PA image of a healthy breast where the arrow indicates the deepest point from the skin surface. The figure is adopted and reprinted from Toi et al.[204] under Creative Commons Attribution 4.0 International license

Manohar et al. conducted one of the first clinical investigations of PAI in breast imaging with Twente Photoacoustic Mammoscope. This breast imaging system employs a single near-infrared (NIR) laser with a wavelength of 1064 nm for excitation and an ultrasound detector. The system undertook a few updates to capture the photoacoustic (PA) signal and achieve a resolution of approximately 3.5 mm from a 9 x 8 cm^2 field of view.[205] Using this PAI system, high-intensity lesions can be detected with different types of appearances. These lesions can be broadly characterised as mass-like, ring-like, non-mass or scattered. The pattern of the observed lesions in the PAI system shows a degree of similarity to images acquired from dynamic contrast-enhanced MRI and histopathologic analysis of breast malignancies' vasculature. This PAI system has high accuracy in detecting lesions, with 32 of 33 lesions successfully identified.[206]

The utility of PAI further pushes breast cancer screening to another level by overcoming the difficulty associated with dense breast tissue. Breasts containing dense fibroglandular tissue often

presents difficulty in cancer diagnosis with an X-ray mammogram. A volumetric three-dimensional PA handheld probe has demonstrated a potential solution for such diagnosis.[207] Deán-Ben et al. investigated the utility of PAI in screening volunteers with dense breasts and achieved sufficient image contrast without compromising imaging performance. The group applied a single wavelength (800 nm) for excitation and mapped a volumetric view of the vascular anatomy of the fibroglandular-dominated breast. They also derived blood oxygenation parameters such as HbO_2, Hb and total haemoglobin content (HbT) with a tunable optical parametric oscillator laser to monitor multiple wavelengths.[208] The PA images demonstrated vasculature and haemoglobin content within the dense breast offered high-resolution imaging quality at depths beyond 2 cm. Therefore, PAI stands out as a promising tool for breast cancer screening as well as assessing angiogenic process through investigating blood oxygenation parameters.

1.6.4 PAI in Dermatologic Imaging

Skin is the largest organ in the human body and has a complex multilayer architecture. Despite being easily accessible, skin disorders often rely on visual examination and biopsies followed by histopathological analysis. Although these examination methods are the current gold standard in skin diagnosis, these methods are either subjective or invasive. The non-invasive nature of PAI serves as a potential complementary alternative for faster and objective diagnosis of skin disorders. In addition, PAI can differentiate and monitor the skin components such as melanin and haemoglobins through their respective wavelengths. Hence, PAI could act as a potential future diagnostic tool in the field of dermatology.

Psoriasis and eczema are skin conditions caused by systemic inflammatory diseases that can be potentially imaged and monitored through PAI. Augirre et al. visualised the psoriasis skin's morphology, architecture, and vasculature with raster-scanning optoacoustic mesoscopy (RSOM).[209] The group also applied a single wavelength to identify and quantify inflammatory landmarks without exogenous contrast agents. Under RSOM, psoriatic skin revealed increase in epidermal thickness, dilated and elongated capillary loops. Moreover, the dermal vasculature became more extensive and denser, which

matched the histological analysis. The inflammatory biomarkers derived from the PA signal correlated with the clinical Psoriasis Area Severity Index (PASI) demonstrated the potential PAI utility for objective diagnosis in dermatological conditions.

Chronic hyperkeratotic hand eczema has a similar clinical feature to psoriasis in which both might display a thick scale on the palm. Therefore, similar clinical feature causes difficulty in differentiating eczema from psoriasis. Zabihian et al. used high-resolution photoacoustic tomography and optical coherence tomography (OCT) in examining eczema patients.[210] Patients with chronic hyperkeratotic hand eczema displayed hypervascularisation where the demarcation of capillary loops was smaller compared with healthy subjects. A significant difference in vascular patterns between healthy and eczema patients was also revealed. Furthermore, patients with dyshidrotic hand eczema exhibited narrower vascular plexus than healthy subjects. The deep penetration property of PAI provides an in-depth physiological condition that OCT may not be able to provide. Therefore, the combination of OCT and PAI provides extra valuable information to assist clinicians in diagnosing dermatological diseases and monitoring treatment outcomes.

1.6.5 PAI in Ocular Diseases

Despite the promising results in clinical breast and dermatological imaging, the progression of PAI in ocular examination remains in laboratory settings. The eye is a fragile organ, and the delicate photoreceptors at the posterior segment are highly vulnerable to external damage.[211] The constant eye movement also adds an extra challenge to ocular imaging.[212] Furthermore, the optical power and refractive index of both cornea and crystalline lens are essential to focusing light on the retina. These contribute several obstacles to ocular imaging and must be overcome to achieve a successful imaging. First, the laser intensity for ophthalmic imaging must be within the guidelines set by International Commission on Non-Ionising Radiation Protection (ICNIRP) broadband guidelines and American National Standard for Safe Use of Lasers (ANSI).[213,214] Overexposure to inadequate laser energy can potentially cause permanent damage to the retina through photochemical damage, thermoacoustic damage and thermal damage.[215,216] Second, an ideal and appropriate ocular imaging modality should

possess non-invasive and non-contact nature. This is largely related to patient compliance. The modality should avoid causing discomfort during imaging and prevent nausea induced by using exogenous contrast agents through intravenous injection. Third, high-speed imaging process should be implemented to avoid any eye movement as it will likely induce blurring, distortion, and motion artefacts.

The abnormal change in retinal sO_2 and melanin concentration in retinal pigment epithelium (RPE) has been demonstrated in some sight-threatening diseases such as diabetic retinopathy (DR), glaucoma, and age-related macular degeneration (AMD). Thus, precise measurement of these factors is essential for ocular disease diagnosis. Quantitative measurement of sO_2 and RPE melanin concentration has drawn much attention and efforts in the past decades. Several techniques have been developed to achieve these goals. Non-contact multi-wavelength fundus photography could provide a way to investigate the retinal sO_2.[217–219] Unfortunately, the light scattering hinders its performance and results in inaccurate measurements.[220] Other methods including oxygen-sensitive microelectrode measurements and fluorescence life-time imaging have been explored in detecting retinal partial pressure of oxygen in experimental animal studies. However, the invasive nature limits their progression and utility in clinical settings.[221,222] Visible-light optical coherence tomography (Vis-OCT) is a non-contact modality that has been shown to successfully measure choroidal and retinal sO_2 with high-resolution image quality.[223–225] Although it is able to provide ocular sO_2, the sO_2 measurements at other anatomical regions are yet to be verified.

Techniques such as spectroscopic fundus photography (SFP) and near-infrared autofluorescence (NIR-AF) imaging have been exploited to investigate and measure *in vivo* RPE melanin.[226–228] The SFP relies on a mathematical optical model (MOM) to deduce the optical density of melanin. However, the simplified MOM employed in SFP may not be able to truly reflect the actual RPE melanin and result in unreliable measurement. The NIR-AF uses the coincidence from the emission signal of melanin that is excited by AF and NIR to quantify its concentration.[228] Unfortunately, a precise mathematical model for melanin concentration in the NIR-AF technique is under development.

Thus, the usability of NIR-AF in melanin quantification is currently limited. Therefore, a non-invasive modality for accurately quantifying ocular sO_2 and melanin is warranted.

The encouraging results obtained in clinical breasts and skin with PAI have driven the development of PAI in the ocular examination. Several groups have applied PAI to examine ocular tissues in the past.[229] Liu et al. utilised optical-resolution photoacoustic microscopy (OR-PAM) to image mice with CNV.[230] They used an excitation wavelength of 532 nm to image the cornea (Figure 1.10). Initially, the signal of the corneal vessels was not clearly visible due to stacking with the signal from melanin in the iris. The group conducted a B-scan of the corneal vessels and iris followed by a segmentation to obtain a map of clear corneal vasculature. This study demonstrated the potential utility of PAI to visualise CNV without the use of an exogenous contrast agent. Despite the ability to visualise corneal vessels, the system requires a water tank to be placed on top of the object being scanned. The role of the water tank is to relay the ultrasonic signal to the detector. However, this set-up hinders the clinical application of PAI for ocular imaging.

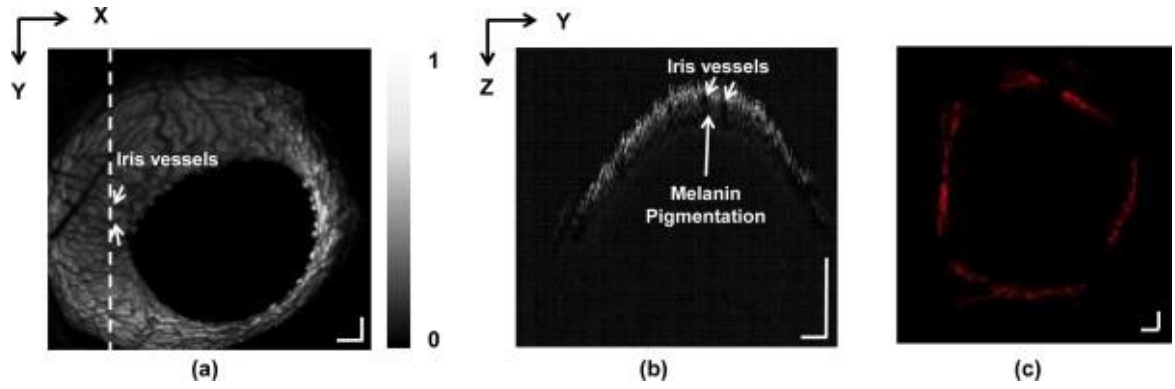

Figure 1.10 Image of a control eye with optical-resolution photoacoustic microscopy (OR-PAM)

(a) OR-PAM image of mouse eye. (b) B-scan image of the eye. (c) Anti-CD31 staining of the whole cornea. Reprinted with permission from ref. 230. Copyright 2014 Elsevier

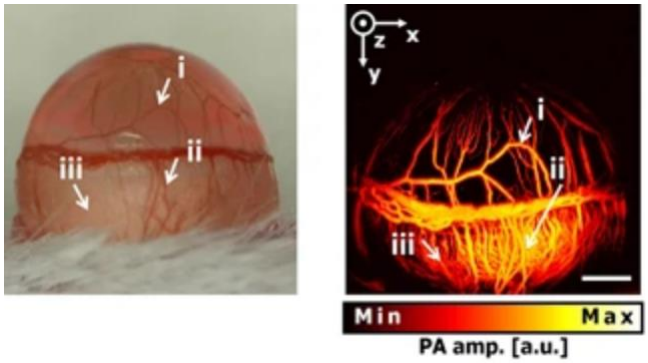

Figure 1.11 Corneal blood vasculature of mouse eye

Photograph (left) shows the corneal vasculature of mouse eye; PA image (right) of the vasculature. The figure is adapted and modified from Jeon et al.[231] with permission to reprint under Creative Commons Attribution 4.0 International license

Photoacoustic imaging of the posterior segment is more difficult than anterior segment imaging. The lens significantly attenuates ultrasonic signals leading to a poor signal-to-noise ratio (SNR) and subsequently poor image quality. Hariri et al. demonstrated the utility of PAI to detect chorioretinal oxygen saturation (CR-sO_2) with rabbit ocular ischemia model.[195] The group employed a commercially available PAI modality, Vevo LAZER by FUJIFILM VisualSonics for the detection of CR-sO_2. Briefly, the system is equipped with a Q-switch Nd:YAG laser and linear array transducer for inducing laser energy and detecting ultrasound signal, respectively. This system demonstrated the PAI utility in monitoring the change of CR-sO_2 level under ischemia condition. However, this system could not discriminate against individual blood vessels owing to limited spatial resolution.

The emergence of photoacoustic ophthalmoscope (PAOM) breaks through the obstacle of poor image quality. Jiao et al. developed a non-invasive PAOM to image retinal blood vessels and retinal pigment epithelium shown in Fig 1.12.[232]

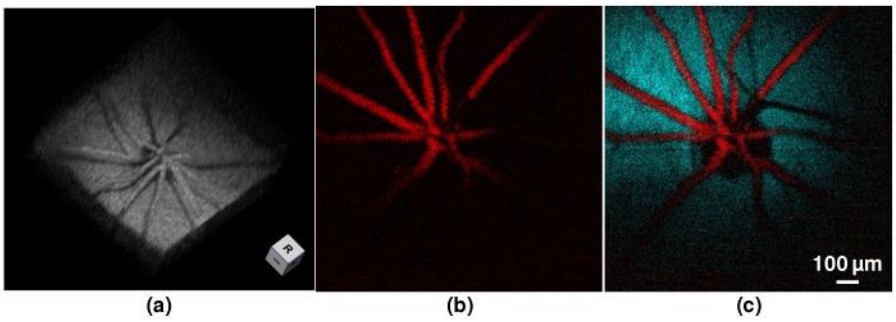

Figure 1.12 Visualisation of retinal pigment epithelium and retinal blood vessels with PAOM

(a) Image of retinal structure captured with PAOM. (b) Segmentation reveals retinal blood vessels (labelled in red colour). (c) Overlaid pseudo-coloured imaged of retinal structure. The figure is adopted from Jiao et al. [232] and reprinted under permission of Creative Commons Attribution-Noncommercial-No Derivative Works 3.0 Unported License

Briefly, the design has two outputs: one output source acts as the excitation source, and the other one is responsible for the compensation of laser intensity variation. An ultrasound gel was applied to couple the eyelid and an needle ultrasonic transducer to detect the PA signal induced by the laser. Numerous investigations have successfully utilized PAOM in posterior segment imaging and achieved excellent image quality for retinal/choroidal vasculature and melanin in RPE.[233–237] Overall, PAOM possesses several outstanding properties over OR-PAM for ocular posterior segment imaging. First, the imaging speed of PAOM is significantly faster than OR-PAM, which makes it an ideal imaging modality for ocular examination. Moreover, this type of imaging modality does not require a water tank to relay the ultrasound signal; instead, it only requires ultrasound gel to couple the object being imaged with the transducer. Furthermore, the design of PAOM overcomes the attenuation problem associated with lens where the needle transducer at the eyelid detects almost every ultrasonic signal. Thus, PAOM can deliver images with a high SNR, making it a valuable imaging modality for retinal imaging.

1.7 Nanotechnology in Drug Delivery

CNV requires medical attention due to its potential to compromise visual acuity and, subsequently, quality of life. Clinical treatment for CNV often employs topical corticosteroids as first-line treatment. However, the structural barriers of the eye pose numerous challenges to ocular drug

delivery. Common ocular drug administration routes such as topical administration and ocular injection have their strengths and weaknesses. Over the past decades, tremendous efforts have been made to overcome ocular drug delivery challenges through the use of nanomedicine. This section will review the problem associated with ocular drug delivery and potential solution with nanomedicine.

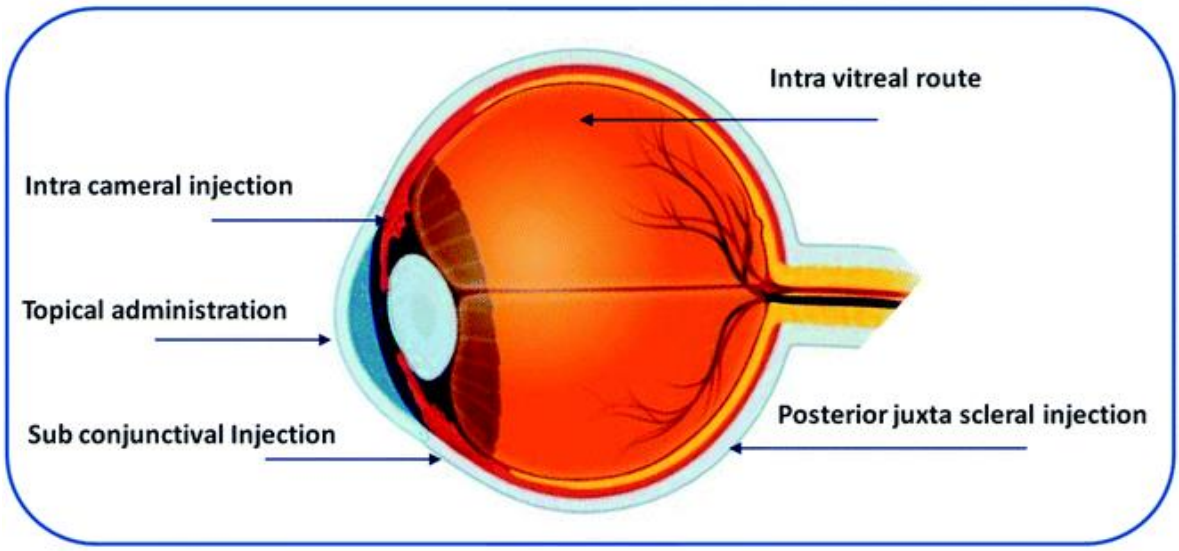

Figure 1.13 Schematic illustration of different administration routes

The figure is adapted and reprinted from Gorantla's work[241] under the permission of copyright 2020 RSC Advances Creative Commons Attribution 4.0 International License

1.7.1 Administration Route for Ocular Drug Delivery

Common ocular drug administration routes include, but are not limited to topical administration, subconjunctival injection and intravitreal injection. Each administration route has distinct merits and liabilities; thus, the choice of ocular drug delivery method shall depend on the nature of the disease.

1.7.2 Topical Administration

Topical administration is the most common and preferred route for treating ocular diseases owing to its non-invasive nature and excellent patient compliance. Topical administered drugs are often formulated as eye drops, suspensions, and ointments and are generally absorbed through the corneal surface and conjunctival cul-de-sac.[238] However, the physiological and anatomical barriers limit the penetration and absorption of the applied drug, with 95% being wasted.[239,240] Therefore, this leads to

low bioavailability. Physiological barriers include blinking, nasolacrimal drainage, and lacrimation rate. Corneal epithelium and stroma are considered as anatomical barriers, whereas dynamic barriers refer to lymph flow, conjunctival blood and lachrymation.[241] These barriers prevent entry of the applied drug, thus contributing to low bioavailability.

Apart from these barriers, tear film also plays an important role in preventing drug absorption through topical administration. Tear film, a natural lubricant, comprises of lipid, aqueous and mucus layer. Under a normal physiological condition, the flow rate is approximately 1.2 mL per minute and renews every 5 minutes. Upon topical administration, the induction of reflex stimulation leads to an increase of lachrymation to approximately 300 mL per minute. This generates a high turnover rate of the mucus layer and lacrimal fluid. Therefore, the applied drug is diluted and washed away upon administration. Furthermore, the mucin within the tear film assembles a hydrophilic layer on the ocular surface. This serves as a protective layer from cell debris and foreign materials. Consequently, this acts as an additional layer for topically administered drugs.[242]

Despite the numerous preventive mechanisms for drug permeation, topical administration is still the most preferable route owing to its non-invasive nature. However, because of the low bioavailability, frequent administration is required to retain drug concentration to exert therapeutic effects on the ocular surface. Unlike eye drops, the sticky and thick nature of ointment can prolong the surface retention time and thus, enhance the bioavailability. However, the physical property ointment often results in blurred vision and compromises patient compliance. In addition, over secretion of lacrimal fluid under an inflammatory state further compromised the efficacy of eye drops as it tends to dilute the topically applied drugs.[240,243] All in all, topically administered drugs are effective in treating ocular anterior segment diseases to a certain extent, whereas posterior diseases require another administration route for efficient treatment outcomes.

1.7.3 Ocular Injections

Besides topical application, ocular injection is also a common route for administrating an ocular drug. Figure 1.13 shows the different types of ocular injection sites. Intravitreal injection is one

conventional way to administer ocular drug into the vitreous cavity. Due to limited space, only 20 – 100 µL of drugs in either solution form or suspension can be injected for therapeutic purposes. Furthermore, a higher gauge needle such as 27 or 30 gauge shall be used during practice.[244] The vitreous cavity is filled with clear, viscous liquid known as the vitreous body. The composition of the vitreous body contains hyaluronan and glycosaminoglycan, which plays a vital role in drug distribution. The negatively charged glycosaminoglycan exerts electrostatic attraction towards drugs being administered into the vitreous cavity and thus, this may affect the distribution.[245] Moreover, drug molecular weight and pathophysiological condition also influence the drug distribution.[246] The shape and molecular weight of the drug have an impact on the retention time. Small molecular weight (< 500 Da) has a shorter retention time, whereas large, linear (> 40 kDa) and globular (> 70 kDa) molecules exhibit a greater retention time. The injection route can bypass the natural mechanical and physiological barriers and increases drug bioavailability. However, the invasive nature can lead to severer complications such as vitreous haemorrhage, retinal detachment, cataracts and infection.[247] Other injection routes such as intracameral, subconjunctival and posterior juxta scleral are considered less invasive compared to intravitreal injection although drugs administered through these routes have a shorter retention time.[248]

1.7.4 Nanomedicine in Ocular Drug Delivery

Chronic nature of various ocular diseases requires frequent drug administration regardless of topical or injection routes.[249] The development of nanocarriers stands as a promising solution to overcome current obstacles imposed by current ocular drug administration methods. Furthermore, the smart nanocarriers are capable of providing targeted and sustained release therapy that conventional administration methods fail to achieve.[250,251] Nanocarriers are defined as particulate systems with dimensions ranging from 10 to 1000 nm. However, a more recent definition describes nanoparticle as a particle with novel properties which a bulk particle typically does not possess. Therefore, the definition of a nanoparticle is not primarily based on its size but also considering its unique properties.[252] The ultimate purpose of nanocarrier is to develop a clinically applicable formulation for disease treatments. Thus, nanocarriers that are able to enhance drug solubility, precise delivery and improve treatment efficacy shall be an attracting point. Many drugs (e.g. anti-cancer drugs) are often associated

with poor water solubility, which requires unpleasant excipients (e.g. Cremophor EL) to dissolve the active pharmaceutical compounds. Improving solubility through the use of nanocarrier shall increase the safety profile, thereby diminishing toxic side effects while enhancing bioavailability.[253–255]

Nanomedicine can be generally categorised into polymer-drug conjugate and nanoparticulate system. However, the boundary between these categories is not clear. Materials such as liposomes, dendrimers, solid lipid nanoparticles have been widely investigated and utilised in the past. Among all these, polymeric nanomaterial has exhibited great potential in different medical applications. Synthetic polymer enables a flexible design that fits the intended purpose in a well-controlled and reproducible manner.[256] Poly Lactide-coglycolide (PLGA), a synthetic polymer, has demonstrated outstanding capability and is a valuable alternative for natural polymers such as chitosan and alginate.[257,258] Regardless, different fabrication methods have been developed for assembling nanoparticles. These methods include, but are not limited to single-/double-emulsion, and nanoprecipitation.

1.7.5 Single-/Double-Emulsion

The single-/double-emulsion methods are one of the most frequently employed methods for synthesising nanocarrier to encapsulate drugs with different solubilities. The choice of method depends on the hydrophilicity of the drug to be encapsulated. The single-emulsion method is preferred when the encapsulated agent is hydrophobic, whereas double-emulsion method is used for hydrophilic drugs. Regardless of the method, the system requires emulsifying a suitable organic solvent with an aqueous solution.

In the case of single-emulsion, polymer and hydrophobic pharmaceutical compound are co-dissolved in a water-immiscible, volatile organic solvent such as dichloromethane or chloroform. The organic solvent is dropped into an aqueous solution containing a surfactant (e.g. polyvinyl alcohol (PVA)) under vigorous homogenisation or ultrasonication to generate an emulsion.[259] Therefore, this method is denoted as O/W (oil in water) emulsion. After emulsification, the organic solvent is removed with continuous stirring at ambient temperature or under reduced pressure to form nanoparticles. Quenching with a large amount of water or other medium is also a way of removing the organic solvent

for nanoparticle formation.[260] The solidified nanoparticles are then collected and washed using centrifugation or ultrafiltration, followed by freeze-dying for long-term storage.[261] Apart from acting as a drug carrier, this method has recently been used for the preparation of vaccine.[262]

The double-emulsion method shares similar procedures with the single-emulsion, except this fabrication process is used when the encapsulating agent is hydrophilic such as protein and peptides. With this method, the active agent and polymer are first dissolved in aqueous and organic solvent, respectively. The aqueous phase is mixed with the organic phase to produce a primary emulsion (W/O). The resultant primary emulsion is emulsified into a second aqueous phase (W/O/W) to yield the nanoparticles.[263] The nanoparticles are then isolated and washed with centrifugation or ultrafiltration to remove unencapsulated pharmaceutical agents and surfactants. A recent *in vivo* experiment revealed that insulin-loaded nanoparticles fabricated from this method could maintain normoglycaemia for 24 hours. This shows the capability of sustained-release property and enhances bioavailability through the use of nano-formulation.[264]

Adjustment of experimental factors offers a certain degree of control in the size of nanoparticles produced and amount of drug loaded. Factors to be considered during synthesis include drug-to-PLGA ratio, choice of organic solvent, stirring speed/power of ultrasonication and surfactant concentration. However, the double emulsion methods are often associated with some drawbacks when the encapsulated target is either protein or peptide. Biological molecules are susceptible to denature at the aqueous-organic phase, while the harsh stress induced by homogenisation or ultrasonication might induce aggregation or cause protein tertiary structure to unfold.[265] Several excipients such as sugars, polyethylene glycol (PEG), and bovine serum albumin (BSA) have been employed to minimise protein denaturation during encapsulation.[266–268] Despite preventive measures employed, the emulsion methods still suffer from batch-to-batch variation, poor size homogeneity and variable release kinetic.[269]

1.7.6 Nanoprecipitation

Nanoprecipitation, also known as the solvent displacement method, is an easy and mild fabrication process for nanoparticle formation with high reproducibility.[270] The method relies on mixing

a water-miscible organic solvent into an aqueous phase. In general, the precursor material (e.g. polymer) and substance to be encapsulated are dissolved in a polar and water-miscible organic solvent such as DMSO, acetone and acetonitrile.[271–276] The resultant mixture is dropped into the aqueous phase under stirring, which may contain surfactants. Although the use of surfactants can enhance the stability of a colloidal suspension, their presence is not necessary in some cases.[277] Upon addition, the organic solvent rapidly diffuses into the aqueous phase, which leads to the instantaneous formation and precipitation of nanoparticles. The nanoparticle properties can be controlled by the molecular weight of precursor material, precursor material-to-drug ratio and solvent choice.[278] Aside from the easy processing, this method also offers well-defined nanoparticle size as well as narrow size distribution, which emulsion methods have problems achieving.[279] This method is frequently employed to produce polymeric nanoparticle with size of 100 nm.[280] Despite the above advantages, this method is preferred for encapsulating hydrophobic agents rather than hydrophilic drugs. The nanoparticle produced with this method can either be nanospheres or nanocapsules.[281] The production of nanospheres or nanocapsules depends on the phase in which the active agent is dissolved. If the active substance is dissolved in the organic phase where the nanomaterial precursor is, the resulting nanoparticle product will be nanospheres. Nanocapsules can be obtained upon dispersion of emulsion into the aqueous phase when the drug is first dissolved in oil, followed by emulsification with an organic solvent.[282,283] Several research groups have used this method to encapsulate aldendronate sodium for osteoporosis, while a modified protocol was used to encapsulate simvastatin with a PLGA hybrid nanocarrier.[284,285]

Regardless of the method employed for nanocarrier fabrication, nanotechnology stands out as a potential formulation for ocular drug delivery. Advantages of nanocarrier includes improving active agent solubility, enhancing drug delivery, and reducing toxicity. However, the high surface area-to-mass ratio of nanoparticles deserves a thorough investigation to examine its potential toxicity. Furthermore, when a bulk material changes into a nanoscale, the material may acquire unexpected toxicological properties.[260] Nevertheless, a statement in Schrur's nano-toxicology editorial notes that arbitrary experimental conditions and inconsistent experiment results complicates the determination of safe profile.[286] Common materials used in drug delivery are chitosan, PLGA, and liposomes. Despite

the well-documented safety profile of these materials, long-term nanoscale safety requires a comprehensive investigation for pharmaceutical utility.

1.8 Drug Discovery and Potential Candidate for Ocular Diseases

Angiogenesis, triggered by several cellular signal pathways, can be observed in various devastating diseases. Existing clinical treatment for ocular angiogenesis commonly involves the use of monoclonal antibodies and corticosteroids. However, these agents either suffer from high cost, rigorous storage condition, or unpleasant side effects. Thus, there is an urgent need to expand the arsenal for an effective treatment of ocular angiogenic diseases.

1.8.1 Tyrosine Kinase

Tyrosine kinase is part of the phosphotransferases family that transfers a phosphate group from adenosine triphosphate (ATP) to target substrates. This transfer enables signal transmission from cellular surface to cytoplasmic components, thus regulating physiological functions. In the human genome, 90 out of 518 protein kinases are tyrosine kinases.[287] The tyrosine kinase comprises of around 30 families and can be categorised into receptor and non-receptor (cytoplasmic) tyrosine kinase. The category of the tyrosine kinase has a specific role in its function. Receptor tyrosine kinase is crucial for extracellular signal transduction, whereas non-receptor tyrosine kinase is responsible for relaying intracellular communication.

A receptor tyrosine kinase possesses three domains: a C-terminal intracellular domain, am N-terminal extracellular ligand-binding site and a transmembrane domain. The receptor tyrosine kinase has a unique bi-lobar structure to exert its functionality. The first lobe is between the N- and C-terminal, whereas the second lobe lies in the C-terminal domain. The N- and C-terminal lobe allows ATP binding capacity, while the lobe on the C-terminal domain is an activation loop, which is also known as the DFG motif. D, F, and G denotes the amino acid combination at the beginning, i.e. aspartic acid, phenylalanine and glycine, respectively. Hence, this loop is named after the combination of amino acids. The conformation of this loop is important for anti-angiogenic medication to exert its power. The extracellular ligand-binding site regulates its kinase activity through the autophosphorylation of

tyrosine residues.[288] Moreover, other phosphorylation sites are also responsible for controlling protein interactions. Once activated, the receptor recruits signalling protein, which activates signalling pathway and results in biological responses.[289] These biological responses are important for cell proliferation, migration, survival, differentiation, and vascular permeability.

1.8.2 Involvement of Tyrosine Kinases in Angiogenesis

The family of tyrosine kinase is well known to possess an important role and function in regulating the angiogenic process. Stimulation of the corresponding tyrosine kinase leads to a cascade of signalling pathway in endothelial cells and results in angiogenesis. Src homology 2 (SH2) domain-containing proteins are important molecules that trigger the activation of tyrosine kinases. Examples of signalling molecules include PLC γ, growth factor receptor bound protein 2 (Grb2), T-cell specific adaptor protein (TSAd) and focal adhesion kinase (FAK).[290–292] Therefore, inhibition of the tyrosine kinase family serves as a potent strategy for anti-angiogenesis.

1.8.3 Tyrosine Kinase Inhibitors

The interaction of VEGF and receptor tyrosine kinase (RTK) triggers biological activities, which leads to angiogenesis. As a result, blockage of this type of ligand-receptor binding would be an approach to achieve anti-VEGF treatment. One approach is to utilise monoclonal antibody (e.g. bevacizumab), which acts on either the secreted molecules or cell surface. Another approach is to employ a small hydrophobic molecule to achieve anti-angiogenesis.[293] These molecules are mostly hydrophobic and can penetrate the cell membrane easily. Upon entry, these inhibitors interact with the intracellular signalling molecules or receptor domain. The underlying principle of this strategy is to impede VEGF activities through the inhibition of intracellular signalling pathways and, thus arresting angiogenic response. These agents inhibit a wide variety of RTK such as VEGFR-1, VEGFR-2 and FGFR-1. Drugs in this class of inhibitors include sunitinib, sorafenib and lapatinib (Figure 1.14).

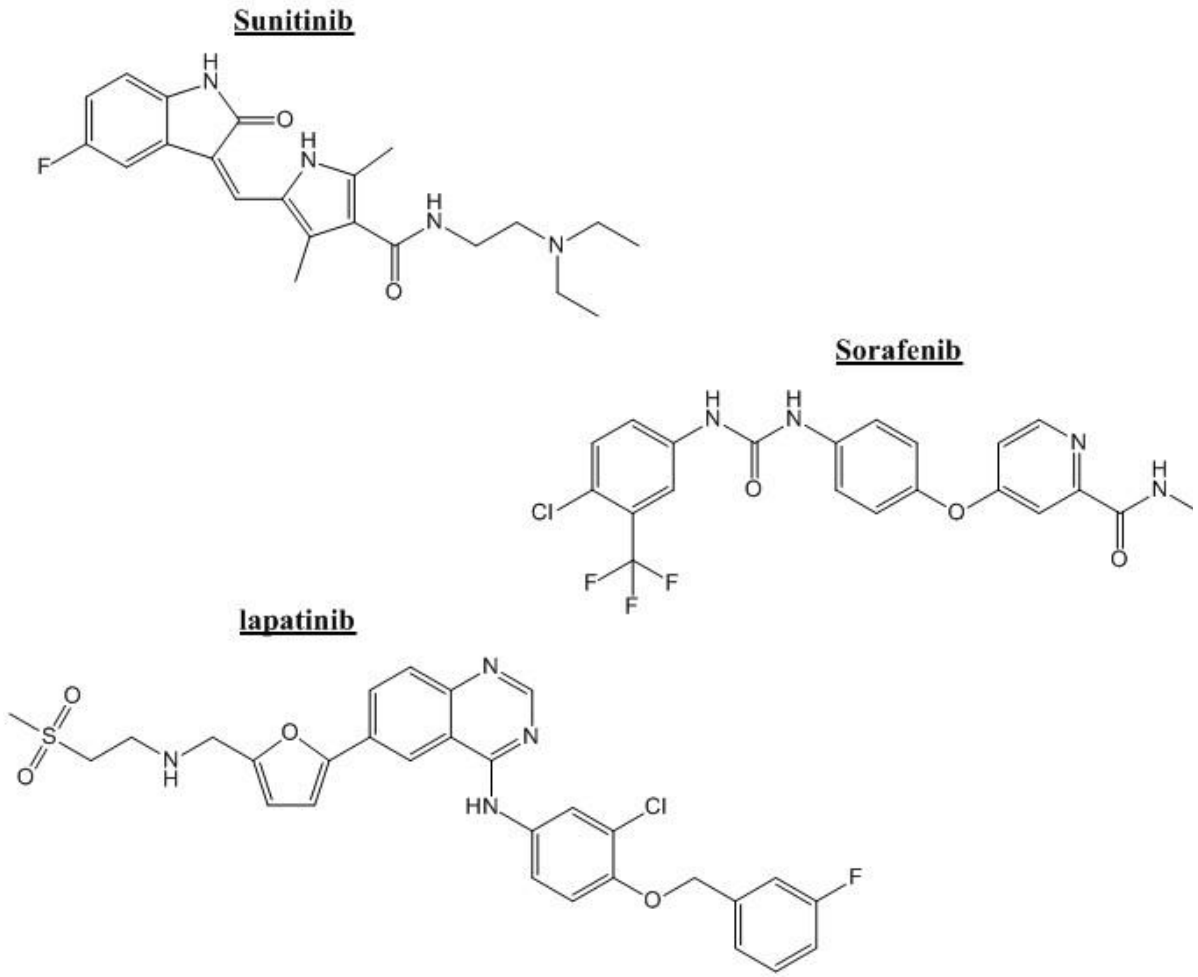

Figure 1.14 Chemical structure of sunitinib, sorafenib, and lapatinib

Sunitinib, an FDA-approved medication, is intended for the treatment of metastatic carcinoma. It is an exceptionally potent RTK inhibitor (RTK-i) which selectively targets epidermal growth factor receptor (EGFR), VEGFR-2, FGF-1 and platelet-derived growth factor receptor-β (PDGFR-β).[294,295] Sunitinib demonstrated its effectiveness in diminishing angiogenesis in an experimental inflammation-induced CNV model. The proposed mechanism is to block the VEGF-2 and VEGFR-2 pathway.[296] Other studies also found that sunitinib is capable of reducing the level of VEGFR-2 and is three times more potent than bevacizumab through an *in vivo* experimental CNV model.[177,297] However, *in vitro* epithelial cytotoxicity was observed when the concentration of sunitinib is above 3.3 µg/ml. Therefore, topical administration safety and dose profiles are yet to be determined.[298]

Sorafenib, an inhibitor of VEGFR-2 and PDGFR, demonstrates its capability to reduce *in vivo* animal CNV through oral administration. It is thought that it inhibits both VEGFR-2 and extracellular signal-regulated kinase (ERK) phosphorylation.[299,300] Despite its anti-angiogenic property, sorafenib also shows a higher degree of *in vitro* toxicity than sunitinib.[298]

Lapatinib is an RTK-i used to treat human epidermal growth factor receptor 2 (HER-2) positive breast cancer. It works by inhibiting EGFR and human epidermal growth factor receptor 2 (HER-2).[301] This drug has shown to be effective in reducing experimental *in vivo* animal CNV through oral administration. Moreover, lapatinib is more effective in treating experiment CNV compared to trastuzumab, a HER2 inhibitor. Upon oral administration, the drug decreases VEGF expression in corneal epithelial and stroma.[302]

Despite RTK-i demonstrating its potent anti-angiogenic property, most studies were conducted in experimental CNV models. Further studies are needed to confirm their clinical utility and safety. Nevertheless, RTK-i stands out as a promising reagent for future CNV treatment options.

1.9 Motivation of Research

Accurate and objective diagnosis with effective drug delivery is crucial for ocular disease treatment. Unfortunately, current clinical ocular examination techniques for CNV are either subjective or unable to provide in-depth molecular information. In addition, ocular drug administration methods suffer from poor absorption profile, low bioavailability, repetitive administration frequency and invasive nature. The current advancement in imaging modality and nanotechnology offers a promising opportunity to break through the obstacles that exist in ocular examination and drug delivery system, while this work also investigates a potential drug candidate for ocular anti-angiogenesis.

In this thesis, I investigated the potential utility of PAI in monitoring CNV progression and treatment outcomes through non-invasive quantification of molecular species. A fast and objective analytical method with a non-invasive nature provides a new pathway to monitor CNV progression by investigating of hemodynamic and sO_2 levels with PAI modality, thus, offering a more comprehensive examination of CNV progression and treatment outcome.

Secondly, a polymeric nanoparticle drug delivery system was developed to enhance ocular drug delivery, while the CNV treatment outcome was monitored by PAI. This polymeric nanoparticle drug delivery system utilises an FDA-approved biocompatible material with surface decoration to further enhance the retention time and penetration ability with peptides. This shall enhance ocular drug bioavailability.

Finally, the anti-angiogenic property of a newly developed hydrophobic drug was investigated with an experimental CNV model. Clinical approach for CNV treatment usually involves the use of steroid, which might induce undesired side effects such as elevation of intraocular pressure (IOP). The safety and efficacy of a newly developed tyrosine kinase were examined through *in vivo* experiments.

Overall, this thesis aims at searching for an advanced imaging technique, a nanoparticle delivery system and a new drug candidate for treating and monitoring CNV with the following objectives:

1. To investigate the utility of PAI in monitoring CNV progression and treatment outcome through hemodynamic and sO_2 quantification.
2. To investigate the utility of an advanced nanoparticle drug delivery system for CNV treatment combined with a non-invasive PA imaging technique
3. To investigate the safety and efficacy of new drug candidate in CNV treatment

1.10 Scope of Work

This work aims to tackle current complications associated with ocular disease diagnosis and drug administration route. Additionally, this work also examines the efficacy of a newly developed anti-angiogenic drug candidate for CNV treatment. Objective diagnosis and effective drug delivery are crucial for the treatment of ocular diseases. PA imaging can detect and monitor the presence of molecular species within a tissue and thus provide in-depth information regarding the disease status. The emergence of nanomedicine in the past decades has shed lights on resolving various biomedical problems such as poor drug bioavailability and enhanced absorption. However, the application of these

technologies is still not available in clinical practices. As such, chapter 1 reviewed the ocular structure and CNV while these advanced techniques are also reviewed.

Chapter 2 elucidates two common nanoparticle (NP) fabrication processes to synthesize polymeric NP (Mal-PEG-PLGA NPs) used in this work. The method for CPP conjugation on the surface of the NP is also presented. Furthermore, the chapter introduces standard analytical instruments for NP characterisation and PA modality used in this work.

Chapter 3 studies the feasibility of utilising PAI for monitoring CNV progression and treatment outcome using Metformin eye drops. This study investigates the possibility of PAI in detecting haemoglobin species that are only present in diseased cornea. This function is rarely seen in conventional clinical practice unless coupled with exogenous contrast agents. Moreover, data obtained using PAI may provide an objective quantification to reflect disease condition that the traditional technique fails to achieve. Thus, PAI may set up a new pathway to objectively monitor CNV disease progress and respect treatment outcome.

Ocular drug delivery has been a major obstacle for formulation scientists due to the protective nature of ocular tissues. Chapter 4, looks into the synthesis of R_8-conjugated PEG-PLGA NP through nanoprecipitation method. Different analytical techniques are employed to characterise and examine the size, zeta potential and drug encapsulation of R_8-PEG-PLGA NP. *In vitro* cell uptake experiment is also studied with R_8-PEG-PLGA/Rh. Finally, treatment efficacy is compared with free FK506, R_8-PEG-PLGA/FK506 and PEG-PLGA/FK506 using an experimental CNV model.

Chapter 5 will investigate the efficacy of a newly developed anti-angiogenic drug (KX2-4245) in CNV treatment. Prior to *in vivo* CNV model, an *in vitro* experiment was conducted to elucidate the cytotoxicity profile of KX2-4245. After determination of concentration, the drug will be tested in experimental *in vivo* CNV model and compared with an anti-VEGF drug. In addition, other drug concentrations will also be applied to the ocular surface to elucidate potential *in vivo* toxicity toward the corneal surface.

Chapter 6 will summarize the works in this thesis and present potential future direction of these techniques in the field of ophthalmology.

2 Methodology

This chapter will discuss nanoparticle surface modification method and the techniques utilised to examine and evaluate the chemical and physical properties of the nanoparticle produced.

2.1 Nanoparticle Surface Modification

Surface modification of polymeric nanoparticles can be achieved through electrostatic or covalent attachment. However, due to high stability and site selectivity, conjugation of cell-penetrating peptides onto the surface of the polymeric nanoparticles prefers using covalent attachment. The conjugation relies on the reaction between maleimide and thiol group as illustrated in Figure 2.1.

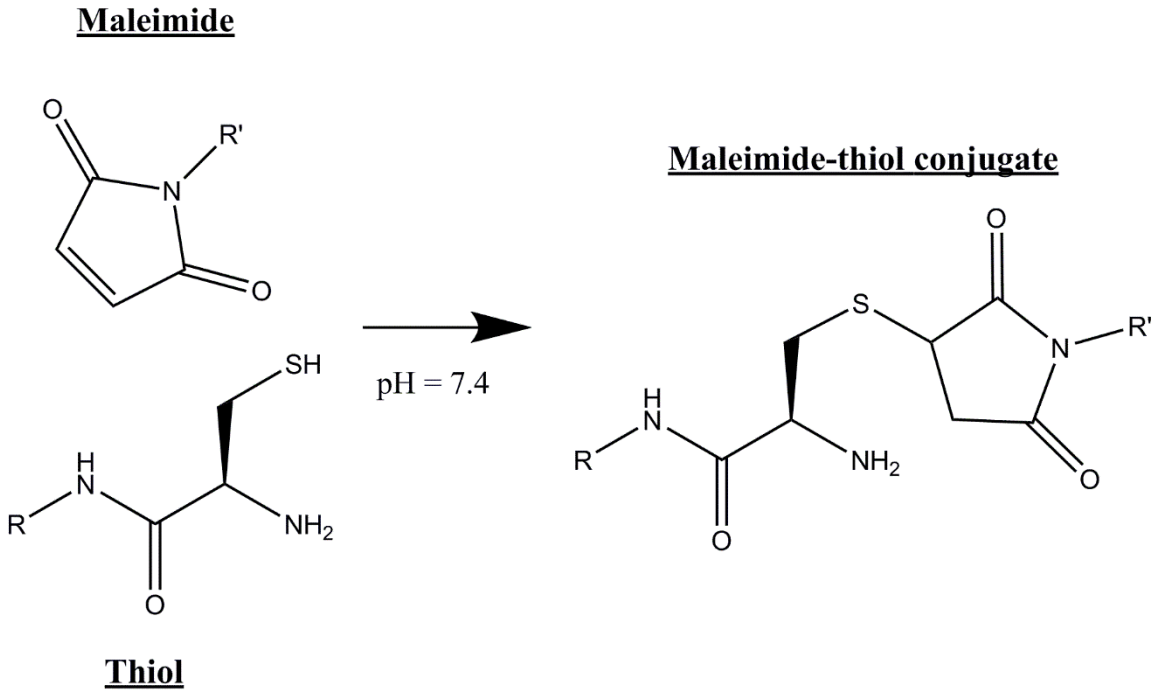

Figure 2.1 Conjugation of maleimide and thiol

2.2 Characterisation Techniques

2.2.1 Dynamic Light Scattering (DLS)

Dynamic Light Scattering (DLS) is a common spectroscopy technique for determining particle size distribution. The instrument equips a laser which emits monochromatic incident light that collides

into a solution containing particles in Brownian motion. The collision results a Rayleigh scattering pattern where size distribution can be obtained based on the particle size. As the scattering pattern correlates to the size of the particle and thus, size distribution can be acquired through a build-in mathematical algorithm. Briefly, polymeric nanoparticles were diluted with MilliQ water and subjected to a DLS instrument (Zetasizer Nano, Malvern Instruments Ltd.), as shown in Figure 2.2. Default settings were used to conduct each measurement and the settings were as follows: temperature: 25℃; equilibration time: 120 seconds; measurement angle: 173° Backscatter (NIBS default); number of measurements: 3.

Zeta potential was also measured with the same instrument. Electrophoresis is the motion of particle under the influence of an applied electric field. The interaction between the particle surface charge and applied electric field causes the particle to move with a medium. The particle movement direction and velocity are the function of the applied electric field, particle surface charge and the medium. The Doppler shift in the scatter light can provide information regarding the particle velocity. The particle velocity is proportional to the strength of the applied field and the particle electrical potential, therefore optical measurement can assist in the measurement of zeta potential. Default settings were used to measure zeta potential and the settings were as follow: temperature: 25℃; equilibration time: 120 seconds; measurement duration: automatic; number of measurements: 3.

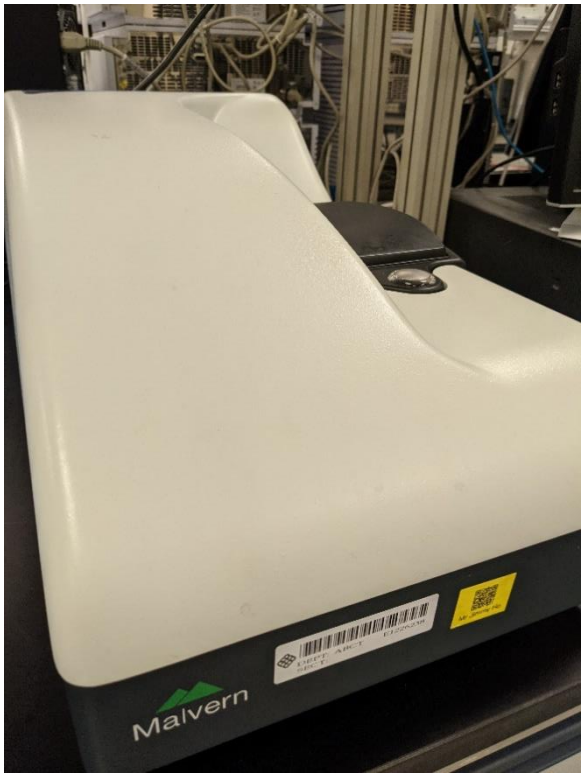

Figure 2.2 A photograph of Zetasizer Nano instrument for DLS measurement

2.2.2 Transmission Electron Microscopy (TEM)

Another technique commonly utilised to examine the morphology of nanoparticle is Transmission electron microscopy (TEM). A JEM-1210 (JEOL Ltd., Tokyo, Japan) was used to investigate the morphology and size of the polymeric nanoparticle. The system operated at 200 keV, giving off a high voltage electron beam that interacts with the sample on the carbon grid. Electron signals were generated upon interaction and, subsequently, collected to construct an image to reveal particle morphology as well as the size can be obtained. To perform TEM, a drop of polymeric nanoparticle solution is transferred onto a carbon grid and air-dried. Once dried, the sample grid is placed inside the TEM instrument for imaging procedures.

2.2.3 Fourier Transform Infrared Spectroscopy (FTIR)

Fourier-transform infrared (FTIR) spectroscopy is extensively employed to identify functional groups of a chemical compound. Each functional group has a distinct vibrational and stretching mode corresponding to a specific infrared (IR) energy; thus, the characteristic IR peaks could reflect the

groups within a compound. With the merit of this technique, it stands out as an easy and quick analytical method to verify successful conjugation. To prepare a sample for FTIR, analyte and dried potassium bromide (KBr) power were mixed and ground to produce a thin pellet. The KBr acts as a sample carrier in the IR measurement, and it is optically transparent in the wavenumber (4000 – 400 cm^{-1}). Therefore, avoid interference in IR absorbance. The pellet was quickly measured to avoid absorbing surrounding moisture, leading to an unwanted intense O-H stretching band. FTIR spectra of the samples were collected using NICOLET iS50 FT-IR (Thermo Scientific, USA) with an IR range of 500 – 4000 cm^{-1}.

Figure 2.3 A photograph of NICOLET iS50 FT-IR for structural characterisation

2.2.4 Ultra-performance Liquid Chromatography-Tandem Mass Spectrometry (UPLC-MS)

Ultra-performance liquid chromatography-tandem mass spectrometry (UPLC-MS) is an analytical technique to separate and determine chemical compounds within a sample. In this work, this

technique was employed to quantify the amount of drug encapsulated inside the polymeric nanoparticle. Agilent 1290 UPLC – Agilent 6460 electrospray ionisation triple quadrupole mass spectrometer equipped with a Zorbax Eclipse Plus C18 column (Agilent; 2.1x50mm; 1.8 μm) was used to determine the encapsulation content. The column temperature was maintained at 45°C, and the flow rate was set as 0.3 mL/min. The two predominant precursor ions produced were sodium adducts $[M+Na]^+$. The peak areas of the selected mass transitions were used for the quantification of FK506 (m/z 826.5→616.0) and ascomycin (m/z 814.5→604.2). Fragmentation of FK506 and ascomycin was set as 100 V and 160 V, while the collision energy for optimal fragmentation was 35 eV for both compounds.

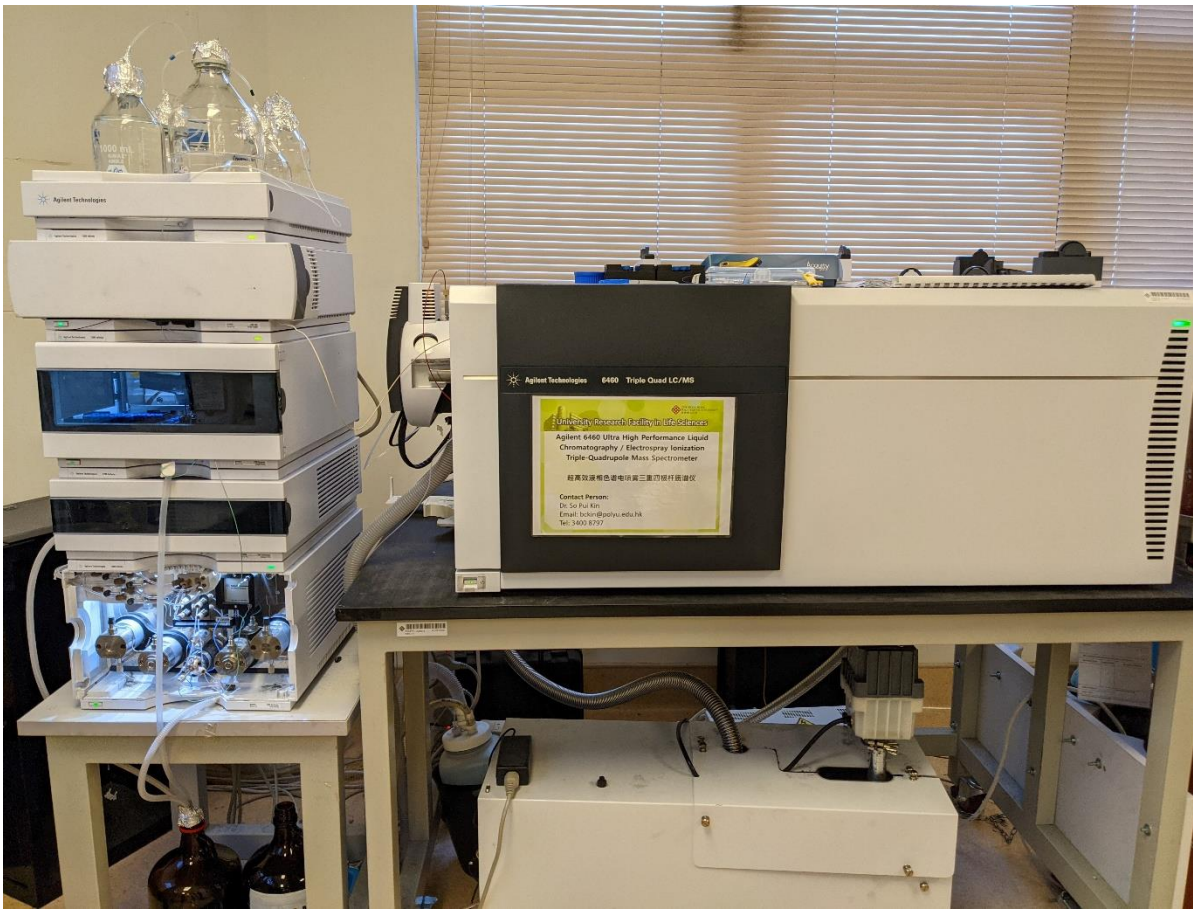

Figure 2.4 UPLC-MS for determination of drug loading and encapsulation efficiency

2.3 Photoacoustic Imaging (PAI) Instrument

The combination of ultrasound and photoacoustic imaging modality offers numerous opportunities to investigate various biomedical applications such as cardiology and vascular biology.

Furthermore, a PAI modality simultaneously captures ultrasound and photoacoustic images to provide anatomical and molecular information at a specific wavelength. With these advantages, the Vevo LAZR Photoacoustic Imaging System (FUJIFILM VisualSonics) was utilized to capture ultrasound and PA images of ocular tissues. Transducers LZ-250 (21 MHz) and MS-550D (32 MHz) were used to record ultrasound, PA signal and doppler signal. The resultant signals acquired were combined in one image for further analysis.

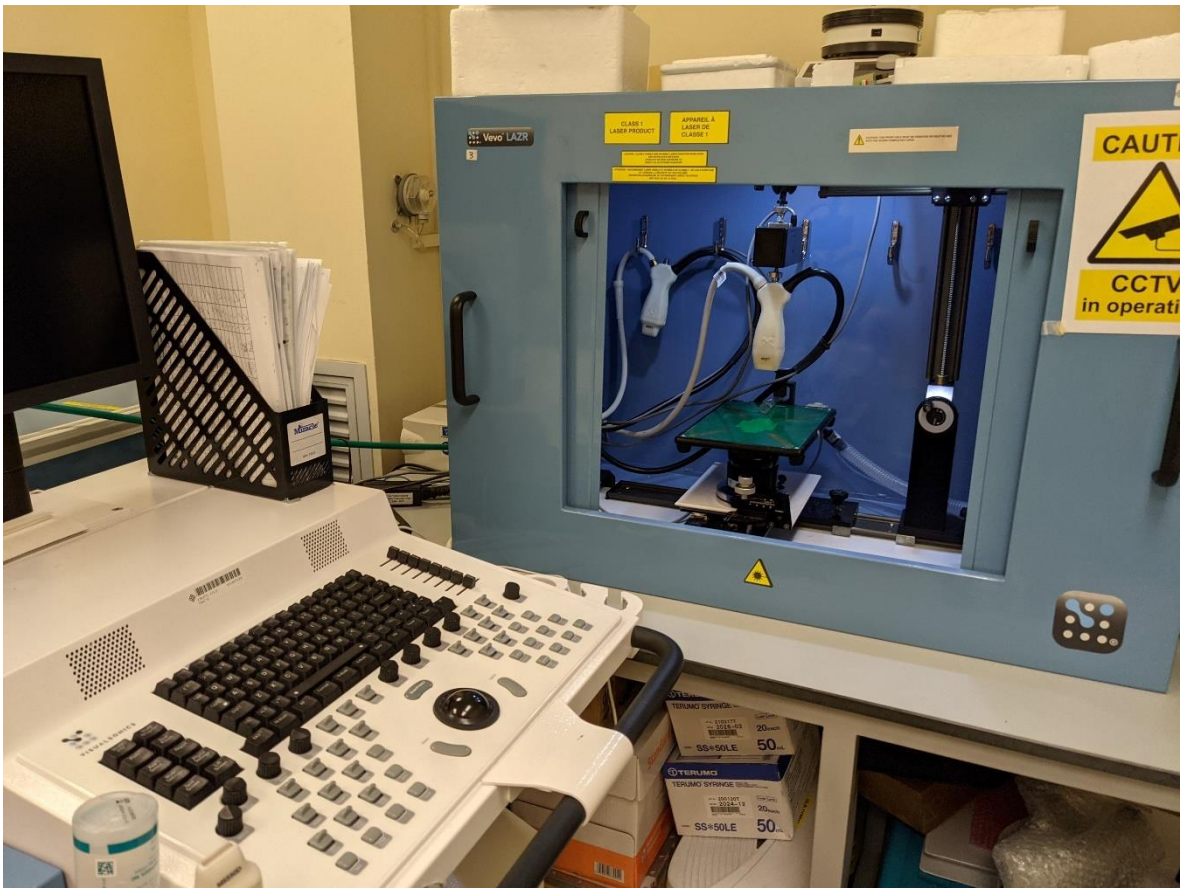

Figure 2.5 A photograph of FUJIFILM VisualSonics Vevo LAZR Multi-modality Imaging Platform

3 *In vivo* PA Imaging for Monitoring CNV Progression and Treatment Outcome with Metformin Eye Drops

3.1 Introduction

Accurate and objective examination techniques are crucial for monitoring ocular diseases. Corneal neovascularisation (CNV) is a sight-threatening ocular condition that could affect corneal transparency and visual acuity. A reliable ocular examination technique and treatment are vital to assist a physician to provide necessary treatment for an individual with ocular diseases. Traditional ocular examination often employs a slit-lamp and corneal angiography to access blood vessels on the diseased cornea. Although both equipment/techniques can provide the status of the cornea, these techniques come with certain disadvantages. A slit-lamp equipped with a digital camera can capture the condition of an ocular surface image during ocular examination and undergo computerised analysis. However, image analysis requires high image quality for further processing.[303] Furthermore, a computerised analysis could be subjective to a certain extent. Thus, it might not be able to deliver representable results. On the other hand, corneal angiography could reveal blood vessels on the cornea using of chemical dyes such as fluorescein or indocyanine green.[107,304,305] This technique can identify blood vessels even with corneal scaring which is generally difficult to visualise with slit-lamp examination. However, potential side effects associated with administration of chemical dyes must not be neglected. Patients with liver or renal dysfunction and those at risk of anaphylaxis must pay extra cation when receiving corneal angiography.[306] As a result, there is a need to establish a technique with non-invasive and objective nature for future ocular examination.

With the promising results demonstrated by preclinical and clinical PAI technique in various biomedical applications, it stands out as a promising technique for ocular examination.[307,308] It has been utilised to image ocular vasculature in recent studies with encouraging results.[231,309] However, studies mostly focused on vessel visualisation rather than haemoglobin and sO_2 quantification.

Metformin, an FDA-approved hypoglycemic agent, exhibits anti-angiogenic effects in different *in vitro* and *in vivo* experimental cancer models.[310–315] The anti-angiogenic property is also demonstrated

in various ophthalmic disease models such as choroidal neovascularisation, oxygen-induced retinopathy (OIR) and diabetic retinopathy (DR). However, these investigations utilise intraperitoneal injection or oral gavage as an administration method.[316–319] Thus, conventional ophthalmic drug administration routes with metformin are yet to be determined. Liu et al. recently reported the co-administration of metformin and levofloxacin using hydrogel through subconjunctival injection is effective in demolishing CNV.[320]

To this end, this study aims at investigating the following objectives with PAI and slit-lamp to (i) assess the efficacy of topically administered metformin against CNV, (ii) examine *in vivo* CNV model haemodynamic status, and (iii) quantify sO_2 levels in CNV.

3.2 Experimental Details

3.2.1 *In vivo* Alkali-induced Rat CNV Model

Health SD rats (n=24; Male; 200-300 g; Age 6-14 weeks) were employed in this investigation. Prior to all experimental procedures, general anaesthesia and corneal anaesthesia were induced by 3% isoflurane inhalation and tetracaine eye drop (Bausch & Lomb Pharmaceuticals, Inc). Additionally, topical administration of 1% tropicamide was given to the experimental eye for pupil dilation. Once the corneal surface numbness was achieved, a circular filter paper previously soaked in 1.0 M sodium hydroxide solution was placed on the central cornea under a microscope for 30 seconds. After removing the filter paper, the corneal surface was quickly rinsed with 10 mL of PBS.

Immediately after the rinse, rats were randomly divided into four groups (n = 6 per group) and received 50 µL of solution for 14 days. Topical administration of saline and metformin eye drops with different concentrations (4, 40 and 200 mg/mL) was given to the injured eye 4 times per day. Eyes were evaluated and examined by slit-lamp microscope on day 0 (pre-op), 4, 7 and 14. Corneal images were taken and analysed automatically with ImageJ software (Wayne Rasband, National Institutes of Health, USA). The corneal vascularised area was measured and presented as mean percentages ± SD.

3.2.2 *In vivo* PAI on Ocular CNV

Vevo LAZR Photoacoustic Imaging System (FUJIFILM VisualSonics) was utilized to capture B-mode ultrasound images, PAI and Doppler sonograph. The system is equipped with a tunable Nd:YAG laser system (OPOTEK Inc. 680-980 nm, 20Hz repetition rate, five ns pulse width, 50 mJ pulse peak energy) to imitate acquisition and excite tissue with optical pulses to generate the PA effect. The following parameters were used for this study: Transducer LZ-250, Frequency 21 MHz, Depth: 14.00 mm, Width: 23.04 mm, Wavelength: 750/850 nm, Threshold HbT: 20, Acquisition: sO2/HbT. A different transducer was employed to record Doppler sonography: Transducer MS-550D, Frequency 32 MHz, Pulse Repetition: 4 kHz, Depth: 10.00 mm, Width: 14.08 mm, Beam Angle: 0°, Sensitivity: 4, Wall Filter: Low. Photoacoustic/Doppler signals and ultrasound scans were acquired simultaneously and combined into one image in both transducer settings.

The animals were imaged at designated time points to acquire PA and doppler images for further analysis. Prior to imaging procedures, animals were anesthetised with inhalable anaesthetic and tetracaine eye drops. Once animals were anaesthetised and placed on a heated platform, a layer of ultrasound gel was applied over the cornea. Transducers were then carefully aligned and examined the cornea at 750 and 850 nm wavelengths to acquire HbR and HbO2 PA signals. Acquired data (haemodynamic data, sO2 and doppler signals) were then analysed with a built-in oxygenation-haemoglobin measurement package in workstation software (Vevo LAB, FUJIFILM VisualSonics, Toronto, Canada). Quantification of haemodynamic status, sO2 level and doppler signals were accomplished by tracing the cornea as the region of interest. The sO2 levels were calculated from pixels with an estimation of oxygen saturation, and resultant data were reported as average %sO2. The Doppler signals were treated in the same way as sO2, except the data were presented as percentage of vascularity.

3.2.3 Histological Analysis

At the end of the study period, all animals were euthanised, and ocular tissues were obtained for histological analysis. Immediately after enucleation, eyeballs were fixed in paraformaldehyde 4% solution and sectioned for H&E and CD31 analysis.

3.2.4 Statistical Analysis

All data were analysed with GraphPad Prism 5 (GraphPad Software Inc.) and expressed as mean ± standard deviation. Student's t-test and one-way ANOVA (for multiple group comparison) were performed with $*p < 0.05$ considered statistically significant, whereas ns represent no significance.

3.3 Results and Discussion

3.3.1 Metformin Eye Drops Exhibit Anti-angiogenic Effect and Reduce Experimental CNV

This work studied the feasibility of PAI as a tool for CNV progression and treatment outcome with metformin eye drops. PAI technique monitored and quantify the sO_2 to deliver an objective assessment of CNV and treatment outcome. Our data demonstrated that metformin 40 mg/mL was effective against CNV while PAI provide a non-invasive and objective analysis of the outcome.

3.3.1.1 Colour Images and Computerised Quantitative Analysis

In this study, a well-established alkali-induced CNV model was employed to investigate the therapeutic efficacy of metformin eye drops against experimental CNV. Topical administration is the most convenient and non-invasive route for ocular drug delivery.[238,243] Ocular absorption is generally hindered by the ocular anatomy and several other factors, and thus, we examined three different concentrations to probe the potential therapeutic range. The metformin concentrations employed in this study were 0, 4, 40 and 200 mg/mL which are designated as control, low, medium, and high concentration groups.

The representative colour images obtained with a slit-lamp revealed newly formed blood vessels in saline and metformin 4 mg/mL groups on day 4. The blood vessels continued to sprout and reach the central cornea on day 14 in the control and metformin 4 mg/mL group. Quantitative analysis demonstrated an increased vascularised area throughout the whole study period in both groups. The calculated mean vascularised area in saline group were 49.01 % ± 9.42, 51.52 % ± 10.91 and 68.52 % ± 9.69 on day 4, 7, and 14 respectively.

The metformin 4 mg/mL group also exhibited an increased vascularised area with mean area of 19.93 % ± 5.75, 35.89 % ± 2.96 and 48.28 % ± 11.55 on day 4, 7, and 14. Liu et al. demonstrated that subconjunctival injection of metformin 3 mg/mL and levofloxacin hydrochloride 3 mg/mL remarkably inhibited CNV formation.[320] In our study, the metformin 4 mg/mL did not show obvious angiogenic inhibitory effect compared with the study conducted by Liu's group. However, the severity and mean vascularised area of metformin 4 mg/mL was slightly lower compared with the saline group. This indicated that metformin has a certain degree of anti-angiogenic effect *via* topical administration.

Upon increasing the metformin concentration by 10 and 50 folds, the drug significantly inhibited angiogenesis, as shown in Figure 3.1. The groups exhibited a mild increase in newly formed blood vessels on day four and maintained low levels throughout the study. Quantitative analysis revealed that both groups demonstrated a similar vascularisation area with a mean of 12.72 % ± 5.47, 6.33 % ± 0.61 and 2.25 % ± 0.61 on day 4, 7, and 14, respectively. Table 3.1 summarised the vascularised area in rats received saline and metformin treatment.

Although quantitative analysis of the colour images provided information regarding the vascularised area, it cannot offer any molecular insight of CNV progression. Moreover, the natural dome shape of the cornea poses difficulties in focusing and capturing all vessels in one single image.[321] Furthermore, scarring and oedema on cornea after injury also hamper blood vessel visualisation from colour images.[304] Therefore, the quantitative results derived from colour images pose a dilemma on reflecting the actual corneal condition.

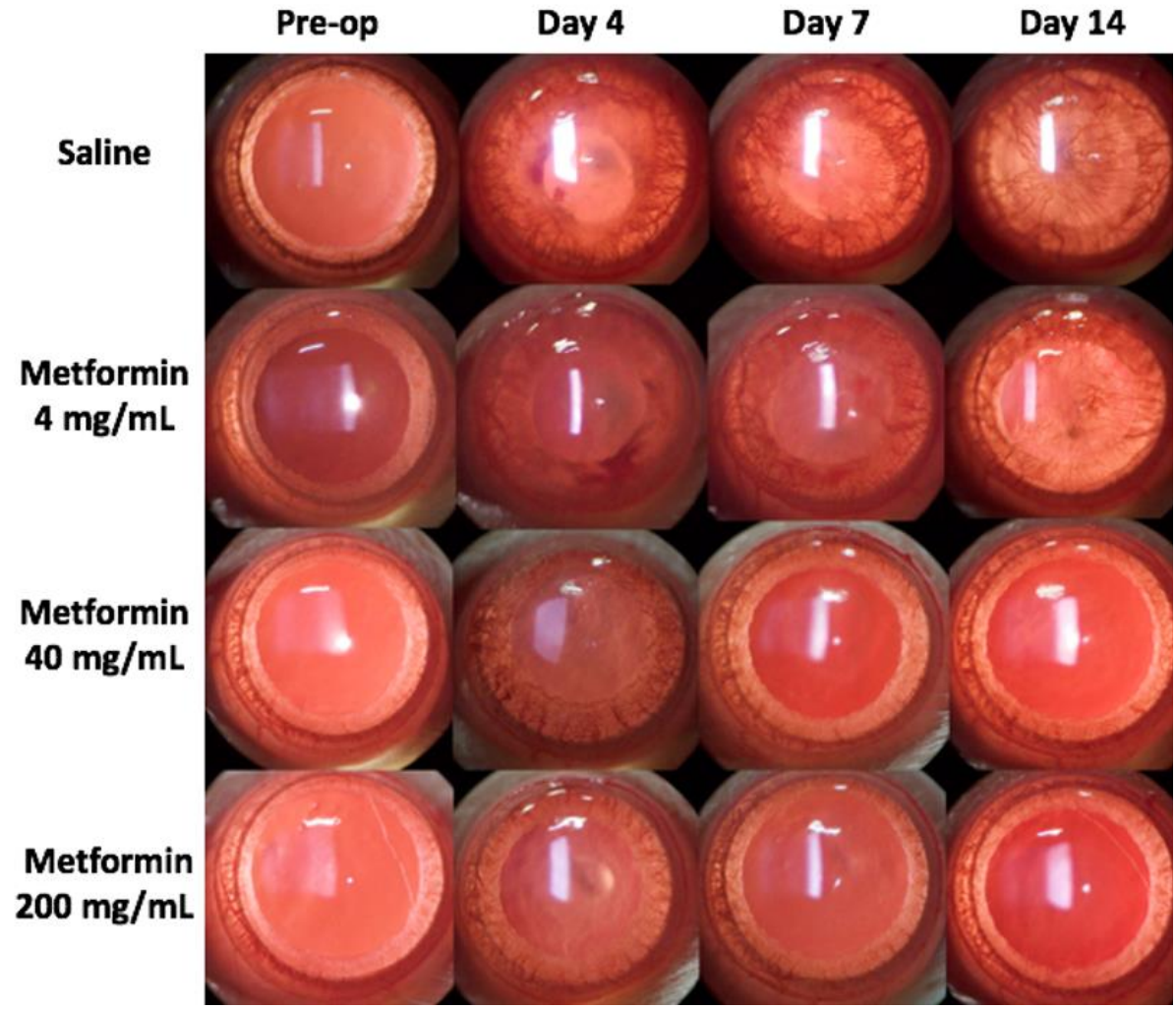

Figure 3.1 Slit-lamp images of rat's cornea after metformin treatment for CNV

Pre- and post-treatment images with control and metformin groups (0 - 200 mg/mL)

	Average % vascularised area		
	Day 4	**Day 7**	**Day 14**
Saline	49.01 ± 9.42	51.52 ± 10.91	68.52 ± 9.69
Metformin 4 mg/mL	19.93 ± 5.75	35.89 ± 2.96	48.28 ± 11.55
Metformin 40 mg/mL	12.25 ± 5.14	6.68 ± 0.68	2.76 ± 0.98
Metformin 200 mg/mL	13.19 ± 5.79	5.98 ± 0.54	1.73 ± 0.23

Table 3.1 Average % vascularised area in rat's cornea received saline and metformin treatment

The unique anatomical barrier of the cornea, tear film, and other factors all contribute to poor bioavailability. Nature defence mechanisms such as tear turnover, reflex blinking and drainage leads to significant drug loss upon administration, with only 5% of topically applied drug being absorbed.[322] Therefore, frequent instillation and higher dosage are needed to overcome the poor bioavailability issues. In this work, our data indicated that metformin 40 mg/mL is the optimal concentration for CNV treatment. Concentration higher than 40 mg/mL does not seem to provide additional benefits or treatment effects. The increased concentration compensates for the poor bioavailability and thus, exhibits an anti-angiogenic effect for CNV treatment. Although colour images can provide quick assessment on CNV and treatment progression, it fails to give an objective and comprehensive information of molecular species presented in the cornea. Therefore, a technique that provide objective assessment and ability to monitor haemoglobin species would be beneficial to CNV assessment.

3.3.1.2 Histological Analysis

The CNV inhibitory effect of metformin was investigated and confirmed with histological analysis using H&E and CD31 staining (Figure 3.2). The neo-vessels were detected in saline and metformin 4 mg/mL, while no apparent vessels can be recognised in metformin 40 mg/mL and 200 mg/mL. The CD31 staining also confirmed the anti-angiogenic effect of topically applied metformin. Strong CD31 immuno-reactivity was observed in saline and metformin 4 mg/mL groups as compared with metformin 40 mg/mL and 200 mg/mL. Therefore, these results indicated metformin is capable of inhibiting CNV through topical administration at an optimal concentration of 40 mg/mL.

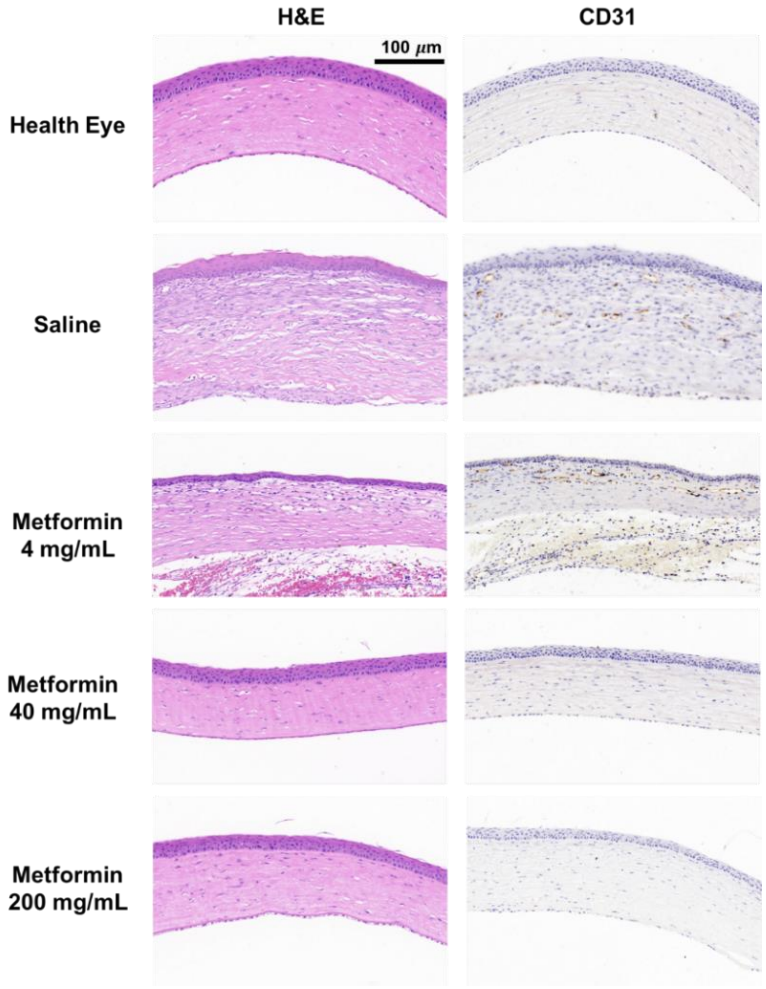

Figure 3.2 Histopathological images of rat's cornea after metformin treatment

H&E (left) and CD31 (right) images revealed the treatment effect of metformin eye drops with different concentrations on Day 14 (scale bar 100 μm for H&E and CD31)

3.3.1.3 Anti-angiogenic and Anti-inflammatory Effect of Metformin

Though this study did not investigate the underlying mechanism, numerous studies have demonstrated the anti-angiogenic effects of metformin. Experimental data suggested that metformin is capable of reducing and inhibiting VEGF receptor Flk-1 level, activin receptor-like kinase 1 (ALK-1) expression as well as protein translation of VEGF-A in various ocular disease models.[316–318] Moreover, metformin exhibits anti-inflammatory ability and reduces inflammatory cytokines such as monocyte chemotactic protein-1 (MCP-1) and interleukin-6 (IL-6).[319] Overall, our data demonstrated that topical administration 40 mg/mL of metformin is an effective agent for CNV treatment.

3.3.2 Monitor Change of Corneal Haemodynamic Status with PAI Technique

Conventional ocular examination technique with slit-lamp provides a general condition of the ocular surface. However, it fails to detect molecular information during a diseased state. The use of PAI offers molecular information of CNV without using an exogenous contrast agent. After CNV induction, the presence of haemoglobin species within the blood vessels acts as a natural endogenous contrast agent for imaging purposes. We employed PAI to record and explore the change of HbR and HbO_2 content in the cornea, which is achieved by monitoring two different wavelengths: 750 and 850 nm.

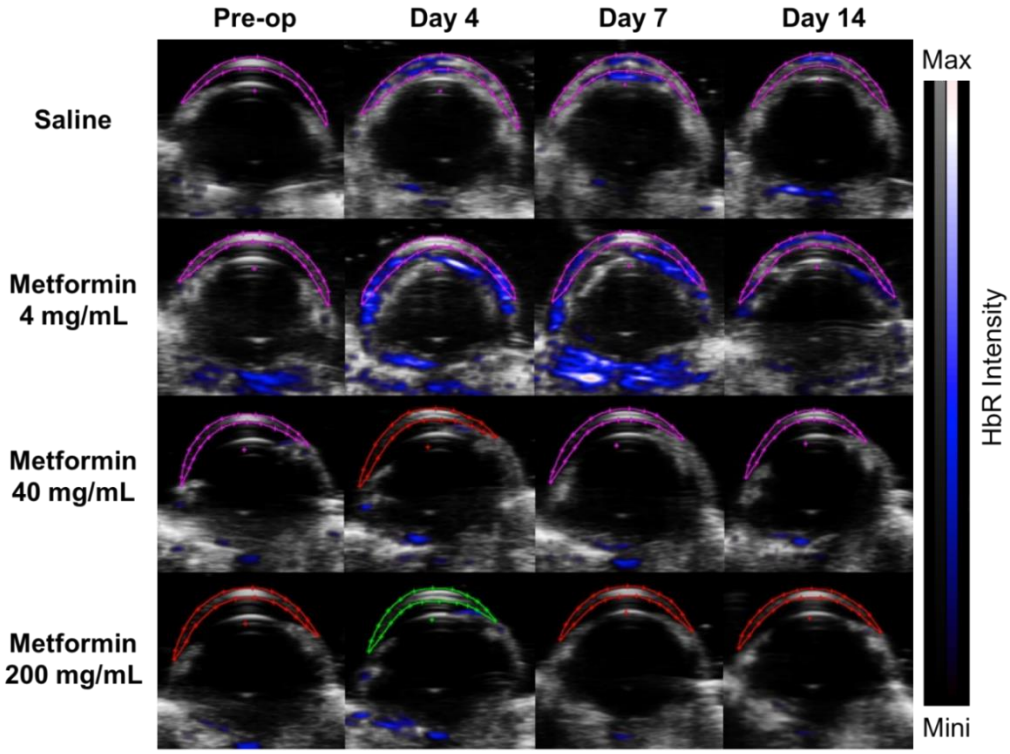

Figure 3.3 Co-registered PA and ultrasound images of HbR status over the study period

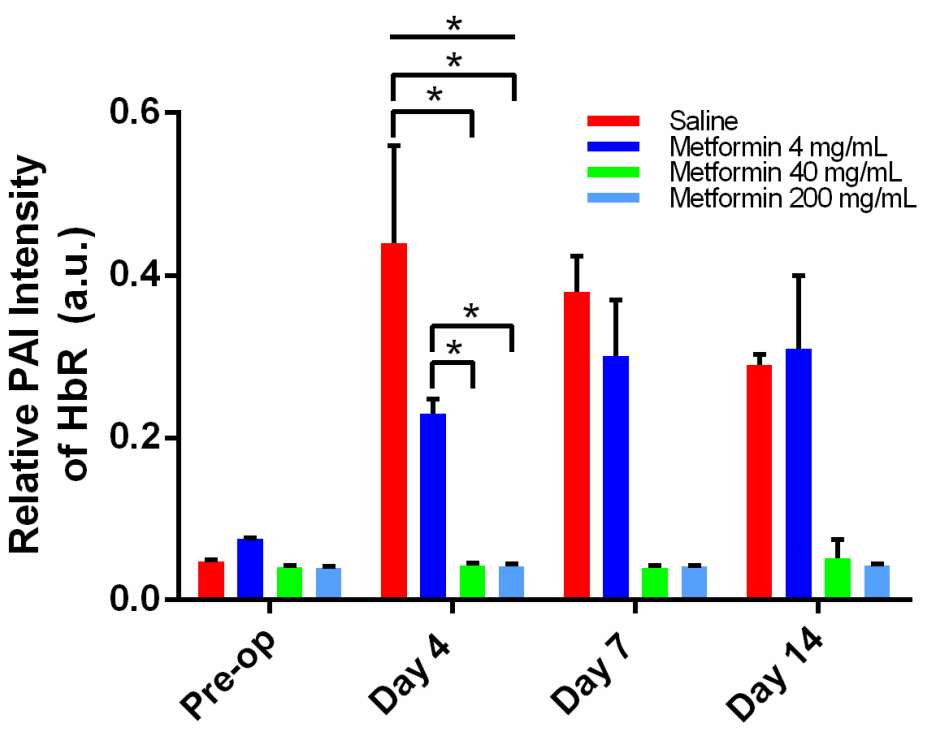

Figure 3.4 Quantitative analysis of PA intensity in HbR signals over the study course *$p < 0.05$

Before the induction of alkali injury, all animals showed low baseline PAI signal value in the cornea. After the alkali injury, a significant increase in HbO_2 and HbR PAI signal was recorded and observed in the saline and metformin 4 mg/mL group (Figure 3.3). Quantitative analysis (Figure 3.4) of saline group revealed an 8.80-fold increase in HbR signal (0.44 ± 0.12) compared to the baseline value of (0.05 ± 0.0013) on day 4. The HbR signal regressed slightly on day 7 and day 14 with values of (0.38 ± 0.044) and 14 (0.29 ± 0.013), respectively. A considerable amount of increase in HbO_2 content (Figure 3.5 and Figure 3.6) was also detected in the saline group with an 8.97-fold increase (0.61 ± 0.14) on day 4. The HbO_2 signal remained at a similar value (0.65 ± 0.022) on day 7 and showed a slight regression (0.54 ± 0.037) on day 14. The significant increase in HbR and HbO_2 PAI signal all points to the formation of new blood vessels on cornea after alkali injury.

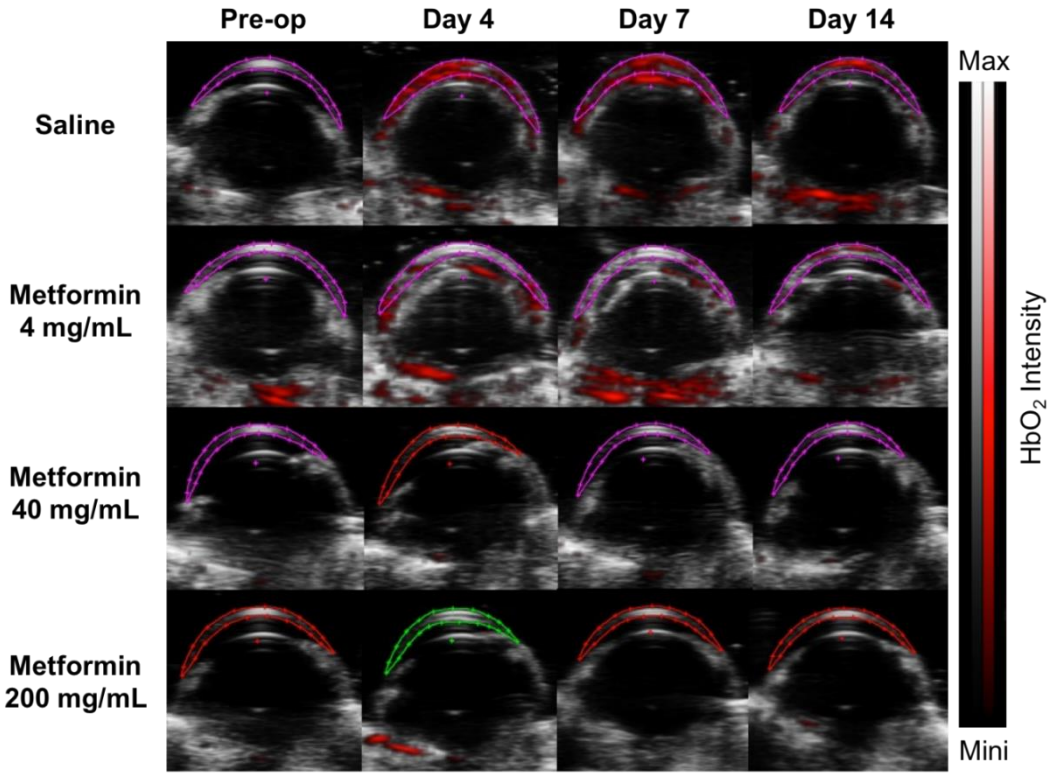

Figure 3.5 Co-registered PA and ultrasound images of HbO_2 status over the study period

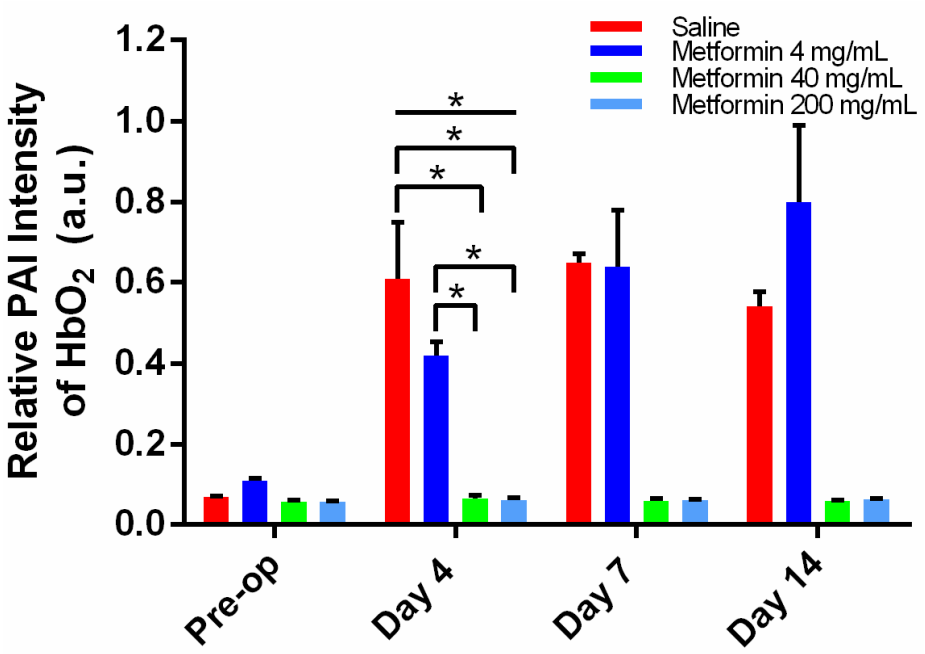

Figure 3.6 Quantitative analysis of PA intensity in HbO_2 signals over the study course $*p < 0.05$

The animals that received metformin 4 mg/mL also exhibited increased patterns in HbR and HbO_2 signals. The HbR signal showed a 3.07-fold increase (0.23 ± 0.018) on day 4 compared with the baseline value of (0.075 ± 0.0016). On day 7 and 14, the HbR signal remained at similar value of (0.30 ± 0.07) and (0.31 ± 0.09) respectively. However, the recorded HbO_2 values were much higher than the HbR and showed a 3.8-fold increase (0.42 ± 0.034) on day 4 compared to the baseline value (0.11 ± 0.0046). However, the HbO_2 of the metformin 4 mg/mL group exhibited an increased trend on day 7 and day 14 with values of 0.64 ± 0.14 and 0.8 ± 0.19. Overall, the signal of HbR and HbO_2 were lower than the saline group. This indicated that the metformin 4 mg/mL exerted a certain degree of anti-angiogenic effect on alkali-injured rat cornea. The incompetence to achieve full inhibitory effect is properly related to the high amount of drug lost upon the topical administration of 4 mg/mL of metformin.

In contrast, the metformin 40 mg/mL and 200 mg/mL groups maintained similar corneal HbR and HbO_2 baseline values throughout the study course. Thus, indicating higher concentration was required to achieve CNV inhibitory effect. Moreover, these data indicated that PAI possesses the ability to detect and measure molecular species within the cornea, which conventional examination techniques fail to achieve.

3.3.3 Monitor Change of sO_2 with PAI Technique

With the capability of PAI technique to measure and quantify haemoglobin species, we next measured the sO_2 status using a built-in mode to examine the non-invasive corneal oxygen saturation throughout the study period. All sO_2 data are presented as average value. Instead of examining two haemoglobin species separately, the sO_2 data offers a more direct and clear indication of angiogenesis as it considers both haemoglobin species. Thus, it gives a more comprehensive condition of corneal haemodynamic status. A healthy cornea is avascular in order to provide optimal vision, whereas a vascularised cornea shall obstruct vision. Thus, this results in an elevation of $\%sO_2$. Figure 3.7 shows the co-registered US and PA images of the changes in $\%sO_2$ over time. The saline and metformin 4 mg/mL groups exhibited a notable rise in sO2 level during the course of study, as revealed by

quantitative analysis (Figure 3.8). On day 4 and 7, the average $\%sO_2$ of saline reached 46.82% $\pm$ 6.12 and 51.04% $\pm$ 1.97, respectively. The average $\%sO_2$ regressed slightly on day 14 with value of 40.09% $\pm$ 5.71. The metformin 4 mg/mL revealed a same pattern as saline group where the average $\%sO_2$ values were 24.07% $\pm$ 5.22, 57.47% $\pm$ 6.9 and 45.47% $\pm$ 7.40 on day 4, 7 and 14. Upon increasing the concentration to 40 mg/mL and 200 mg/mL, quantitative analysis revealed a subtle increase on day 4

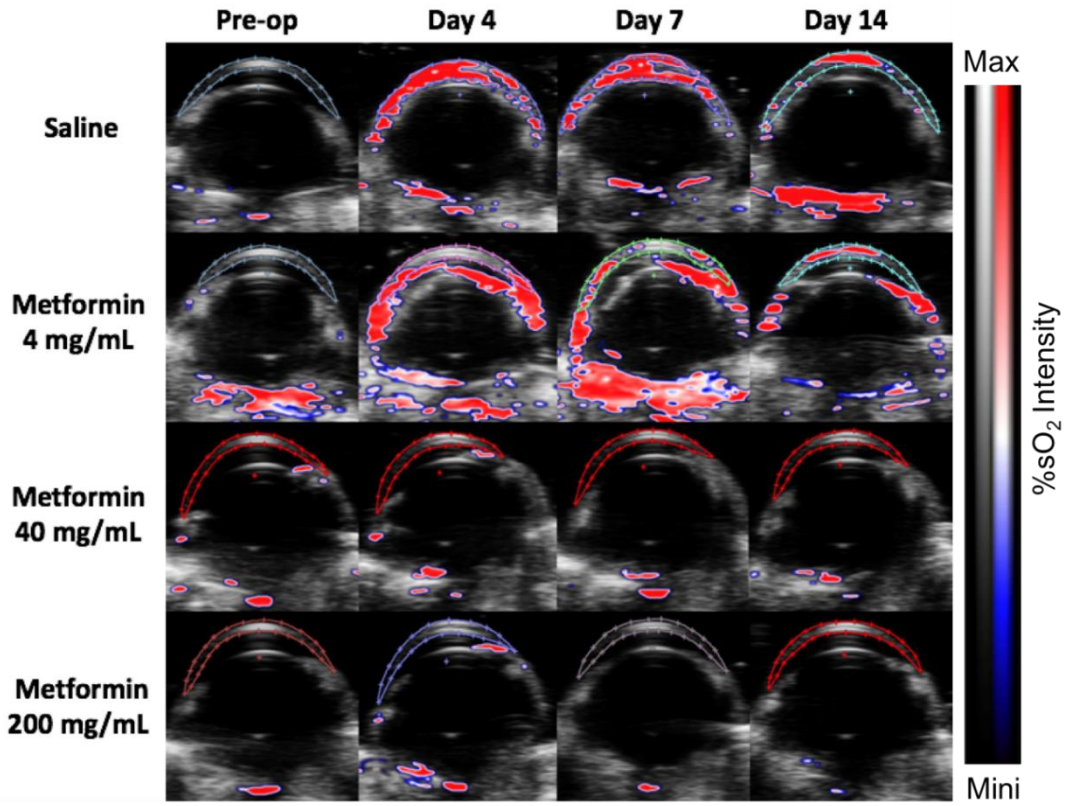

Figure 3.7 Co-registered PA and ultrasound images of pre- and post-corneal $\%sO_2$ after metformin treatment

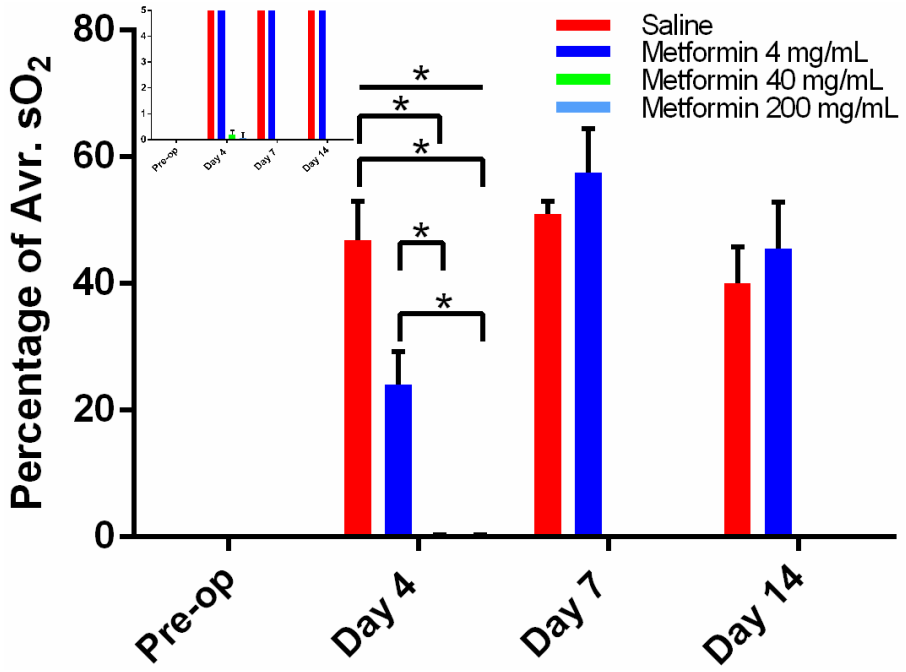

Figure 3.8 Quantitative analysis of pre- and post-treatment $\%sO_2$ with different concentrations of metformin eye drop $*p < 0.05$

with average $\%sO_2$ value of only $0.21\% \pm 0.15$ and $0.08\% \pm 0.20$ individually. The average %sO2 returned to the pre-op level on day 7 and 14. These data indicated that metformin effectively inhibits CNV progression with an optimal concentration of 40 mg/mL.

The average $\%sO_2$ data is complementary with data obtained in haemodynamic status, the colour image analysis and the severity of CNV observed. Hence, this demonstrated $\%sO_2$ is capable of providing a new path in assessing and monitoring CNV progression and treatment outcome through natural endogenous contrast agents.

The PAI technique demonstrated in the above data revealed it possesses unique advantages over fluorescent angiography as it does not involve the intravenous injection of chemical dyes. The natural endogenous contrast agents (HbR and HbO_2) only exist during CNV status. Hence, it avoids the potential interference signal from other the surroundings. Furthermore, the PAI technique does not require exogeneous contrast agents, thus is free of any potential side effects associated with chemical dyes. In addition, PAI reveals molecular information that slit-lamp fails to achieve. Therefore, this technique stands out as a promising imaging modality for additional ocular examination in the future.

3.3.4 Doppler Sonography of CNV

Doppler sonography is a useful US technique to examine superficial tissues and provide information regarding the blood flow. In this part of the experiment, we utilised the power Doppler mode to investigate the percentage of vascularity within the cornea. The percentage of vascularity increased in the saline and metformin 4 mg/mL groups, as shown in Figure 3.9. The saline group revealed a continued increase in the percentage of vascularity with values of 4.24% $\pm$ 0.38 and 15.95% $\pm$ 0.51 on day 4 and 7, respectively (Figure 3.10). The percentage of vascularity exhibited a reduction on day 14 (11.85% $\pm$ 1.6). However, the metformin 4 mg/mL group exhibited a continuous increase in signal with value of 3.73% $\pm$ 0.73, 9.12% $\pm$ 2.32 and 12.41% $\pm$ 1.47 on day 4, 7 and 14. The percentage of vascularity in the remaining testing concentration groups maintained a pre-op level even after CNV induction, except for a slight increase in Doppler signal that was recorded on day 4 in metformin 40 mg/mL. It is worth noting that the data in the percentage of vascularity exhibited much a smaller value compared to haemodynamic status and average $\%sO_2$. This is because of the transducer used in the experiment. We employed a different transducer to obtain high-resolution images. However, the transducer's size could not cover the whole cornea, which only allowed recording of part of the vascularised area. Despite this problem, the percentage of vascularity agreed with the $\%sO_2$ data. Both Doppler sonography and $\%sO_2$ demonstrated an increasing trend in saline and metformin 4 mg/mL, indicating CNV progression and ineffectiveness in suppressing CNV with 4 mg/mL.

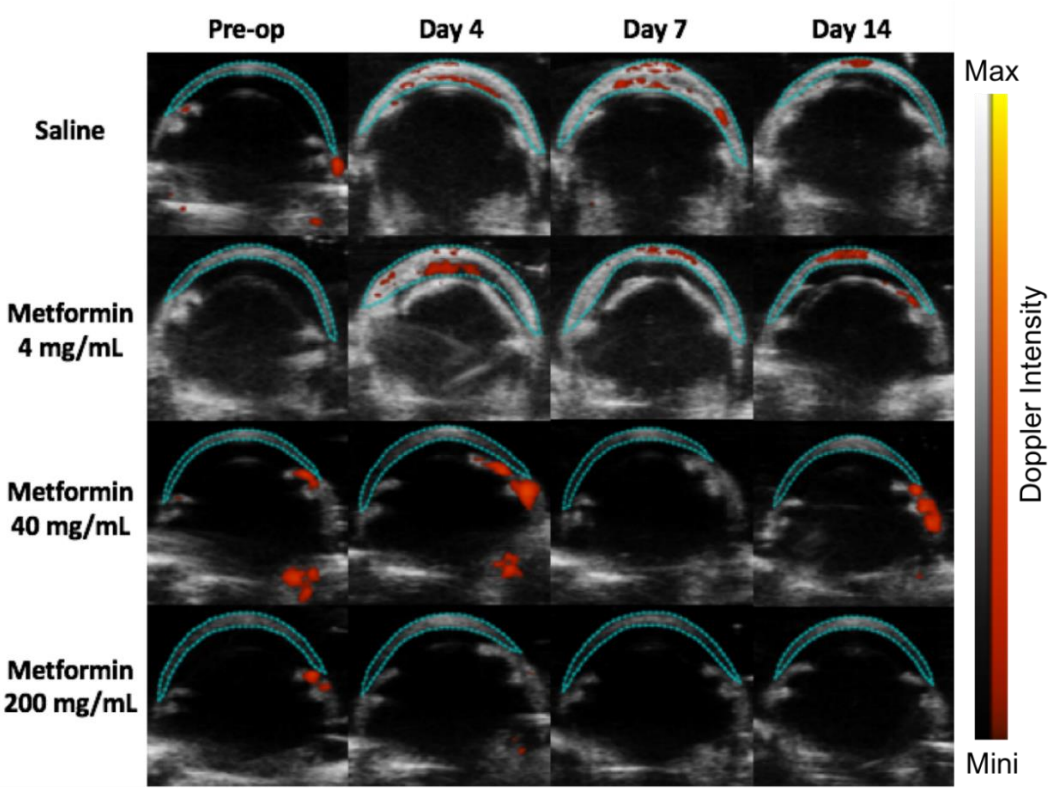

Figure 3.9 Co-registered Doppler and ultrasound images for blood vascularity before and after metformin eye drop treatment

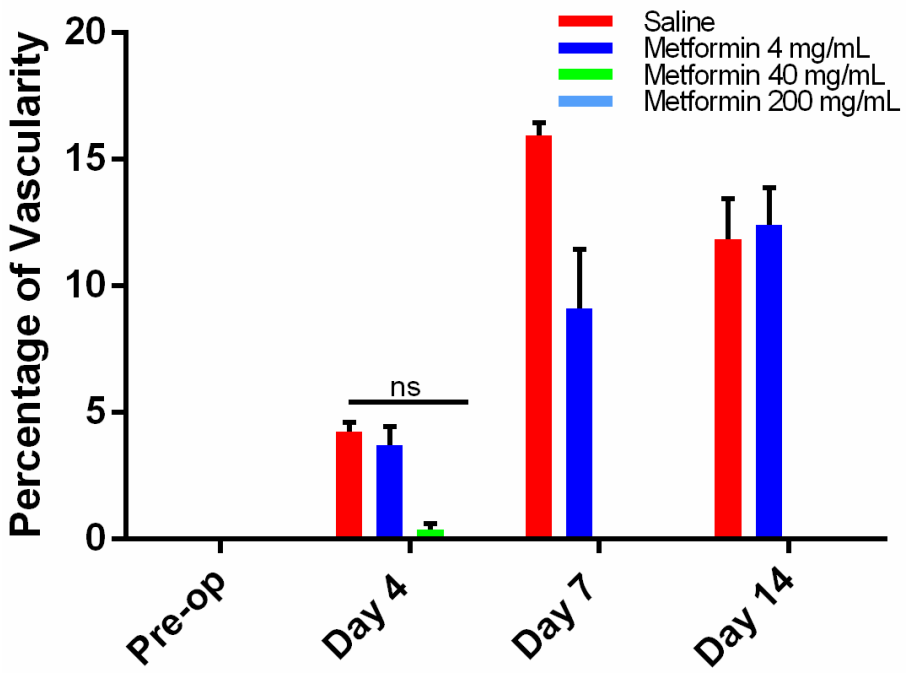

Figure 3.10 Quantitative analysis of pre- and post-treatment Doppler signals with different concentrations of metformin eye drop (ns: not significant)

3.4 Conclusion

In summary, this work utilised PAI to investigate the haemodynamic status, average $\%sO_2$ and Doppler sonography for CNV progression and treatment efficacy of topically applied metformin. Our data suggested that the optimal concentration of metformin to inhibit CNV progression is 40 mg/mL. Coupled with slit-lamp and PAI, the two provide a comprehensive status of CNV through colour image analysis as well as corneal sO_2 information derived from haemoglobin species present during the disease state. Not only PAI could offer molecular information, it also serves as a valuable tool for assessing treatment outcome and exhibit promising potential for monitoring the ocular condition. Corneal transplantation has a high risk of post-transplant blood vessel growth. Thus, monitoring blood vessels with the level of sO_2 through PAI is potentially a promising way for post-operative analysis. Overall, PAI provides a non-invasive and label-free approach for longitudinal ocular examination.

4 Enhanced Ocular Delivery with Cell-Penetrating Peptide-Conjugated Polymer Nanoparticle for CNV Treatment Coupled with PAI as a Tool for Disease Monitoring

4.1 Introduction

Ocular drug delivery has been an enormous challenge over the past decades owing to the unique ocular anatomy, which radically eliminates the passage of foreign materials, leading to poor treatment efficacy *via* topical administration. Corneal neovascularisation (CNV) is a sight-threatening condition that could result in a decline in visual acuity and total vision loss.[155] Statistics revealed that corneal diseases is a major cause of blindness worldwide, with more than 10 million patients requiring corneal keratoplasty to regain vision.[323,324] Among all conventional administration methods, topical administration is the most preferred method for ocular disease treatment owing to its non-invasive nature. However, topically applied drugs suffer from poor bioavailability[238] as the unique and complex anatomy of eye constrains and impedes the penetration of the applied drug into the anterior and posterior segment.[239] Apart from such complexation, tear film and physiological barriers (e.g. reflex blinking, nasolacrimal drainage and lacrimation rate) also prevent drug absorption. Furthermore, the high turnover rate and mucus layer of tear prevent topically administered drugs from entering the eye and dilute the concentration of those that could pass. Thus, the tear film and its components act as a comprehensive defence barrier and pose tremendous problems for topical administration.[325] With these barriers, up to 95% of topically administered drugs are lost upon administration.[240] Therefore, eye drop formulation requires frequent instillations in order to sustain and provide an efficacious treatment outcome.

Nanoparticle (NP)-based drug delivery system has caught massive attention over the past decades due to its enhanced permeability and retention (EPR) effect observed in the research on cancer nanomedicine.[326] Numerous researchers have spent tremendous efforts enhancing ocular drug delivery through NP-based delivery systems. The use of nanocarrier system has been shown to overcome limitations associated with conventional ocular drug administration method. Moreover, the system can

also feature targeted and control released properties to maximise drug availability.[250,251] Different delivery systems have been widely investigated for their efficacy and ability to deliver drugs. Example of these include but are not limited to liposomes and polymeric NPs. Polymeric NPs, particularly those made with biodegradable materials, hold promising features as an outstanding drug delivery carrier for macromolecular drugs. Hence, biodegradable polymeric NPs as delivery vehicles have few advantages over other drug delivery systems.[327,328] First, polymeric NPs protect encapsulated protein-related pharmaceutical compounds from *in vivo* chemical and enzymatic degradation, which increases their half-life.[329–331] Second, nanoscale particles could facilitate and overcome obstacles associated with physiological barriers (e.g. cell membrane and blood-brain barrier).[332–335] Third, polymeric NPs possess sustained and controlled release properties which conventional administration method do not.[331,336–338] Finally, surface modification can empower NPs to target a specific type of organ/tissue/cells while reducing undesired side effects and the frequency of administration.[339–341]

Poly(lactic-co-glycolic acid), also known as PLGA, is a biocompatible and biodegradable material produced from lactic acid and glycolic acid, which undergoes dehydration and cyclisation follows by ring-opening polymerisation.[342] The PLGA material has a long history of being utilised as sutures in clinical settings. It undergoes degradation and metabolises naturally to give its constituent monomers, which can be absorbed by the body and thus exhibiting good biocompatibility, tunable degradation rate and safety profile.[343,344] With its excellent physical properties, PLGA is approved by the FDA to be used as a drug carrier as well as scaffolds in tissue engineering.[260,338,345,346] Over 15 FDA-approved drugs have utilised and incorporated PLGA, indicating its effectiveness and reliability as a drug carrier.[347,348] Apart from its utilisation in FDA-approved medication, attempts have been made in the past to encapsulate various biological compounds to strengthen their efficacy in experimental disease models. Encapsulated drugs include insulin, bevacizumab, plasmid DNA and cyclosporine A.[349–351] In summary, formulations with polymeric NPs exhibit great potential in biomedical application as an effective drug carrier to enhance various chemical and physical parameters.

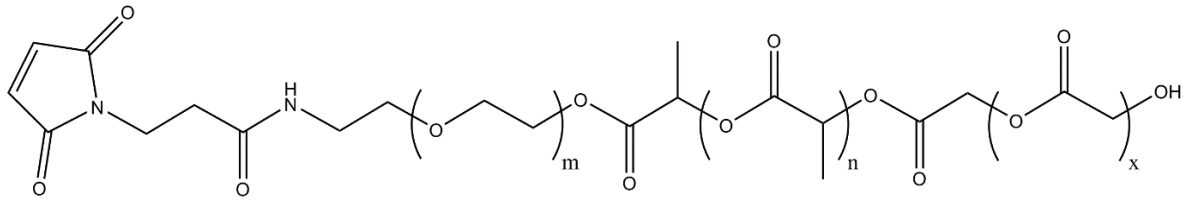

Figure 4.1 Diblock copolymer *m*aleimide-poly(ethylene glycol)-poly(Lactide-co-glycolide) (Mal-PEG-PLGA)

NPs show excellent capability as drug carrier and has been widely employed as a valuable tool to enhance the pharmacokinetic properties of pharmaceutical components. While nano-formulations provide excellent competency in biomedical science, surface modification with cell-penetrating peptides (CPPs) further strengthens intracellular drug delivery properties. Cationic CPPs are small peptides that generally contain 5 to 30 amino acid residues and consist of mostly basic amino acid residues. As a result, CPPs possess an overall positive charge.[352] CPPs can act as a versatile tool for improving the effectiveness of drug delivery because of their high permeability and ability to translocate into a wide variety of cells, as well as possessing low cytotoxicity with no immunogenicity.[353] With these advantageous characteristics, CPP-conjugated NP (CPP-NP) has been developed and investigated in the field of biomedicine and biomedical aspects.

The first CPP discovered was the transactivator protein (Tat 48 - 60) derived from human deficiency virus type 1 (HIV-1) back in 1988.[354] Since then, many other CPPs have been identified and added to the CPP family. Depending on the amino acid sequences, CPP can be divided into cationic, amphipathic and hydrophobic. Poly-arginine peptides falls into the category of cationic CPP due to its high content of basic arginine amino acid. Poly-arginine peptides with arginine amino acid sequence lengths of 5 to 9 are frequently employed to facilitate transportation of nucleic acids or proteins.[355] The structure of octa-arginine peptide is shown in Figure 4.2.

The CPP-NP conjugates present excellent results in a broad spectrum of disease treatments as well as serving as imaging probes. With the enhanced therapeutic efficacy and permeability, CPP-NP has been used to treat dermatological disorders, central nervous system disorders, cancers and as an

advanced imaging probe.[356–359] Recently, our group has successfully conjugated iRGD peptide to PEG-PLGA NPs to enhance accumulation while delivering hydrophobic organic dyes to act as a contrast agent for PA imaging as well as photothermal therapy (PTT) for cancer treatment.[360] The peptide-conjugated NPs were revealed to have a longer circulation time and accumulation profile than non-conjugated NPs. These results indicated the advantageous property of peptide-conjugated nanoparticles for biomedical applications and provided further evidence of enhanced permeation through smart surface decoration.

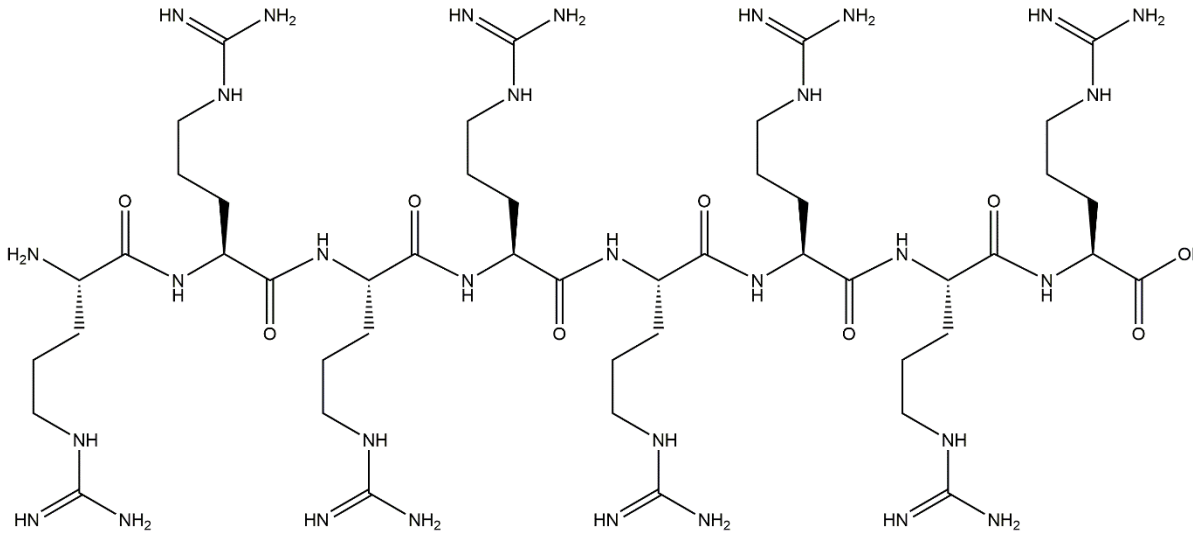

Figure 4.2 Structure of octa-arginine (R_8)

Tacrolimus (FK506) is a powerful immunosuppressive agent that can prevent allograft rejection and is often prescribed to patients who have undergone heart, liver and kidney transplantation. FK506 is a 23-membered macrolide lactone antibiotic (molecular weight 804 g/mol) with 100-fold effectiveness than cyclosporine A, another well-known immunosuppressant.[361–363] FK506 has been shown to be effective in corneal allograft rejection through topical administration and subconjunctival injection.[364–367] However, the lipophilicity of FK506 hinders its utility to a certain extent as the cornea generally favours hydrophilic molecules rather than lipophilic drugs. Therefore, frequent administration or a higher drug concentration is needed which might lead to undesired side effects and poor patient compliance.[368] Thus, encapsulating FK506 in CPP-conjugated polymeric nanoparticles might serve as a promising approach to over the corneal barriers as well as its physical characteristic.

In this study, an experimental CNV model was employed to investigate and evaluate the treatment efficacy of octa-arginine peptide (R_8)-conjugated PEG-PLGA/FK506 NP, with the aim to achieve the following objectives: (i) to compare the treatment efficacy of cysteine-modified octa-arginine peptide (CR_8)-conjugated FK506-encapsulated PEG-PLGA NPs (R_8-PEG-PLGA/FK506 NPs) and non-conjugated NP (PEG-PLGA/FK506 NPs) under topical administration, (ii) to evaluate the treatment efficacy by topical administration twice per day, (iii) to examine the *in vitro* cellular uptake of R_8-PEG-PLGA NP vs non-conjugated NP with fluorescence microscopy and (iv) to evaluate the *in vivo* haemodynamic status and quantify the sO_2 level with PAI.

4.2 Materials and Methods

4.2.1 Materials

Tacrolimus (FK506) and Ascomycin (FK520) were purchased from MedChemExpress. Diblock copolymer Maleimide-poly(ethylene glycol)-poly(Lactide-co-glycolide) (Mal-PEG-PLGA), MW of PEG to PLGA 2000: 15000, molar ratio of lactide to glycolide 75:25, MW= 15000 Da) (PEG-PLGA 75:25) was purchased from Shanghai ToYongBio Tech. Inc (Shanghai, China). Cysteine modified octa-arginine peptide (CR_8) and cysteine were purchased from ChinaPeptide Co., Ltd (Shanghai, China) and Sigma-Aldrich. Rhodamine (Rh) was purchased from Thermo Scientific for cellular uptake experiment. Solvents for nanoparticle synthesis were purchased from Sigma-Aldrich. Methanol (HPLC grade, 99.9%), acetone, ethyl acetate, dichloromethane (DCM) and chloroform were used without further purification. Amicon® ultra centrifugation filters (MWCO 100 kDa) were purchased from Merch Millipore, United States.

4.2.2 Preparation of R_8-PEG-PLGA/FK506 and R_8-PEG-PLGA/Rh NPs with Nanoprecipitation Method

The synthetic procedures were adapted from Ahmed et al.[369] with slight modification. Briefly, polymer (8 mg) and FK506 (0.2, 0.5, 1 and 4 mg) were co-dissolved into acetone and drop into PVA solution (1%, 2%, 4%; 4 mL) under sonication. The NPs suspension was stirred to evaporate the organic solvent. The NPs were collected and washed with MilliQ water using Amicon® ultra centrifugation

filters. The washed NPs were subjected to low-speed centrifugation to remove aggregates before further use. The resultant NPs were conjugated with CR_8 peptide through interaction between the Mal group on the polymer and thiol group on the CR_8. After conjugation, the unreacted Mal was quenched with excessive cysteine. The R_8-PEG-PLGA NPs were washed with MilliQ water to remove cysteine, followed by DLS and UPLC/MS measurements described below.

For *in vitro* cellular uptake experiment, NPs synthetic procedures remained the same except FK506 was replaced with 1mg of Rh.

4.2.3 Preparation of Mal-PEG-PLGA/FK506 NPs with Single-emulsion (O/W) Method

The synthesis of Mal-PEG-PLGA/FK506 NP was repeated to encapsulate FK506. Briefly, Mal-PEG-PLGA (8 mg) and FK506 (0.5 mg) were firstly co-dissolved into an organic solvent (chloroform or DCM) and emulsified with an aqueous phase containing PVA using a probe sonicator (TL-ST150, Tenlin, China). The primary emulsion was quickly transferred to 10 mL of 1% PVA solution and stirred (100 rpm) at room temperature for solvent evaporation. After solvent evaporation, the NPs were collected and washed with MilliQ water to remove free FK506 and PVA. The resultant NPs were subjected to DLS and UPLC/MS measurements described below.

4.2.4 *In vitro* Charged-induced Aggregation and Peptide Quantification Analysis

Human umbilical vein endothelial cells (HUVECs) were incubated in a 12-well plate with 5% CO_2 atmosphere at 37 ℃ for 24 hours. R_8-PEG-PLGA NPs with different zeta potentials were diluted with cell culture medium and incubated at 37 ℃ for 24 hours. After the incubation period, the cells were washed with PBS, followed by observation under an inverted microscope and photographs were taken during examination. Peptide quantification was done by using Pierce™ Quantitative Colorimetric Peptide Assay kit (Thermo Scientific, USA). Briefly, sample and working reagent were mixed and pipetted into a 96-well microplate, followed by incubation at 37 ℃. After incubation, the sample mixture was sent to a microplate reader and measure at a wavelength of 480 nm. The experiment was repeat in triplicate.

4.2.5 Size distribution, Zeta Potential, Polydispersity (PDI) and Structural Analysis

The mean size, zeta potential and PDI of FK506-loaded PLGA NPs were determined by dynamic light scattering (Zetasizer, Malvern Panalytical, USA) with a measurement angle of 173° at 25 ℃. Structural analysis was performed with FTIR. All measurements were performed in triplicate.

4.2.6 Morphological Examination

The morphology of PLGA NPs were analysed with transmission electron microscopy (STEM, JEM-2100F, Japan). Briefly, NP dispersion was transferred and dried on a carbon film-supported copper grid. The sample was then stained with 2 % uranyl acetate and dried in air overnight prior to TEM evaluation.

4.2.7 FK506 Encapsulation Efficiency and Drug Loading with UPLC/MS

The drug loading (%DL) and encapsulation efficiency (%EE) of R_8-PEG-PLGA/FK506 NPs were determined by UPLC/MS. The UPLC column, Zorbax Eclipse Plus C18 column (Agilent: 2.1x50 mm; 1.8 µm), was employed and maintained at 45 ℃ throughout the analytical procedures. The precursor ions produced for FK506 and ascomycin (internal standard; IS) were sodium adducts, $[M+Na]^+$. The peak area of two mass transitions was selected for quantification, FK506 (m/z 826.5→616.0) and IS (m/z 814.5→604.2). The collision energy of 35 eV was set to cause optimal fragmentation, while fragmentation for FK506 and IS was 100 and 160 V, respectively. The mobile phase consists of methanol/0.1% formic acid, whereas mobile phase B consist of MilliQ/0.1% formic acid and the system operates at a flow rate of 0.3 mL/min. A calibration curve was prepared at concentration of 0 – 2000 ppb with a fixed amount of ascomycin as internal standard (IS). To extract FK506 from NPs, a fixed amount of lyophilised NPs was dissolved in acetone, followed by a brief sonication and solvent evaporation. After solvent evaporation, the samples were reconstituted with methanol and centrifuged to remove large polymeric debris. Same amount of IS was also added to the sample to be analysed and sent for analysis. The concentration of the encapsulated FK506 was calculated and obtained through the respective calibration curve. The %DL and %EE were determined with the following equations:

$$\%DL = \frac{Mass\ of\ FK506\ extracted\ from\ NPs}{Total\ mass\ of\ lyophilisd\ NPs} \times 100\% \quad (1)$$

$$\%EE = \frac{Mass\ of\ FK506\ extracted\ from\ NPs}{Total\ mass\ of\ FK506\ feed} \times 100\% \quad (2)$$

4.2.8 *In vitro* Drug Release Profile

The *in vitro* drug release profile was performed with dialysis method under sink condition. Briefly, PLGA NPs dispersion (equivalent to 0.5 mg FK506) was added into a dialysis bag (Spectra/Por® 4 Dialysis Membrane MWCO: 12 – 14 kDa) and submerged in a glass vial containing 40 mL of pH 7.4 phosphate-buffered saline (PBS) and Tween 20 (0.5% w/v) with stirring at 100 rpm at 37 ℃. A second set of samples was stored at 4 ℃ to evaluate the release pattern at storage condition. At designated time points (0, 2, 4, 6, 8, 10, 24, 48, 72 h), a fixed amount (1 mL) of the solution was collected and replaced with fresh medium. Each time point was repeated three-time and data was expressed as mean ± standard deviation (SD). The FK506 content was determined by UPLC/MS described above.

4.2.9 *In vitro* Cellular Uptake

HUVECs (15,000 cells per dish) were seeded and incubated with 5% CO_2 atmosphere at 37 ℃ for 24 hours. After incubation, the cells were washed with PBS and treated with free Rh, R_8-PEG-PLGA/Rh NPs and PEG-PLGA/Rh NPs. The same amount of Rh was used in three groups. At designated time points (3 and 6 hours), the cells were rinsed twice with PBS followed by labelling with DAPI (4',6-diamidino-2-phenylindole). The cells were then visualised immediately with a confocal laser scanning microscope (Leica TCS SPE confocal microscope, Germany). Image acquisition and process was performed with LAS X software.

4.2.10 *In vivo* Alkali-induced Rat CNV Model

Health SD rats (n=20; Male; 200-300 g; Age 6-14 weeks) were employed in this investigation. Prior to all experimental procedures, general anaesthesia and corneal anaesthesia were induced by 3% isoflurane inhalation and tetracaine eye drop (Bausch & Lomb Pharmaceuticals, Inc). Additionally, topical administration of 1% tropicamide was given to the experimental eye for pupil dilation purposes.

Once the corneal surface numbness was achieved, a circular filter paper previously soaked in 1.0 M sodium hydroxide solution was placed on the central cornea under a microscope for 30 seconds. After removing the filter paper, the corneal surface was quickly rinsed with 10 mL of PBS.

Immediately after the rinse, rats were randomly divided into 4 groups (n = 5 per group) and received 50 µL of solution for 14 days. Topical administration of saline, free FK506 eye drops (0.5 mg/mL), R_8-PEG-PLGA/FK506 (equivalent to 0.5 mg/mL FK506) and PEG-PLGA/FK506 (equivalent to 0.5 mg/mL FK506) were given to the injured eye twice per day. Eyes were evaluated and examined by slit-lamp microscope and underwent PAI on day 0 (pre-op), 4, 7 and 14. Corneal images were taken and analysed automatically with ImageJ software (Wayne Rasband, National Institutes of Health, USA). The corneal vascularised area was measured and presented as mean percentages ± SD.

4.2.11 *In vivo* PAI on Ocular CNV

Vevo LAZR Photoacoustic Imaging System (FUJIFILM VisualSonics) was utilized to capture B-mode ultrasound images, PAI and Doppler sonograph. The system is equipped with a tunable Nd:YAG laser system (OPOTEK Inc. 680-980 nm, 20Hz repetition rate, 5 ns pulse width, 50 mJ pulse peak energy) to imitate acquisition and excite tissue with optical pulses to generate PA effect. The following parameter were used for this study: Transducer LZ-250, Frequency 21 MHz, Depth: 14.00 mm, Width: 23.04 mm, Wavelength: 750/850 nm, Threshold HbT: 20, Acquisition: sO_2/HbT. Photoacoustic signals and ultrasound scans were acquired simultaneously and combined into one image in both transducer settings.

The animals were imaged at designated time points to acquire PA images for further analysis. Prior to imaging procedures, animals were anesthetised with inhalable anaesthetic and tetracaine eye drops. Once animals were under anaesthesia and placed on a heated platform, a layer of ultrasound gel was applied over the cornea. Transducers were then carefully aligned and examined the cornea at 750 and 850 nm wavelengths to acquire HbR and HbO2 PA signals. Acquired data (haemodynamic data and sO2 signals) were then analysed with built-in oxygenation-haemoglobin measurement package in workstation software (Vevo LAB, FUJIFILM VisualSonics, Toronto, Canada). Quantification of

haemodynamic status and sO2 level were accomplished by tracing the cornea as region of interest. The sO2 levels were calculated from pixels with estimation of oxygen saturation and resultant data were reported as average %sO2.

4.2.12 Histological Analysis

At the end of the study period, all animals were euthanised, and ocular tissues were obtained for histological analysis. Immediately after enucleation, eyeballs were fixed in paraformaldehyde 4% solution and sectioned for H&E and CD31 analysis.

4.2.13 Statistical Analysis

All data were analysed with GraphPad Prism 5 (GraphPad Software Inc.) and expressed as mean ± standard deviation. Student's t-test and one-way ANOVA (for multiple group comparison) were performed with $*p < 0.05$ and $**p < 0.01$ considered as statistically significant.

4.3 Results and Discussion

4.3.1 Optimisation, Preparation, and Characterisation of FK506-Loaded NPs

The FK506-loaded NPs were prepared through two commonly employed methods, nanoprecipitation and single emulsion. In general, the Mal-PEG-PLGA undergoes self-assembly to form NPs for drug delivery purposes. Attempts to maximise %DL and %EE can be achieved by tunning different experimental parameters such as choice of solvent, surfactant concentration, drug concentration and stirring speed.

Prior to encapsulating FK506, blank Mal-PEG-PLGA NPs were fabricated with nanoprecipitation method without adding FK506. These blank NPs were used to optimise the CR_8 conjugation process. Different amount of CR_8 solution was added and conjugated with blank Mal-PEG-PLGA NPs to yield distinct zeta potential values, as summarized in Table 4.1.

Sample	CR_8 sol. added (µL)	Size (nm) ± SD	PDI ± SD	Zeta Potential (mV) ± SD	Peptide conc. (μg/mL) ± SD
a	0	156.4 ± 0.06	0.17 ± 0.02	-19.2 ± 0.40	N/A
b	80	178.3 ± 4.04	0.23 ± 0.02	-2.03 ± 0.09	653.7 ± 0.45
c	100	173.8 ± 5.47	0.16 ± 0.02	13.2 ± 0.40	860.7 ± 3.43
d	400	196.4 ± 2.05	0.16 ± 0.03	21.8 ± 0.62	1072.1 ± 2.02

SD: Standard deviation; Conc.: Concentration

Table 4.1 Size, zeta potential and peptide conc. of non-conjugated PEG-PLGA NPs (sample a) and R_8-PEG-PLGA NPs (sample b to d)

Conjugation of CR_8 to NPs can be achieved with either electrostatic interactions or covalent coupling. Although electrostatic interaction is a more straightforward method to attach CPP to the surface of NP, it provides lesser control over the amount of CPP attached.[370] Another CPP conjugation method is covalent attachment, which other studies have widely employed in the past.[371–373] Specifically, the thiol group on the CR_8 interacts with the maleimide on the NP through Michael addition.[370] The attachment of cationic octa-arginine peptide leads to zeta potential shifted from negative to positive, indicating successful conjugation. The change of zeta potential values and peptide concentration after conjugation are summarised in Table 4.1. As illustrated in Figure 4.3, positively charged NPs aggregated in cell culture (Figure 4.3 c and 4.3 d) while aggregation was absent with NPs possessing a negative charge (Figure 4.3 b). Cells possess a negatively charge on their surface, and thus they attract oppositely charged species. Although the R_8 has excellent cellular permeability[374], excess amount of R_8 conjugation does not seem to enhance uptake as demonstrated in our data as shown in Figure 4.3. The excess amount of positively charged NPs aggregated on the surface of the plasma membrane rather than provide enhanced cellular uptake. Furthermore, studies pointed out that highly charged species may disrupt the integrity of the membrane and lead to undesired cytotoxicity.[375–377] Therefore, the optimal CR_8 conjugation ratio was the method produced in sample b. Thus, this method was used for the later part of NP surface modification.

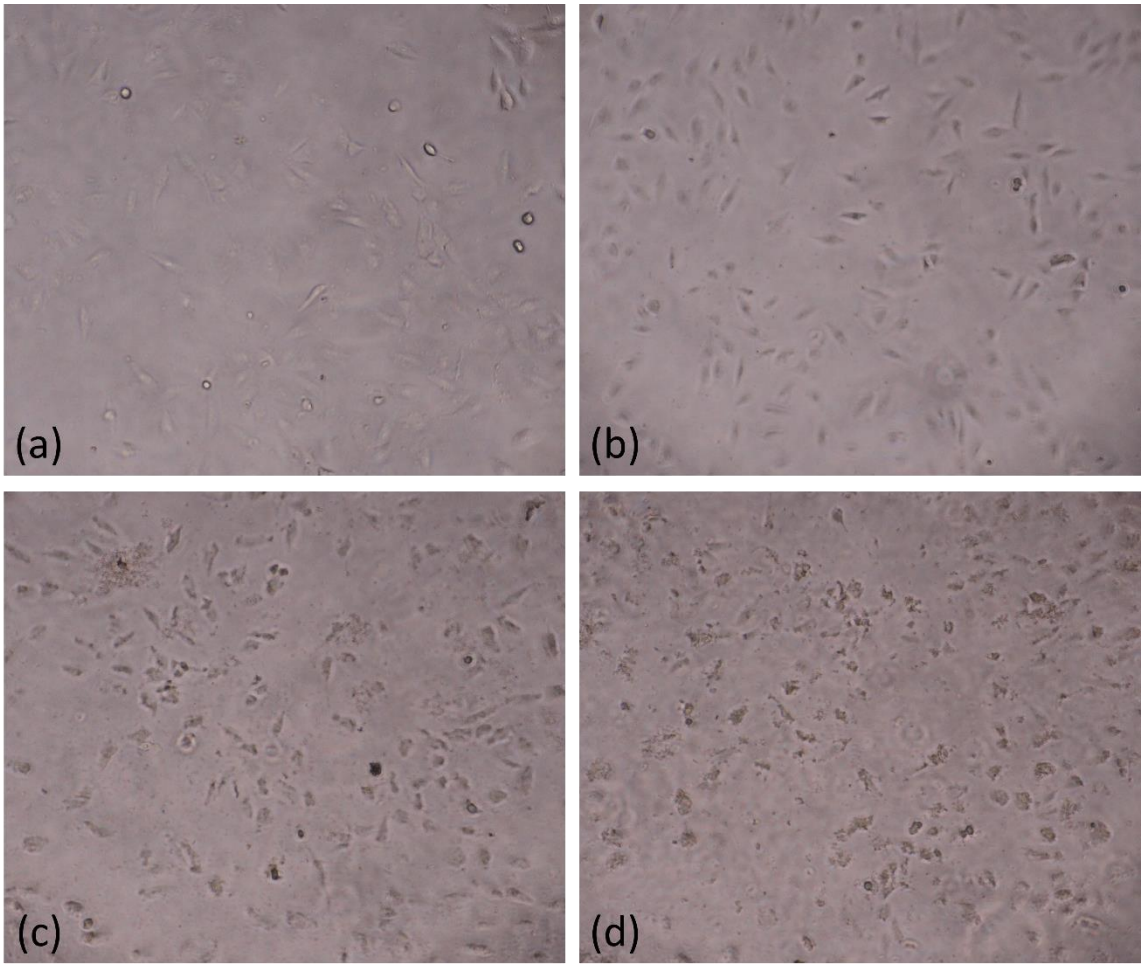

Figure 4.3 Incubation of HUVECs with different surface charge PLGA nanoparticles

(a) Sample a (zeta potential: -19.2 ± 0.40 mV); (b) Sample b (zeta potential: -2.03 ± 0.09 mV); (c) Sample c (zeta potential: 13.2 ± 0.40 mV); (d) Sample d (zeta potential: 21.8 ± 0.62 mV)

To optimise drug loading (%DL) and encapsulation efficiency (%EE) with the nanoprecipitation method, acetone was employed as solvent for dissolving the polymer and FK506 while different surfactant concentrations were firstly investigated. The nanoparticle size, zeta potential, drug loading and encapsulation efficiency were summarized in Table 4.2. Acetone was employed because of its volatility compared to other water-miscible solvent such as dimethyl sulfoxide (DMSO).

As PVA concentration increases, the size, %DL and %EE increase, while the zeta potential exhibited a decrease trend. Despite repetitive washing procedures, small amount of PVA remains adhered to the NPs which leads to size increase.[378] While the change in zeta potential is attributed to the

presence of PVA, it shields the surface charge and results in decrease in zeta potential.[379] Furthermore, the low polydispersity index (PDI) indicated the NPs were suitably homogeneous.[380] Overall, the removal of PVA exposes the carboxyl groups presence on surface of PEG-PLGA NPs which gives negative charge.

Solvent	FK506 (mg)	PVA conc. (%)	Size (nm) ± SD	PDI ± SD	Zeta Potential (mV) ± SD	DL (%)	EE (%)
Acetone	0.5	1	152.0 ± 10.68	0.12 ± 0.07	-21.7 ± 0.35	0.55	8.78
		2	153.35 ± 3.18	0.14 ± 0.01	-19.8 ± 0.15	0.69	11.09
		4	**171.65 ± 6.15**	**0.15 ± 0.01**	**-18.0 ± 0.15**	**1.21**	**19.28**

DL: Drug loading; EE: Encapsulation efficiency

Table 4.2 The effect of solvent and PVA concentration in %DL and %EE with Mal-PEG-PLGA/FK506 NPs fabricated from the nanoprecipitation method

FK506 (mg)	Size (nm) ± SD	PDI ± SD	Zeta Potential (mV) ± SD	DL (%) ± SD	EE (%) ± SD	Size after conjugation ± SD	Zeta Potential after conjugation (mV) ± SD	Peptide conc. (μg/ml) ± SD
0.2	177.03 ± 6.11	0.15 ± 0.03	-18.13 ± 0.43	0.50 ± 0.14	19.93 ± 5.51	–	–	–
0.5	166.87 ± 7.28	0.16 ± 0.03	-18.43 ± 0.61	1.19± 0.09	19.05 ± 1.41	–	–	–
1	**163.95 ± 4.03**	**0.11 ± 0.02**	**-20.20 ± 1.56**	**2.68 ± 0.44**	**21.21 ± 3.93**	**185.2 ± 4.45**	**-6.55 ± 0.94**	**661.3 ± 7.22**
2	162.13 ± 6.81	0.18 ± 0.04	-20.80 ± 1.55	2.80 ± 0.39	11.21 ± 1.56	–	–	–

DL: Drug loading; EE: Encapsulation efficiency

Table 4.3 Maximising %DL and %EE with different amounts of FK506 added in Mal-PEG-PLGA/FK506 NPs fabrication

Apart from surfactant concentration, the amount of drug added also influenced the %DL and %EE. Our data suggested that FK506 2 mg does not significantly increase %DL and even resulted

in a drop in %EE as shown in Table 4.3. Hence, the optimised protocol utilised acetone and 4% PVA to encapsulate FK506. This protocol produced R_8-PEG-PLGA/FK506 NPs with mean diameter of 185.2 ± 4.45 nm, and zeta potential = -6.55 ± 0.94 mV while the %DL and %EE were 2.68% ± 0.44 and 21.21% ± 3.93 respectively.

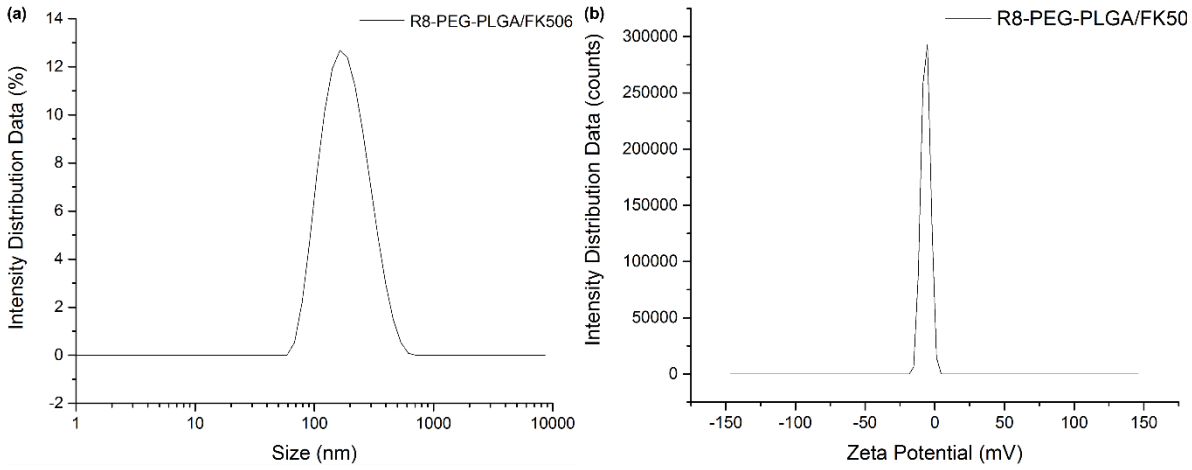

Figure 4.4 DLS (a) and zeta potential (b) measurement of R_8-PEG-PLGA/FK506

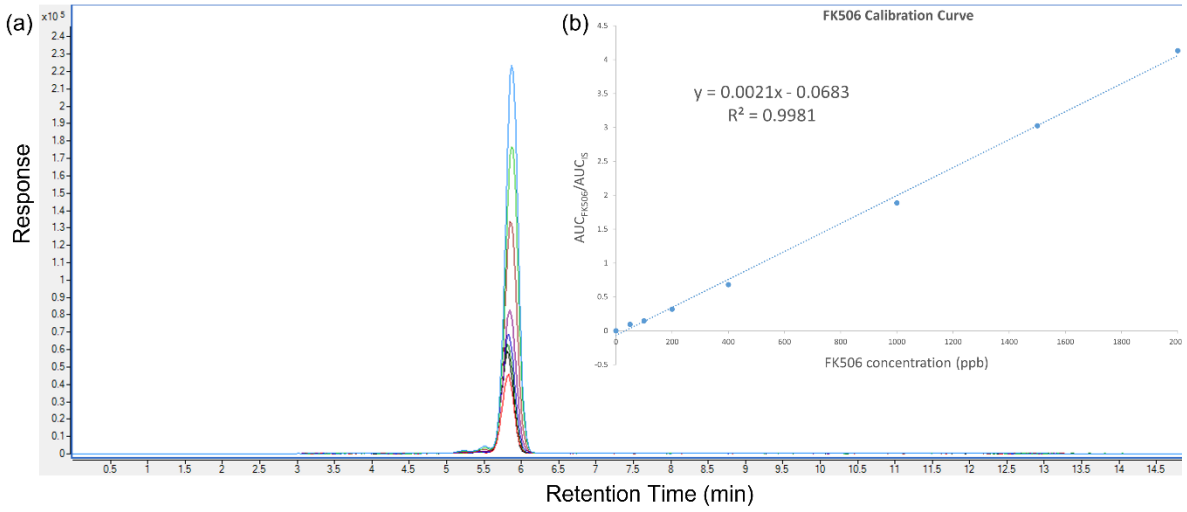

Figure 4.5 Chromatogram (a) and calibration curve (b) of FK506 obtained with UPLC-MS

Apart from the nanoprecipitation method, a single emulsion method was also employed to fabricate and encapsulate FK506 to investigate whether this method yields higher %DL and %EE. Three different organic solvents and solvent evaporation speed were investigated and found that most conditions resulted in the formation of large aggregates (Table 4.4). Only DCM and chloroform with

low solvent evaporation rate successfully produced the desired polymeric NPs and they were subsequently used to encapsulate FK506 (0.5 mg). Despite %DL and %EE being higher with single emulsion method (Table 4.5), the sizes and PDI were more significant than the NPs produced with the nanoprecipitation method. It has been suggested that a polymeric NP with size around 100 nm possesses 2.3-fold cell uptake property than other NP sizes.[381] Thus, NPs produced with the single-emulsion method might not be suitable for ocular drug delivery purpose. Compared to the two methods, the nanoprecipitation method is relatively simple for NP fabrication. For these reasons, nanoprecipitation method was selected to produce NP for the following experiments.

Solvent	**Evaporation speed (rpm)**	**Size (nm) ± SD**	**PDI ± SD**	**Observation**
Ethyl Acetate	1400	216.8 ± 3.46	0.321 ± 0.01	Large Aggregates
	500	218.2 ± 4.06	0.291 ± 0.01	Large Aggregates
	100	199.8 ± 1.78	0.255 ± 0.02	Large Aggregates
DCM	1400	263.9 ± 3.42	0.448 ± 0.02	Large Aggregates
	500	247.2 ± 2.17	0.457 ± 0.03	Large Aggregates
	100	**175.0 ± 4.16**	**0.295 ± 0.03**	**No Aggregation**
Chloroform	1400	239.1 ± 0.70	0.419 ± 0.01	Large Aggregates
	500	350.5 ± 1.65	0.533 ± 0.04	Large Aggregates
	100	**204.5 ± 3.78**	**0.308 ± 0.05**	**No Aggregation**

Table 4.4 Size difference of blank Mal-PEG-PLGA NPs produced with different solvent systems and evaporation speed using single-emulsion method

Solvent	FK506 (mg)	Size (nm) ± SD	Zeta (mV) ± SD	PDI ± SD	DL %	EE %
Chloroform	0.5	269.2 ± 1.25	-37.2 ± 0.50	0.468 ± 0.01	1.62	25.89
DCM		210.3 ± 6.67	-32.8 ± 0.35	0.332 ± 0.04	1.14	18.29

DL: Drug loading; EE: Encapsulation efficiency

Table 4.5 %DL and %EE with Mal-PEG-PLGA/FK506 NPs produced with different solvent systems using single-emulsion method

The conjugation of R_8 peptide and FK506 encapsulation were confirmed with FTIR, as demonstrated in Figure 4.4. The R_8-PEG-PLGA/FK506 exhibits characteristic peaks at 1653, 1758, 2825-2936 and 3421 cm^{-1} representing amide I, amide II, C-H bond (FK506) and N-H stretching respectively. The presence of strong, broad N-H stretching and amide bond in R_8-PEG-PLGA/FK506 suggested successful R_8 conjugation on the NP surface. Furthermore, characteristic C-H stretch of FK506 in R_8-PEG-PLGA/FK506 indicated encapsulation of FK506 into the NPs as this peak were absent in FTIR spectrum of Mal-PEG-PLGA starting material. Therefore, the presence of these characteristic peaks in the R_8-PEG-PLGA/FK506 FTIR spectrum confirms successful R_8 conjugation as well as encapsulation of FK506.

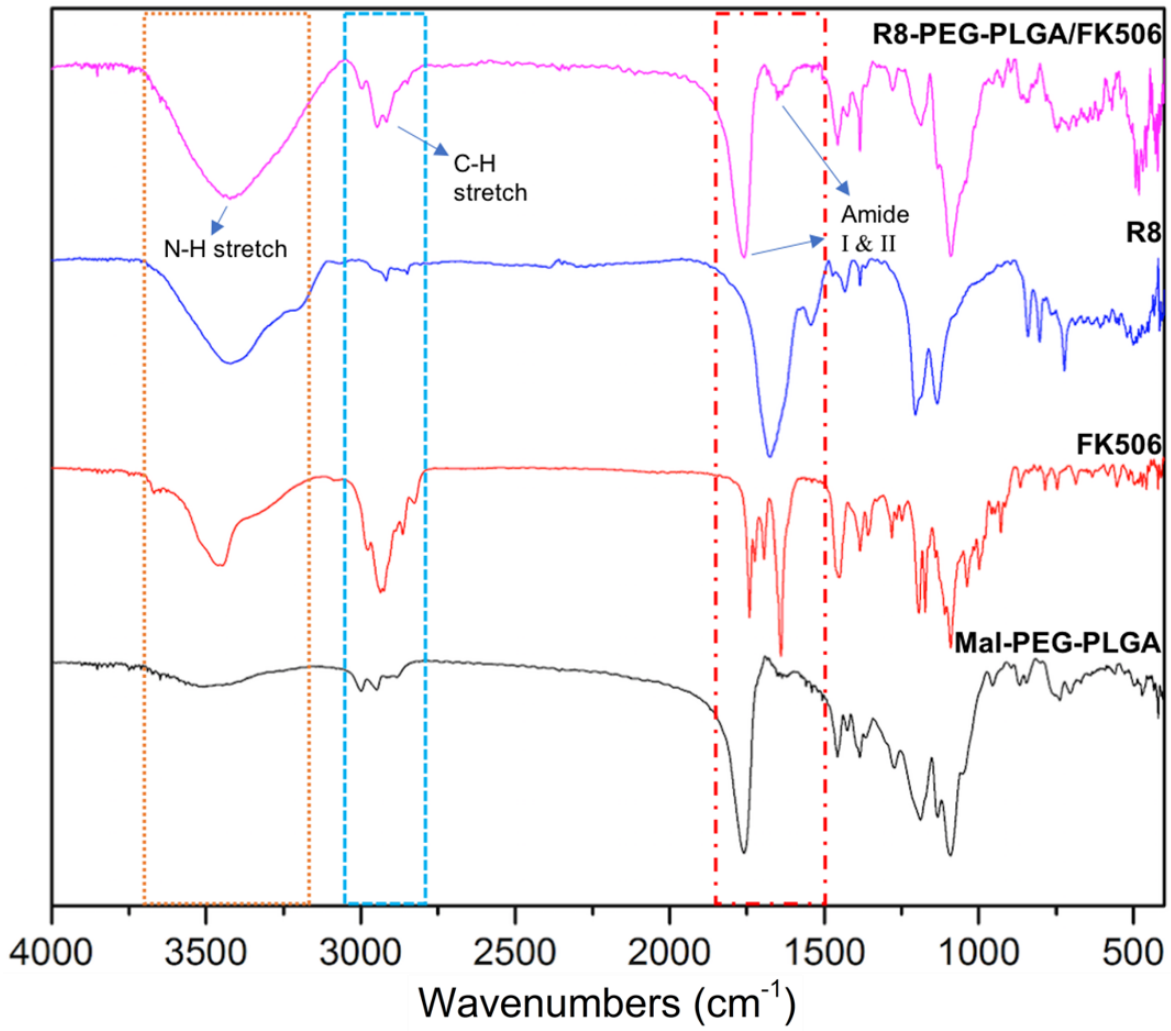

Figure 4.6 FTIR spectra of R_8-PEG-PLGA/FK506 NP and respective raw materials

The morphology of R_8-PEG-PLGA/FK506 NPs (Figure 4.5a) was spherical in size with a mean diameter of 45.63 ± 22.02 nm as measured by TEM (Figure 4.5b), while the size of the NPs measured by DLS was 163.95 ± 4.03 nm. The size discrepancy between the DLS and TEM was due to the technical nature of the analytical method. The TEM characterised and measured the size of dried NPs, whereas the DLS took the hydrodynamic diameters into consideration.[382] Nevertheless, the DLS provides more realistic size data as water is often employed as a medium for drug administration, especially in ocular drug administration. As a polymeric carrier for efficient drug delivery, the size plays a critical part in the rate of cellular uptake. In the case of polymeric NPs, particles with size smaller than 50 nm or larger than 1000 nm do not seem to favour cellular uptake compared to a particle size of

approximately 100 nm.[381] With this regard, the polymeric nanoparticle synthesised with nanoprecipitation method appears to satisfy this requirement for optimal drug delivery purpose.

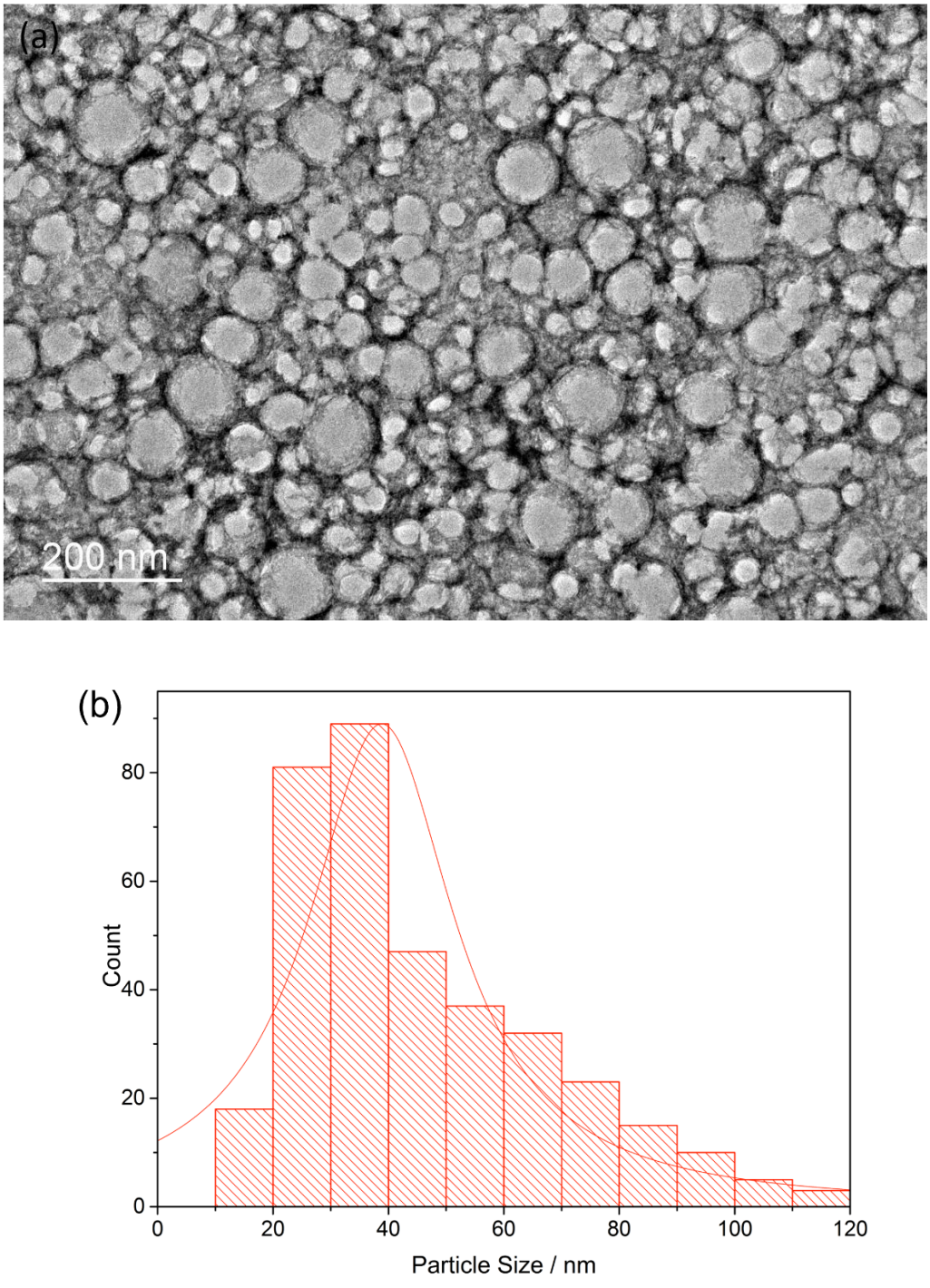

Figure 4.7 TEM image of (a) R_8-PEG-PLGA/FK506 NP and (b) corresponding size distribution

The *in vitro* drug release from R_8-PEG-PLGA/FK506 NPs was performed in PBS buffer with pH 7.4 at 4 and 32℃. The data obtained at 4℃ examined the release pattern at a storage condition,

while 32℃ was chosen to mimic corneal surface temperature. Our data suggested the drug release from NPs remained low at 4℃, which indicated the NPs remained stable at low temperature with only a small amount of drug released (Figure 4.6). At 32℃, the R_8-PEG-PLGA/FK506 NPs exhibited a steady release pattern of FK506 over the study period. The data revealed that approximately 30% of FK506 was released from the NPs during the first 12 hours and more than 50% were released by 24 hours. The NPs demonstrated a slow and steady release pattern with 73% of FK506 released from the nanoparticle by 72 hours. The steady and sustained release pattern of our NPs was unlike the conventional triphasic pattern. The conventional triphasic pattern includes an initial burst release pattern (phase I) follow by a slow-release profile (phase II) and a fast release pattern (phase III) as the final phase.[276]

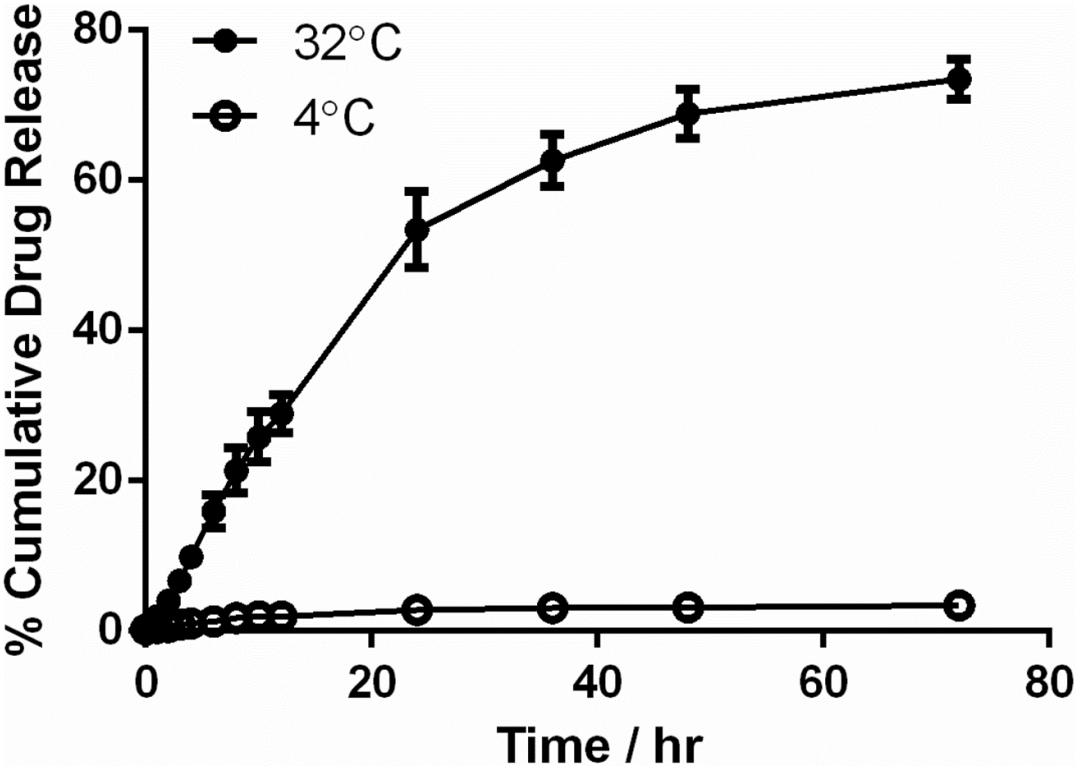

Figure 4.8 Percentage of cumulative drug release pattern at 32 ℃ and 4 ℃

The release of the encapsulated drugs is a combination of diffusion and erosion process of the PLGA NPs. Upon *in vivo* administration or contact with an aqueous medium, the backbone ester bond of the PLGA structure undergoes hydrolysis, which results in a decrease in molecular weight and thus, the structure integrity. The hydrolysis process also generates carboxylic groups, which further

contributes and catalyses the hydrolysis of PLGA NPs.[383] This auto-catalytic process results in heterogeneous degradation within the PLGA, where degradation occurs faster in the centre than on the surface of the PLGA matrix. As the hydrolysis continues, the hydrophobicity of PLGA continues to reduce leading to the structure become water-soluble and diffuses into the release medium.[384] This is known as erosion, and the cause of phase III release pattern in PLGA drug release profile. However, it is worth to note that the conventional triphasic pattern is not necessarily applied to all PLGA NPs. Studies have indicated fast phase II instead of slow-release pattern may follow a slower release profile in phase III.[385,386]

In our experiment, we employed PLGA 75:25 as raw material. The composition of polymer holds a significant role in degradation and release rate. Crystallinity, hydration rate and hydrophilicity of PLGA is correlated to the lactide/glycolide ratio of PLGA composition. The polylactide is less hydrophilic than polyglycolide due to the presence of the methyl side group.[387] Thus, the higher glycolide content, the higher water molecules uptake, resulting a faster rate of degradation and erosion. Therefore, PLGA 85:15 have a slower degradation rate than PLGA 65: 35 and, consequently slower drug release pattern.[388] Furthermore, the ratio also influences crystallinity of PLGA, which exerts an indirect impact on the degradation rate.[260] Study reported that lower lactide content decreases crystallinity which enhances the hydration rate,[389] subsequently leading to faster drug release from the PLGA. In this work, PLGA 75:25 was selected rather than PLGA 85:15 as higher lactide composition may lead to an even slower drug release pattern which might hinder the therapeutic efficacy. With this lactide/glycolide ratio, our data demonstrated a sustained drug release pattern, which suggests that PLGA NP can a valuable tool for drug delivery owing to its tunable property.

4.3.2 *In vitro* Cellular Uptake

HUVEC cell line was selected to investigate the cellular uptake experiment with R_8-PEG-PLGA/Rh NPs. Rh-loaded NPs in HUVECs were observed by a confocal laser scanning microscope (Leica TCS SPE confocal microscope) at different time intervals. As shown in Figure 4.7, both PEG-PLGA/Rh and R_8-PEG-PLGA/Rh NPs were accumulated in HUVEC at 3 hours. However, a time-

dependent increase was observed at 6 hours, where the accumulation of R_8-PEG-PLGA/Rh NPs was significantly higher. The results might be attributed to the conjugation of R_8 on the surface of the NPs. Apart from the EPR effect, the R_8 on the surface of the PLGA NPs facilitate the uptake of the NPs into the cells.[370]

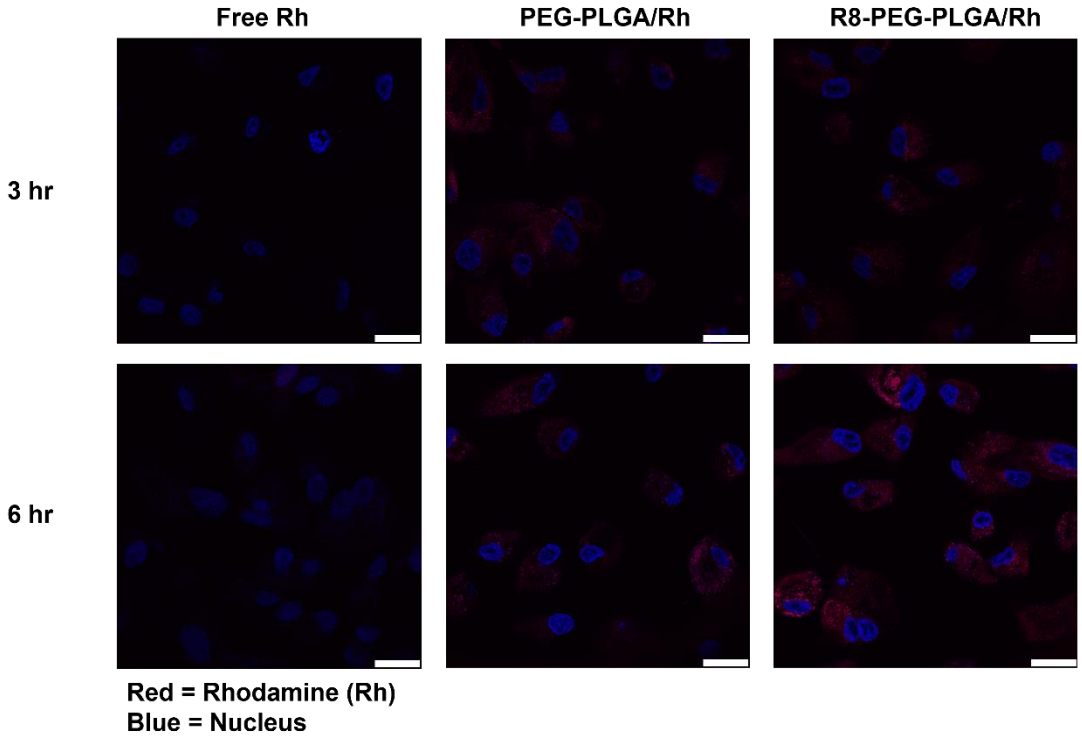

Figure 4.9 Cellular uptake of PEG-PLGA/Rh NPs and R_8-PEG-PLGA/Rh NPs at different time points (Scale bar 25 µm)

However, the mode of uptake mechanism was not discussed in this work. The exact uptake mechanism remains highly debatable despite enhanced cell permeation achieved by CPP-conjugated NPs. The concept of endocytosis is widely accepted as the cellular uptake mechanisms for arginine-rich peptides. Among different types of endocytosis, macropinocytosis has been suggested as the predominant pathway.[390]

Regardless of the mode of uptake mechanism, the R_8-PEG-PLGA/Rh NPs demonstrated a significant uptake compared to non-conjugated NPs. These results showed that the impact of R_8-conjugated NP can potentially break through the obstacles imposed by corneal barriers, thus achieving enhanced uptake and sustain-released drug delivery system.

4.3.3 Treatment Efficacy of R_8-PEG-PLGA/FK506 NPs for *in vivo* CNV Model

The present investigation employed an alkali-induced CNV model to assess the therapeutic efficacy of PLGA-based drug delivery system. Candidates to be evaluated include saline, FK506 eye drops, PEG-PLGA/FK506 NPs and R_8-PEG-PLGA/FK506 NPs. The slit-lamp images (Figure 4.8) revealed newly formed vessels sprouting from the limbus on day 4 and 7 in rat that received saline. The blood vessels continued to extend towards central cornea on day 14, whereas the vascularised area was slightly less severe in group treated with FK506 eye drops. Table 4.6 summarised the corneal vascularised area after received different NP formulation treatment.

The PLGA-based groups demonstrated superior CNV inhibitory effect compared to saline- and FK506-treated rat. Both PLGA NPs (R_8-conjugated and non-conjugated NPs) exhibited increased vascularised area and oedema on day 4. The PEG-PLGA/FK506 NPs demonstrated an inhibitory effect with a mild increase in vessels on day 7 and 14. The R_8-PEG-PLGA/FK506, however, demonstrated excellent inhibitory effect among all treatment groups. Not only did the PLGA NPs offer sustain-released properties, the R_8 peptide also plays a vital role in providing additional cell permeation effect. The R_8 conjugation enhanced NPs' absorption upon topical administration while the cationic R_8 increased the ocular surface retention time. Therefore, these two properties of R_8-PEG-PLGA/FK506 NPs coupled with the EPR effect of NPs further strengthened the delivery of FK506 to the cornea. Thus, the R_8-PEG-PLGA/FK506 NPs were able to demolish and inhibit CNV progression with topical administration twice daily, while conventional FK506 failed to achieve.

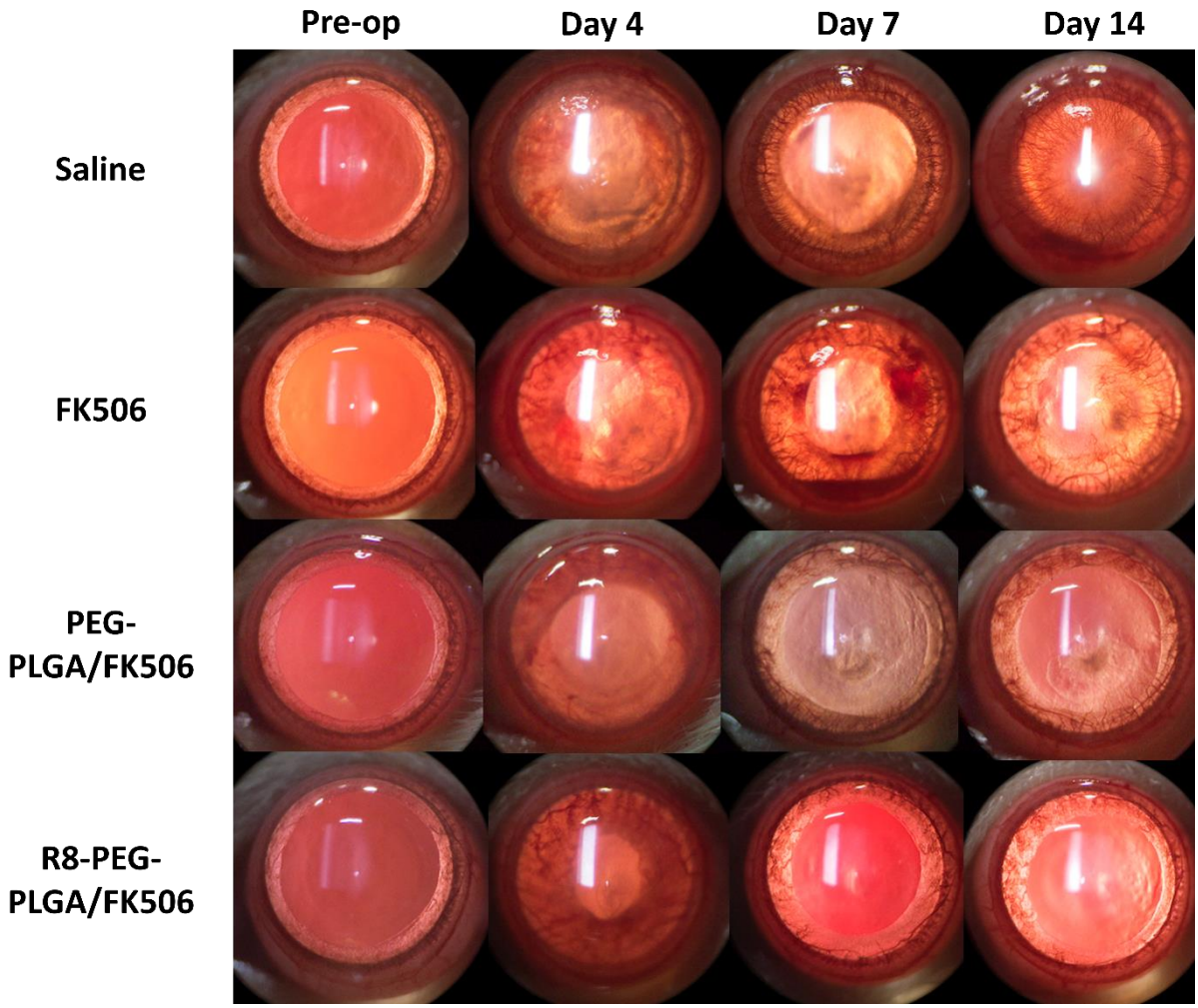

Figure 4.10 Slit-lamp images of treatment efficacy with different NP formulations

	Averaged % vascularised area		
	Day 4	**Day 7**	**Day 14**
Saline	14.74 ± 1.09	35.89 ± 7.82	48.67 ± 6.55
FK506	16.05 ± 1.52	33.92 ± 7.55	46.42 ± 4.98
PEG-PLGA/FK506	11.99 ± 0.36	9.65 ± 0.15	4.27 ± 1.15
R_8-PEG-PLGA/FK506	6.16 ± 0.39	4.19 ± 0.37	2.43 ± 0.60

Table 4.6 Averaged % vascularised area in rat's cornea received different NP formulations

The saline and FK506 groups showed a notable amount of inflammatory cells infiltrating the stroma and a significant number of neo-vessels can be observed (Figure 4.9). The immunohistochemical assay with CD31 also unveiled immunoreactivity in the stroma of the group receiving saline and FK506

eye drop, as illustrated in Figure 4.9. Although slit-lamp images demonstrated the efficacy of FK506, the effect was not extensive. These observations might relate to poor bioavailability with topical administration twice daily.

The representative histological analysis revealed the R_8-PEG-PLGA/FK506 treatment group significantly decreased the inflammatory cells infiltrating the cornea as well as neo-vessels formation. Furthermore, the CD31 immunoreactivity (Figure 4.9) in the stromal region was negligible in R_8-PEG-PLGA/FK506 group. Therefore, the remarkable inhibitory effect might relate to the enhanced delivery of FK506 into the tissue using R_8-conjugated PLGA NPs.

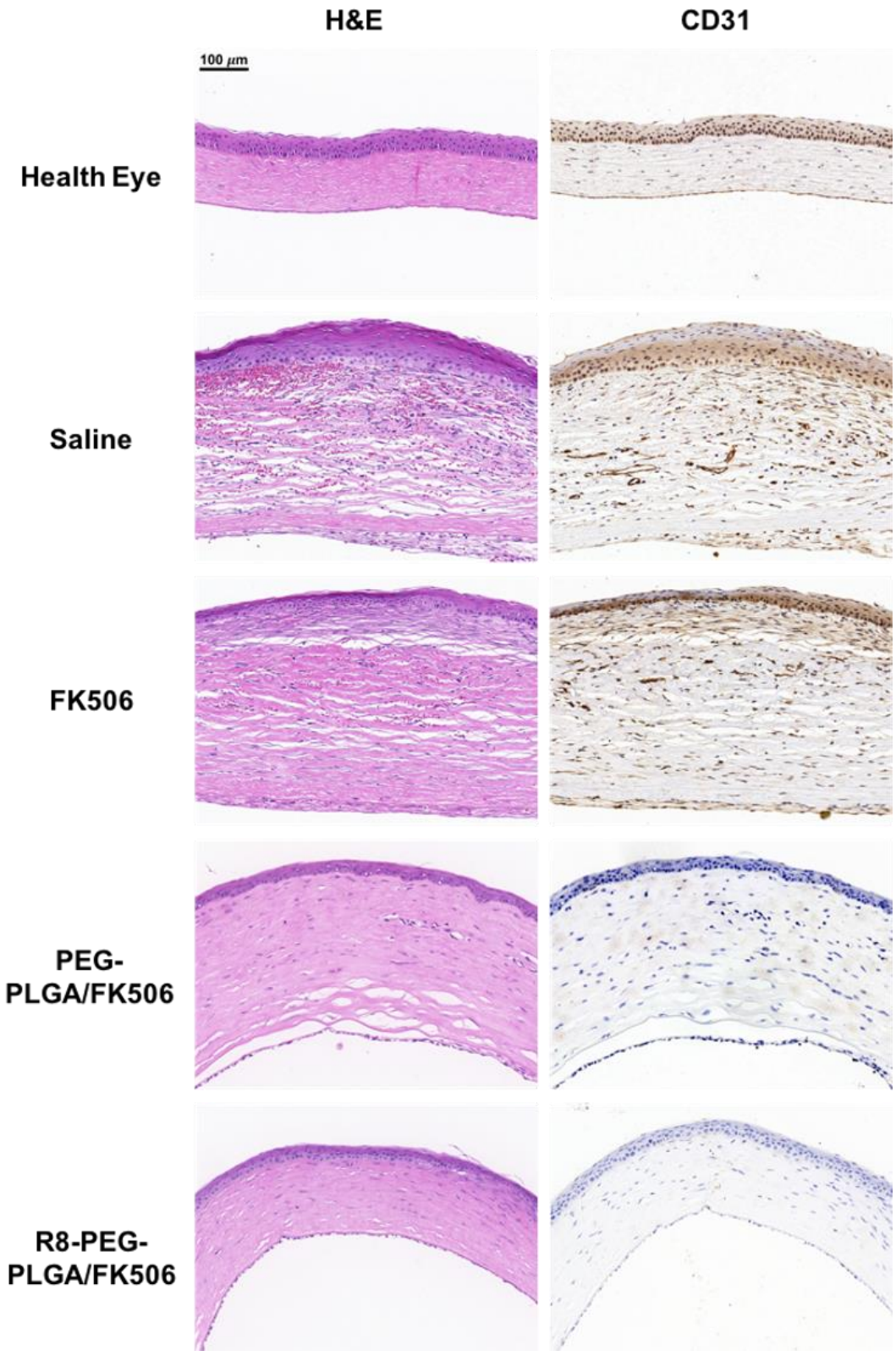

Figure 4.11 Histopathological images of rats received metformin treatment

H&E (left) and CD31 (right) images revealed treatment efficacy of NP formulation on Day 14 (scale bar 100 μm for H&E and CD31).

4.3.4 *In vivo* Corneal Haemodynamic Status with PAI

To provide a more objective analysis of CNV monitoring, PAI was used to assess and quantify the change in corneal haemodynamic status and $\%sO_2$. The corneal HbR and HbO_2 content were monitored and quantified at wavelengths 750 and 850 nm, respectively.

Once alkali injury was inflicted on rat's cornea, a significant increase in HbR and HbO_2 PA signals was recorded in saline- and FK506-treated subjects (Figure 4.10 and 4.12). Quantitative analysis of the saline group revealed a 2-fold increase in the HbR signal (0.12 ± 0.0082) compared to the baseline value (0.06 ± 0.0082) on day 4 (Figure 4.11). The HbR signal in saline group continued to increase on day 7 (0.24 ± 0.066) and 14 (0.30 ± 0.058). In the group receiving FK506 treatment, the quantitative analysis showed a similar trend on day 4 (0.12 ± 0.029) with a 2-fold increase in HbR signal compared to pre-experimental baseline value (0.06 ± 0.036). In the remaining experimental period, the HbR signal of FK506 group continued to rise on day 7 (0.15 ± 0.024) and day 14 (0.27 ± 0.056), respectively.

The PEG-PLGA/FK506 NPs group showed a factor of 1.86 elevation in HbR signal on day 4 (0.13 ± 0.037) followed by continuous decline in HbR signal on day 7 (0.10 ± 0.0055) and 14 (0.09 ± 0.0063). The R_8-PEG-PLGA/FK506 NPs group also revealed a similar trend with slight increase in HbR signal on day 4 (0.09 ± 0.0116) and regressed slightly on day 7 (0.08 ± 0.0075). Subsequently, the signal returned to baseline level (0.07 ± 0.007) on day 14.

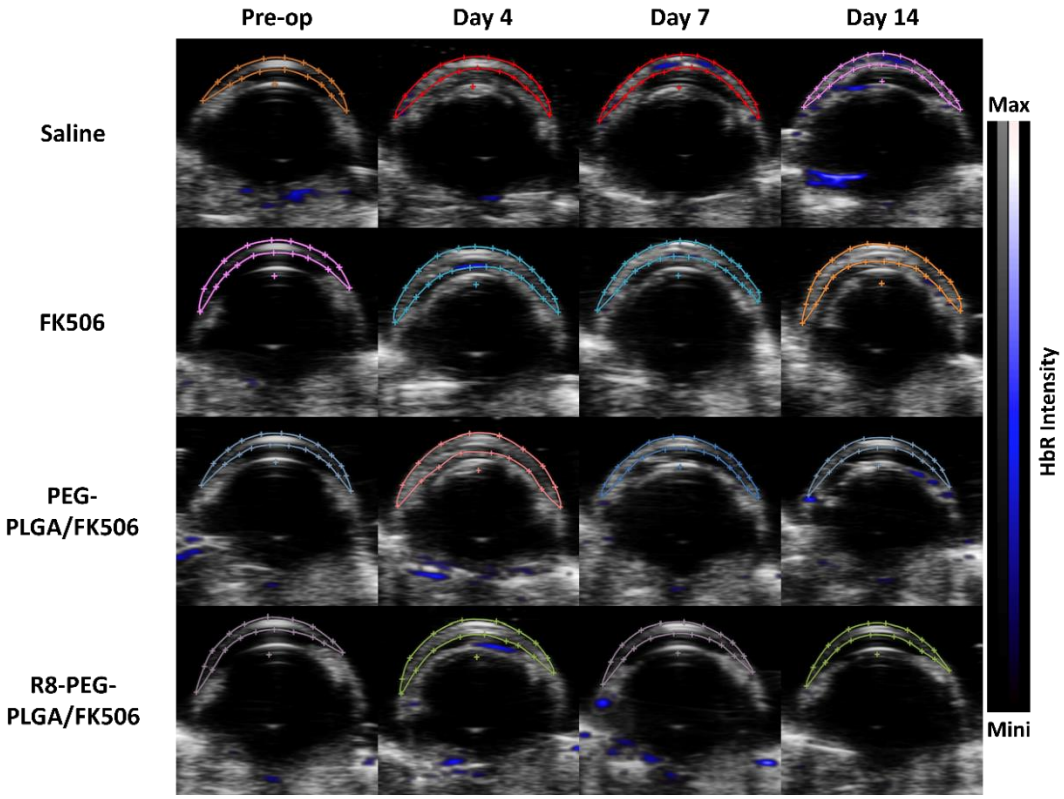

Figure 4.12 Co-registered PA and ultrasound images of HbR status over the study period

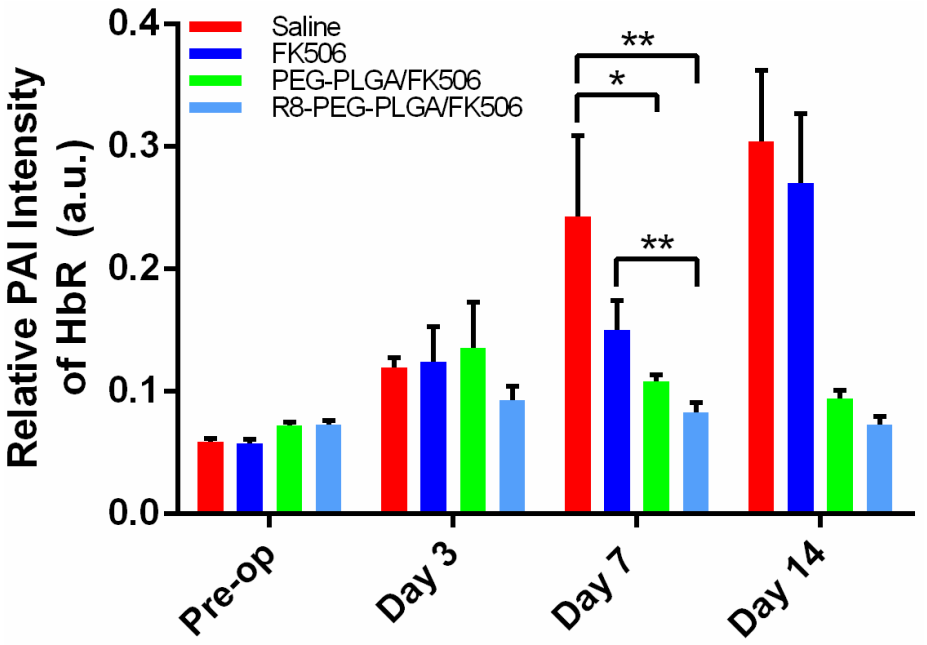

Figure 4.13 Quantitative analysis of PA intensity in HbR signals with different formulations *$p < 0.05$ and **$p < 0.01$

The HbO_2 signal (Figure 4.13) also revealed an increasing trend in the saline group with a 2.33-fold (0.21 ± 0.0225) and 4.33-fold (0.39 ± 0.0597) increase on day 4 and day 7, respectively. At the end of the study period, the HbO_2 increased up to 0.54 ± 0.1196, which was the highest among the study groups. The FK506 group also revealed a similar increase on day 4 (0.23 ± 0.0567), followed by a slight increase on day 7 (0.26 ± 0.0763). However, the PAI recorded a HbO_2 signal of 0.50 ± 0.1065 on day 14, which was a 6.25-fold increase compared to baseline (0.08 ± 0.0064).

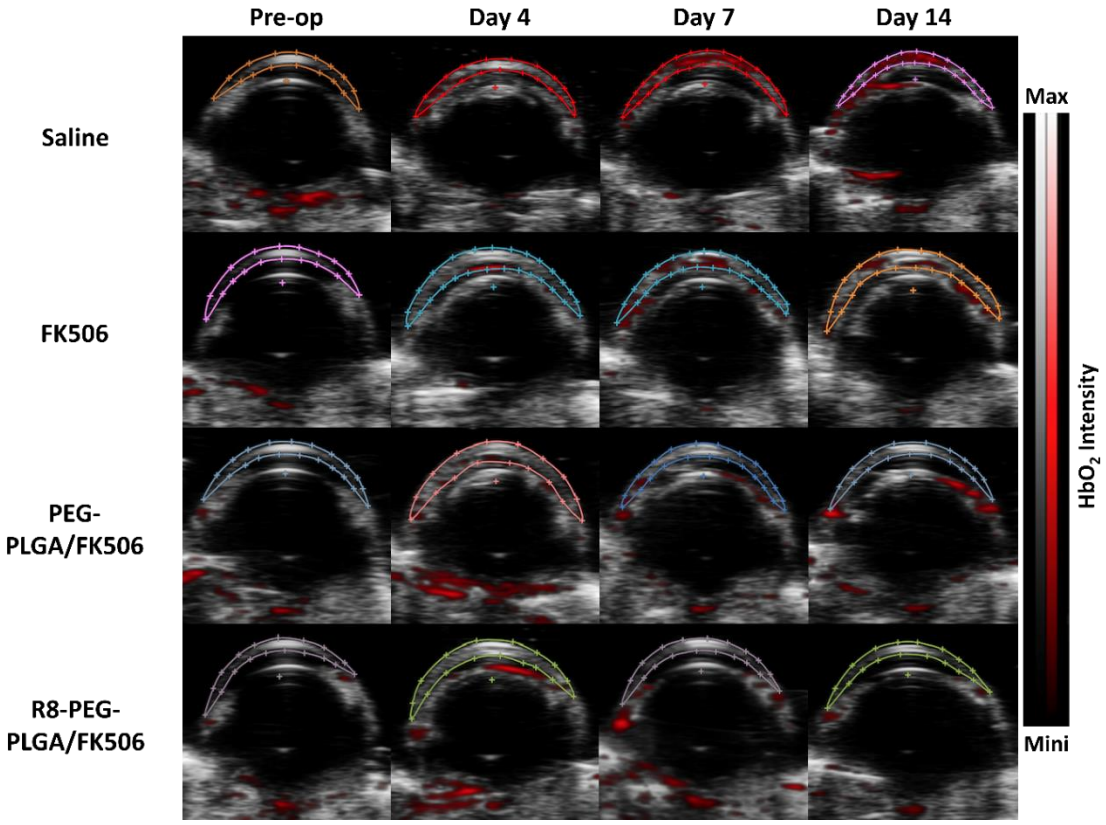

Figure 4.14 Co-registered PA and ultrasound images of HbO_2 status over the study period

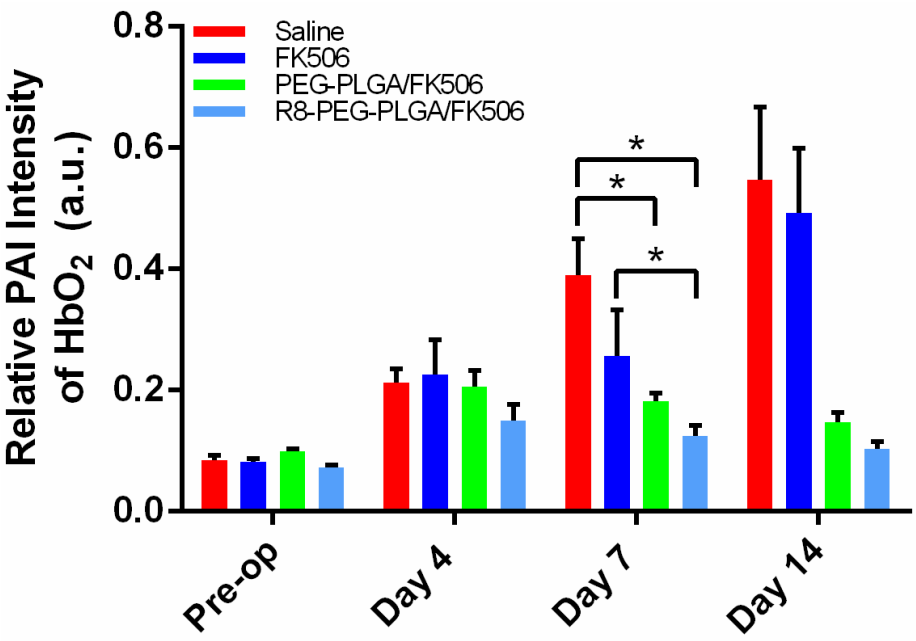

Figure 4.15 Quantitative analysis of PA intensity in HbO_2 signals with different formulations $*p < 0.05$

The PLGA NP groups, however, demonstrated an increase on day 4 followed by regression over the remaining study period. The PEG-PLGA/FK506 NPs group showed a 2.33-fold increase in HbO_2 signal on day 4 (0.21 ± 0.0263) compared with baseline (0.09 ± 0.0034). The HbO_2 signals subsequently regressed on day 7 (0.18 ± 0.0138) and day 14 (0.14 ± 0.0164). Rats that received R_8-PEG-PLGA/FK506 NPs treatment exhibited an increasing trend on day 4 (0.15 ± 0.0266) compared to baseline (0.07 ± 0.0039). Similar to the quantitative analysis observed in PEG-PLGA/FK506 NPs treatment group, the HbO_2 continued to regress on day 7 (0.12 ± 0.0168) and 14 (0.10 ± 0.0119), respectively. The quantitative analysis reflects treatment efficacy of PLGA drug delivery NP through non-invasive monitoring of haemoglobin species in the cornea, which conventional slit-lamp images fail to achieve.

4.3.5 *In vivo* $\%sO_2$ Assessment with PAI

A healthy cornea is a transparent ocular tissue with no blood vessels, while a diseased cornea presents newly formed vessels that obstructs light passing through leading to compromised vision. While slit-lamp images can provide a quick evaluation of cornea status, $\%sO_2$ offers an objective

analysis of CNV progression. Therefore, PAI was utilised to evaluate treatment efficacy with different treatment groups in this study.

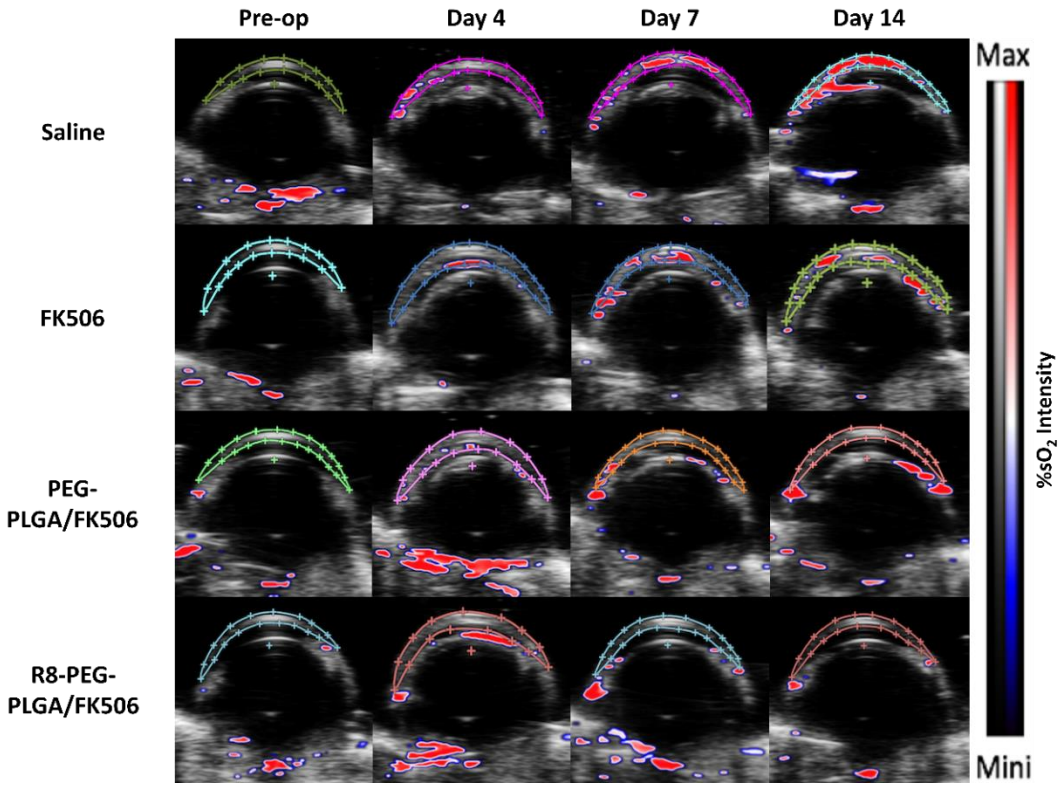

Figure 4.16 Co-registered PA and ultrasound images of corneal sO_2 signals over the study period

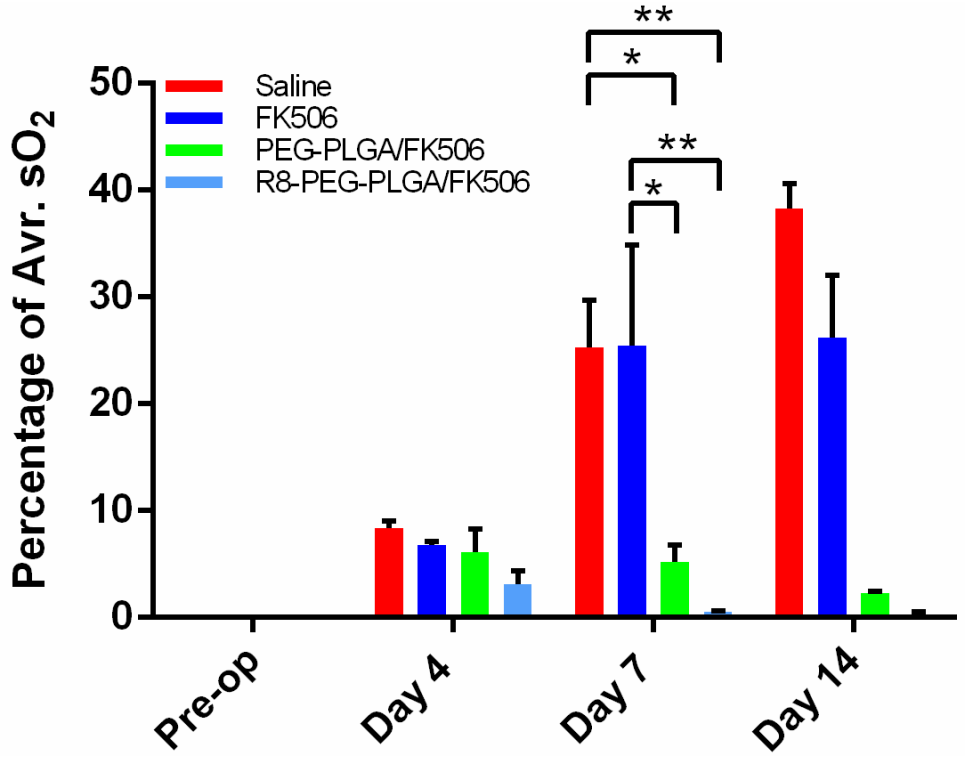

Figure 4.17 Quantitative analysis of PA intensity in $\%sO_2$ signals with different formulations $*p < 0.05$ and $**p < 0.01$

Quantitative analysis (Figure 4.14) revealed that saline-treated animals had a significant elevation in average $\%sO_2$ with 8.39 ± 0.66%, 25.32 ± 4.36% and 38.30 ± 2.34% on day 4, 7 and 14, respectively. The increased trend matches the slit-lamp images and co-registered PA and ultrasound images in Figure 4.14. Moreover, the FK506 treatment group also demonstrated an elevated trend from day 4 (6.77 ± 0.36%) to day 7 (25.43 ± 9.44%) and remained at a similar level on day 14 (26.25 ±5.80%).

Similar to the pattern observed in haemodynamic status, both PLGA NPs treatment groups exhibited an increase of average $\%sO_2$ from pre-op to day 4, followed by continuous regression. The PEG-PLGA/FK506 NPs group showed the average $\%sO_2$ elevated from 0 to (6.17 ± 2.09%) on day 4 and declined to 5.17 ± 1.64% on day 7 and 2.31 ± 0.17% on day 14 respectively. Owing to the EPR effect and enhanced permeability of R_8-PEG-PLGA/FK506 NPs, the overall average $\%sO_2$ revealed a subtle increase on day 4 with average $\%sO_2$ of 3.09 ± 1.32% followed by a continuous decline of average $\%sO_2$ on day 7 (0.52 ± 0.11%) and day 14 (0.30 ± 0.23%).

Overall, the quantitative analysis derived from PAI could provide a more comprehensive view of CNV progression and treatment efficacy. Through the slit-lamp images and PAI analysis, the enhanced drug delivery properties of R_8-conjugated NPs were indirectly demonstrated. Though the molecular mechanism of FK506 was not discussed in this work, the anti-angiogenic properties of FK506 have been discussed elsewhere.[391] Chen et al. concluded that FK506 reduced the expression level of VEGF-A, which is the most important mediator for angiogenic stimulation. Moreover, FK506 reduces the levels of chemokines (MCP-1 and MIP-1α) and inflammatory cytokines (IL-1β and IL-6), thus exerting potent anti-angiogenic properties against CNV.

The cornea possesses multiple barriers for foreign substances to pass through, which leads to poor bioavailability. To overcome such obstacles, higher concentration or frequent dosing are required. However, these strategies might lead to undesired side effects or poor patient compliance. Although FK506 possesses excellent anti-angiogenic ability, poor solubility limits its utility to a certain extend. With the nanotechnology employed in this study, the administration frequency was reduced to twice per day. Despite reduced administration frequency, the therapeutic efficacy was still promising owing to the enhanced cell permeability of R_8-conjugated NPs. Therefore, the data presented in this study demonstrated the enhanced ocular therapeutic response using nanotechnology with a smart surface decoration.

4.3.6 Conclusion

In this chapter, R_8-conjugated PEG-PLGA NPs were fabricated through the nanoprecipitation method with the aim to enhance ocular drug delivery. The physiochemical properties (i.e. nano-size, zeta potential) and surface modification of the PLGA NPs offer a promising ocular drug delivery strategy to enhance drug bioavailability, as demonstrated in the *in vitro* and *in vivo* experiments. The *in vitro* sustained drug release feature, as well as the permeation and accumulation characteristics, suggested its potential capability for delivering FK506 to the cornea. The *in vivo* CNV inhibitory was also examined and evaluated with an objective analysis using non-invasive PAI. PAI provides molecular information that conventional technique fails to deliver, which gives a more comprehensive

framework of disease progression and treatment outcome. Overall, the R_8-PEG-PLGA/FK506 NPs demonstrated a significant CNV inhibitory effect and provided remarkable therapeutic efficacy with topical administration twice daily. In summary, R_8-PEG-PLGA NPs would be a promising drug delivery nanoplatform for ocular drug delivery that might be employed to anterior segment and posterior segment of the eye.

5 Evaluation of High Potency Focal Adhesion Kinase Inhibitor (KX2-4245) Against CNV

5.1 Introduction

Angiogenesis is a complex and essential biological process responsible for embryogenesis and maintaining homeostasis in biological species.[392] The cornea maintains a balance between angiogenic and anti-angiogenic factors to preserve corneal avascularity which is important for visual acuity. However, this balance is disrupted under pathological conditions, which leads to manifestation of various diseases such as CNV, age-related macular degeneration and cancer. VEGF and its counter receptor (VEGFR2) have been identified as one of the key mediators in regulating angiogenesis under physiological and pathological state.[393] Upon binding with VEGF receptors, it induces dimerization, transautophosphorylation and activates a cascade of signalling events. Therefore, the VEGF stimulation triggers a series of angiogenic processes such as proliferation, permeability, migration and survival.

Focal adhesion kinase (FAK), a non-receptor tyrosine kinase, has demonstrated its role in numerous biological activities such as cell migration, proliferation, VEGF production and new blood vessel formation.[394] The cultured endothelial cells express a high degree of FAK as demonstrated in reverse transcription polymerase chain reaction (RT-PCR) and immunostaining assay. This finding suggests the importance of FAK in cell adhesion, migration and integrin signalling, which all relate to the neovascularisation process.[395–397] Apart from VEGF/VEGFR2, the FAK signalling pathway is also mediated by integrin and has been well documented in the past. The integrin mediates FAK to participate in various biological events such as cell adhesion, cell-cell and cell-matrix interaction. These events are thought to be the centre of angiogenesis. Moreover, FAK also acts as a vital element of VEGF/VEGFR2 and Ang/Tie-2 receptors and thus, the FAK is a crucial and multi-functional cell signalling regulator responsible for endothelial cell survival, migration, blood vessels stabilisation and maturation.

Schaller et al. reported two major FAK phosphorylation sites (Y397 and Y925) that play a crucial role in FAK functioning as well as its responsibility in recruiting pro-angiogenic supportive

molecules.[398,399] In the settings of angiogenesis, FAK recruits a multi-functional protein known as c-Src. The c-Src protein involves in regulating diverse normal biological and oncogenic processes such as proliferation and survival. To exert biological function, FAK recruits c-Src and is bound to the phosphorylation site Y397 with the Src homology 2 (SH2) domain. This results in activation of c-Src and subsequently transphosphorylates the phosphorylation site Y925. As a result, this transphosphorylation activates the Ras/MAP kinase pathway *via* the recruitment of Grb-2/mSOS complex.[400] Additionally, the phosphorylation of Y397 generates a docking site for other signalling molecules while it further enhances the FAK activity *via* transphosphorylation at other phosphorylation sites (Y407, Y576 and Y577). Recruitment and activation of the phosphatidaylinositol 3-kinase (PI3-K) induced by integrin ligation and VEGF/VEGFR2 stimulation of FAK results in the generation of downstream signals, which are vital for survival and proliferation.

Corneal neovascularisation (CNV) is a common and sight-threatening complication affecting millions of people worldwide, while CNV is also a risk factor for corneal graft rejection following corneal transplantation.[28,401–403] Treatment intervention employing laser or photodynamic therapy provides closures on newly formed vessels but the effect is only temporary.[404,405] Medical treatment often involves corticosteroids, which is able to suppress proliferating new vessels. However, it is ineffective against matured and established corneal vessels. Furthermore, corticosteroids could result in undesired side effects such as intraocular pressure elevation and cataracts. Other medications such as bevacizumab and ranibizumab target VEGF to achieve anti-angiogenesis. However, these protein drugs are often costly compared to conventional corticosteroids. Therefore, there is a need to enhance the arsenal to combat CNV or other ocular angiogenic diseases.

With the molecular evidence indicating the role of kinase in angiogenesis, inhibition of FAK serves as a reliable strategy to accomplish anti-angiogenesis. Several kinase inhibitors such as sunitinib, sorafenib and lapatinib have been developed to combat angiogenesis, as discussed in Chapter 1.8.3. These agents have demonstrated their anti-angiogenic capability in cancer or experimental CNV model.

This study investigates the anti-angiogenic effect of KX2-4245 with an experimental CNV model, namely (i) the optimal concentration with cultured human umbilical vein endothelial cells (HUVECs) and spontaneously arising retinal pigment epithelial cell (ARPE19), (ii) *in vivo* toxicity with KX2-4245 eye drops and (iii) anti-angiogenic of KX2-4245 with *in vivo* CNV model.

5.2 Materials and Methods

5.2.1 Materials

KX2-4245 was a gift from Kinex Pharmaceuticals (Buffalo, NY), and bevacizumab (Avastin, 25 mg/mL) was purchased from Roche (Basel, Switzerland). HUVEC and ARPE19 were obtained from American Type Culture Collection (ATCC, Manassa, VA). Endothelial cell growth medium and SupplementMix was purchased from PromoCell. Dulbecco's Modified Eagle Medium/Nutrient Mixture F-12 (DMEM/F12) and fetal bovine serum (FBS) was purchased from ThermoFisher Scientific.

5.2.2 Cell Culture

HUVEC was maintained with endothelial cell growth medium supplemented with heparin, endothelial cell growth supplement, 2% FBS and 100 U/mL penicillin G and 100 µg/mL streptomycin sulfate. APRE19 was maintained with DMEM/F12 containing 10% FBS with 100 U/mL penicillin G and 100 µg/mL streptomycin sulfate.

5.2.3 Cytotoxicity Assay

HUVEC and ARPE19 seeded at a density of 5000 cells per well in a 96-well plate were grown to 90% confluence before incubation with different concentrations of KX2-4245 (0 to 20 nM). Cell viability was examined at day 1, 2, and 3 with 3-(4,5-dimethylthiazol-2-yl)-2,5-diphenyltetrazolium bromide (MTT; 0.5 mg/mL). Cells were lyzed, and formazan was extracted with a mixture of DMSO and ethanol (1:1 v/v) and quantified colourimetrically at wavelength 570 nm with correction of interference at 690 nm. The experiment was repeated in triplicate.

5.2.4 *In vivo* Alkali-induced Rat CNV Model

Health SD rat (n=15; Male; 200-300 g; aged 6-14 weeks) were employed in this investigation. Prior to all experimental procedures, general anaesthesia and corneal anaesthesia were induced by 3% isoflurane inhalation and tetracaine eye drop (Bausch & Lomb Pharmaceuticals, Inc). Additionally, topical administration of 1% tropicamide was given to the experimental eye for pupil dilation purposes. Once the corneal surface numbness was achieved, a circular filter paper previously soaked in 1.0 M sodium hydroxide solution was placed on the central cornea under the microscope for 30 seconds. After removing the filter paper, the corneal surface was quickly rinsed with 10 mL of PBS.

Immediately after the rinse, rats were randomly divided into three groups (n = 5 per group) and received 50 µL of solution for 14 days. Topical administration of saline, avastin eye drops (25 µg/mL) and KX2-4245 (2 nM) were given to the injured eye four times per day. Eyes were evaluated and examined by slit-lamp microscope and underwent PAI on day 0 (pre-op), 2, 4, 6, 8, 10, 12 and 14. Corneal images were taken and analysed automatically with ImageJ software (Wayne Rasband, National Institutes of Health, USA). The corneal vascularised area was measured and presented as mean percentages ± SD.

5.2.5 *In vivo* Toxicity Analysis

Various concentration of KX2-4245 (2 to 12 nM) was topically administered (4 times/day; 50 µL) to the eye for 10 days. At designated time points, the animals were anaesthetised with isoflurane and cornea was stained with topical fluorescein. The eye was subjected to slit-lamp examination with cobalt blue filter. The corneal fluorescein stain where damages on corneal surface will be revealed under a blue light. Moreover, red flex was evaluated with an ophthalmoscope where it provides a general examination to assess the condition of posterior segment. The principle of this technique relies on the transparency of the optical components within the ocular tissues such as cornea, aqueous humor, lens and vitreaous humor. Ocular complication such as cataract and retinal abnormalities require treatment intervention.

5.2.6 Histological Analysis

At the end of the study period, all animals were euthanised, and ocular tissues were obtained for histological analysis. Immediately after enucleation, eyeballs were fixed in paraformaldehyde 4% solution and sectioned for H&E and CD31 analysis.

5.3 Results and Discussion

5.3.1 Cytotoxicity of KX2-4245 on HUVEC and ARPE19

HUVECs and ARPE19 were incubated with various concentrations of KX2-4245 to examine the cytotoxicity profile. Using MTT cell survival/proliferation assay, KX2-4245 inhibited cell growth at concentrations above 2 nM on both cell lines. At concentrations below or at 2 nM, the cells did not show any cytotoxic effect. However, concentrations above 2 nM resulted in cell shrinkage and reduced growth. Therefore, KX2-4245 2 nM was used to examine its anti-angiogenic property in an experimental CNV model.

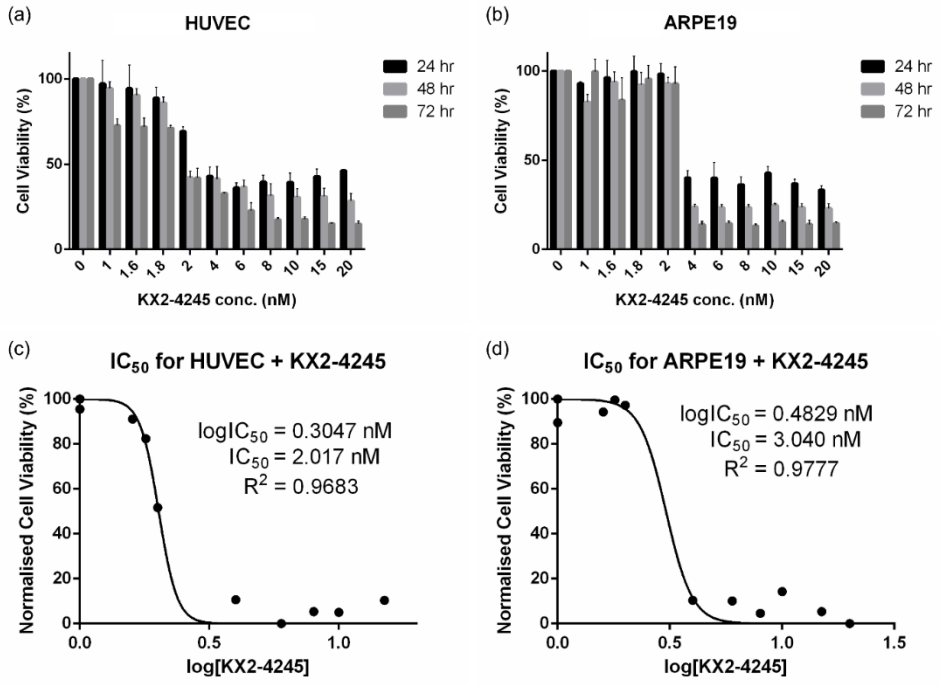

Figure 5.1 Cytotoxicity results of KX2-4245 with different cell lines

(a) Cell viability profile of HUVEC with KX2-4245; (b) Cell viability profile of ARPE19 with KX2-4245; (c) Calculated IC_{50} of KX2-4245 with HUVEC; (d) Calculated IC_{50} of KX2-4245 with ARPE19

5.3.2 Therapeutic Efficacy of KX2-4245 Against *in vivo* CNV Model

In previous studies, the KX2-4245 demonstrated excellent anti-cancer properties in both *in vitro* and *in vivo* experimental cancer models (data not shown). With this regard, the anti-angiogenic effect of KX2-4245 was investigated in an ocular angiogenesis model. The therapeutic efficacy was compared with avastin, a well-known anti-cancer drug that possesses anti-angiogenic properties. Table 5.1 summarised the vascularised area in the rat's cornea after received saline, avastin and KX2-4245.

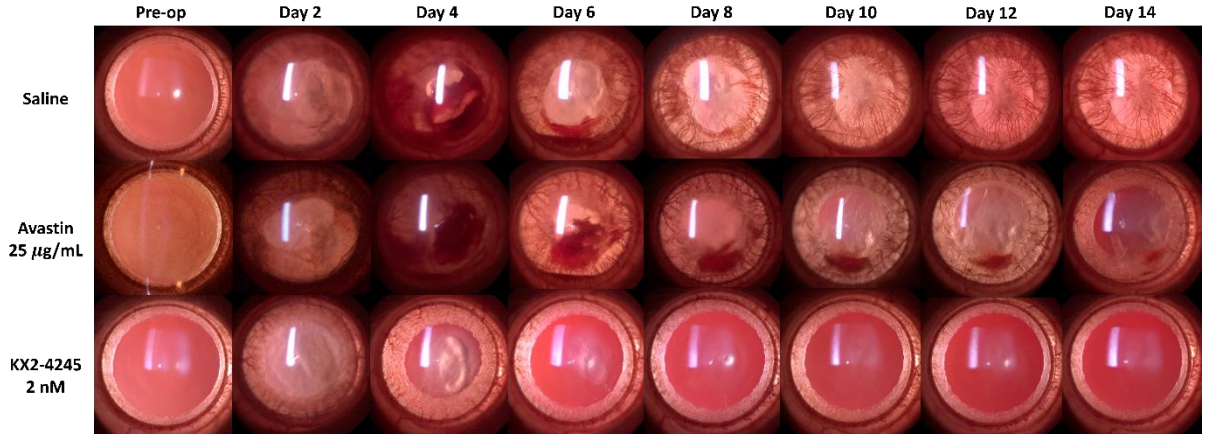

Figure 5.2 Slit-lamp images of rat's cornea treated with KX2-4245 and Avastin eye drops

	Averaged % vascularised areas						
	Day 2	**Day 4**	**Day 6**	**Day 8**	**Day 10**	**Day 12**	**Day 14**
Saline	41.56 ± 2.51	52.26 ± 2.21	53.92 ± 3.19	54.85 ± 2.07	64.95 ± 1.11	74.61 ± 3.31	77.40 ± 2.33
Avastin (25 μg/mL)	23.92 ± 3.86	38.84 ± 2.62	32.06 ± 3.64	31.04 ± 2.82	26.60 ± 3.11	20.11 ± 4.97	15.76 ± 4.11
KX2-4245 (2 nM)	17.07 ± 1.38	9.12 ± 2.14	6.96 ± 0.36	6.17 ± 0.69	2.10 ± 0.21	1.65 ± 0.44	0.95 ± 0.30

Table 5.1 Averaged % vascularised area in rat's cornea received saline, Avastin and KX2-4245

On day 14, the animals that received saline showed substantial growth of blood vessels on the peripheral and centre of the cornea, as shown in Figure 5.2. H&E demonstrated stromal vascularisation and infiltration of inflammatory cells (Figure 5.3). Immunohistochemical assay revealed

immunoreactivity in the stromal region, which indicated the formation of new blood vessels. In contrast, the KX2-4245 significantly inhibited CNV and the vascularised area was markedly reduced with concentration of 2 nM. The H&E staining showed intact stromal structure and reduced inflammatory cell infiltration. Furthermore, no apparent CD31 immunoreactivity was detected. Thus, our data illustrated the anti-angiogenic effect of KX2-4245 with an experimental CNV model.

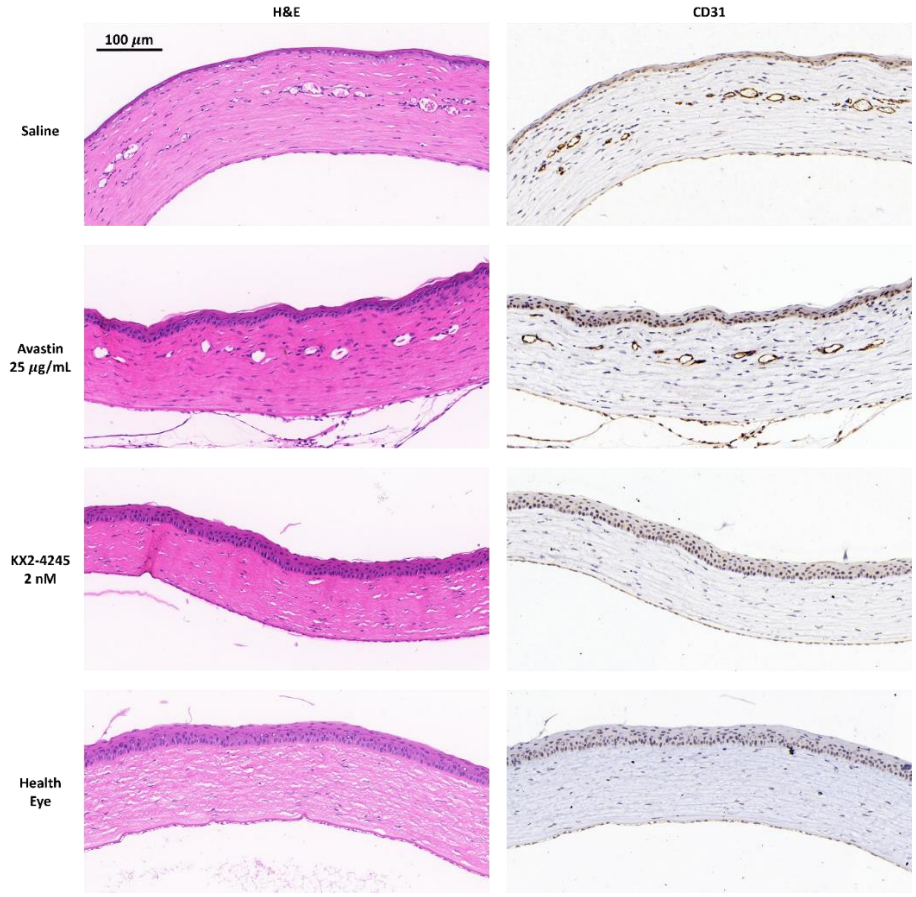

Figure 5.3 Histopathological images of the cornea after receiving KX2-4245 and avastin treatment

H&E (left) and CD31 (right) images revealed anti-angiogenic effect of KX2-4245 treatment effect on Day 14 (scale bar 100 μm for H&E and CD31 image)

The avastin, a VEGF-neutralising antibody, was approved by FDA and has demonstrated clinical usefulness in the treatment of choroidal neovascularisation.[406,407] The drug specifically targets the VEGF signal transduction and thus, ceases VEGF-induced angiogenesis. Apart from choroidal neovascularisation treatment, avastin was also revealed as an effective agent against CNV in clinical settings and experimental animal models.[408,409] In this study, the efficacy of KX2-4245 and avastin eye

drop was compared in an experimental CNV model. The results revealed both medications could reduce and inhibit CNV with KX2-4245 demonstrating superior results. However, avastin might possess a broad anti-VEGF signalling effect which might result in affecting "off-target kinase". Therefore, this results in unexpected side effects on endothelial cells. The KX2-4245 specifically targets FAK which provides an explicit inhibition for angiogenesis.

5.3.3 *In vivo* Corneal Toxicity Assay

Different concentrations of KX2-4245 (ranging from 2 to 12 nM) was topically applied to healthy corneas and they were examined for potential *in vivo* cytotoxicity to corneal epithelial cells. As illustrated in Figure 5.4 – 5.7, the KX2-4245 was well tolerated. Furthermore, no corneal damage can be observed, and red flux also remained normal throughout the study period. These indicated that the corneal surface was intact after receiving KX2-4245 while the posterior segment (i.e. lens, vitreous and retina) remained normal. However, this experiment was only conducted for a short period of time and can only conclude that there is no acute toxicity at this stage. Therefore, a longitudinal study is warranted in the future to examine potential long-term toxicity.

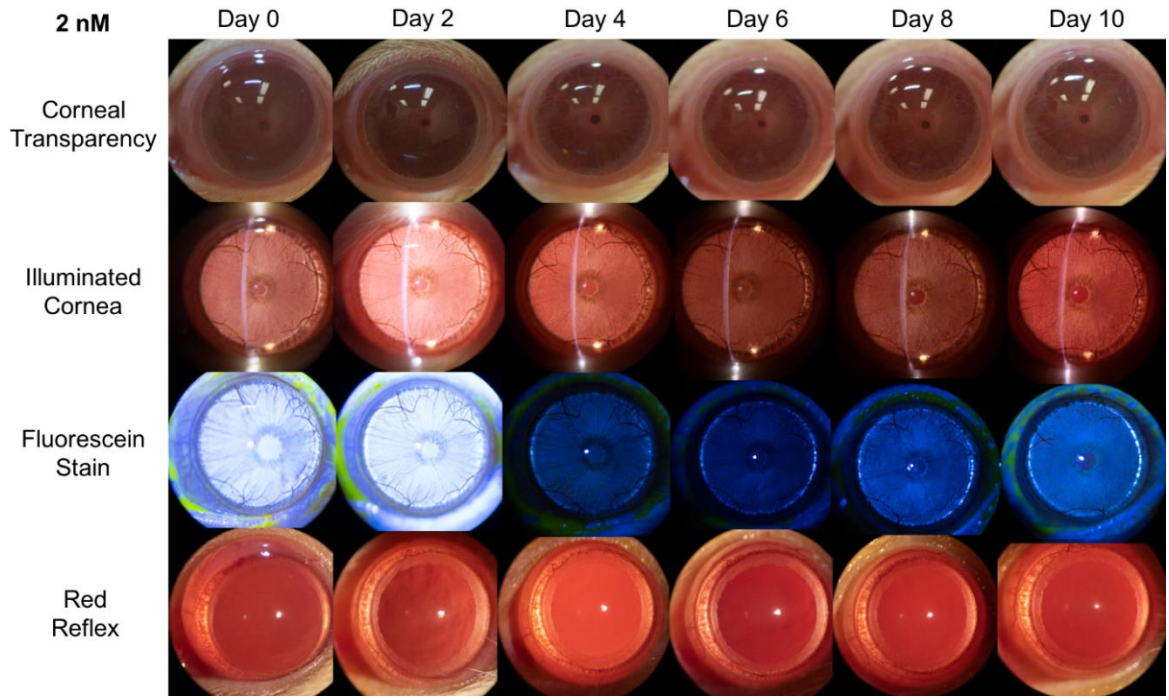

Figure 5.4 *In vivo* toxicity with KX2-4245 (2 nM)

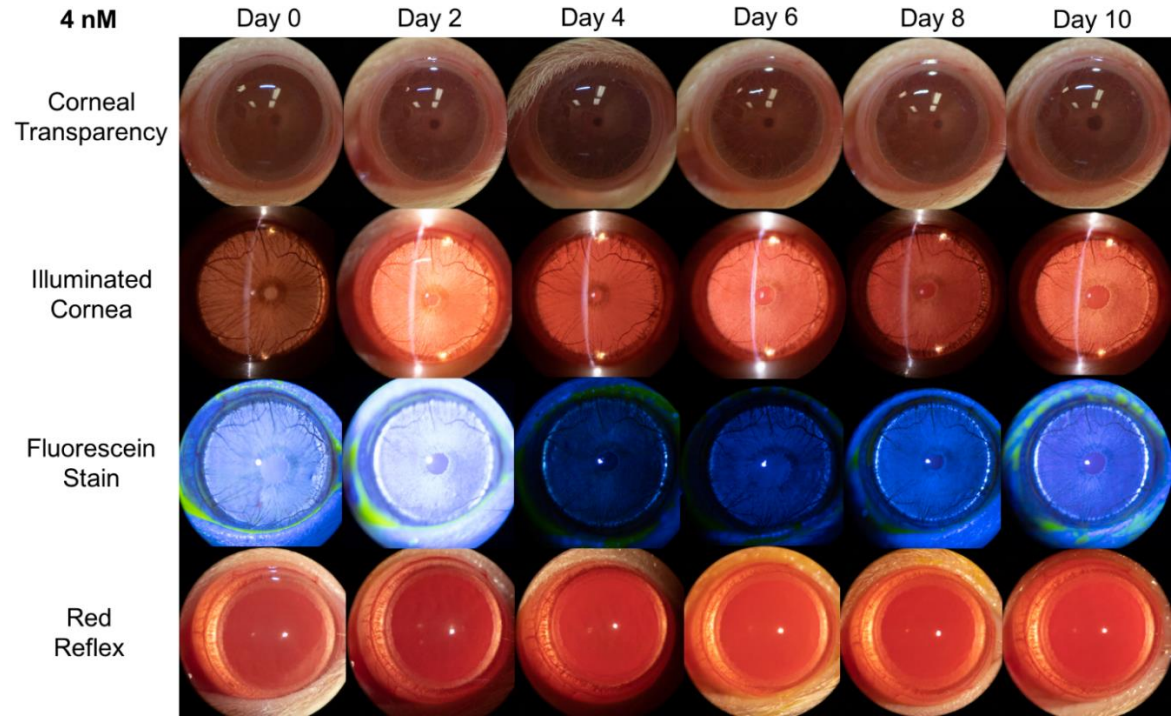

Figure 5.5 *In vivo* toxicity with KX2-4245 (4 nM)

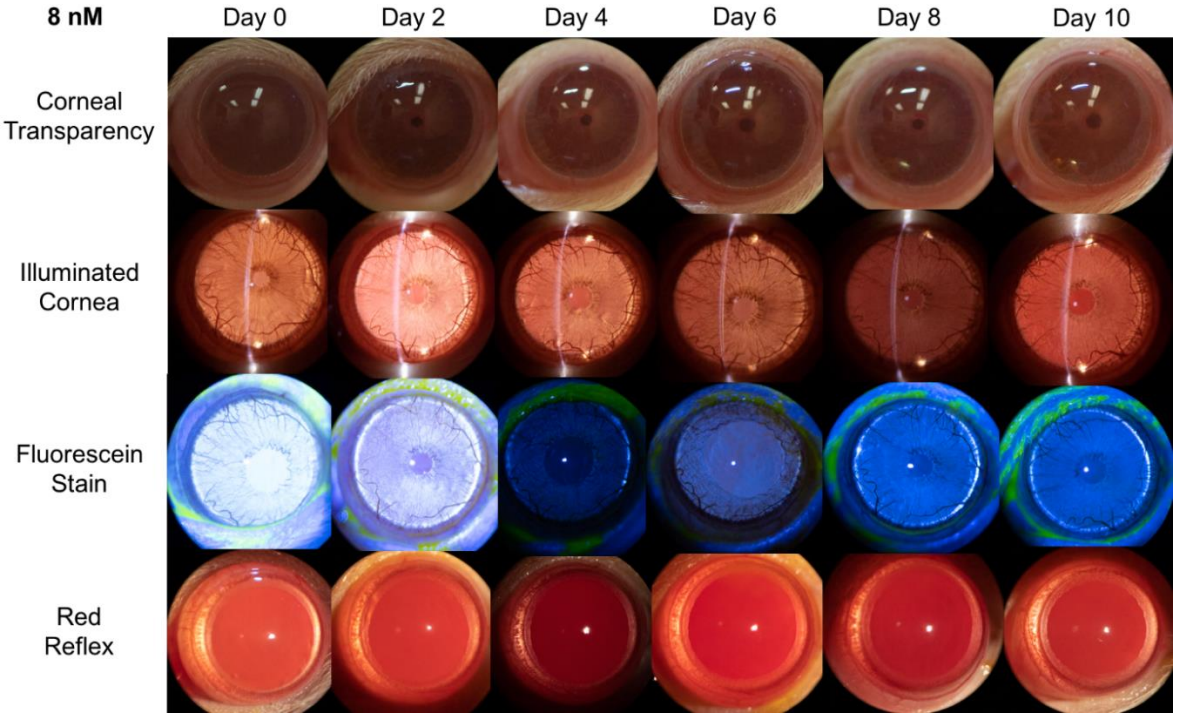

Figure 5.6 *In vivo* toxicity with KX2-4245 (8 nM)

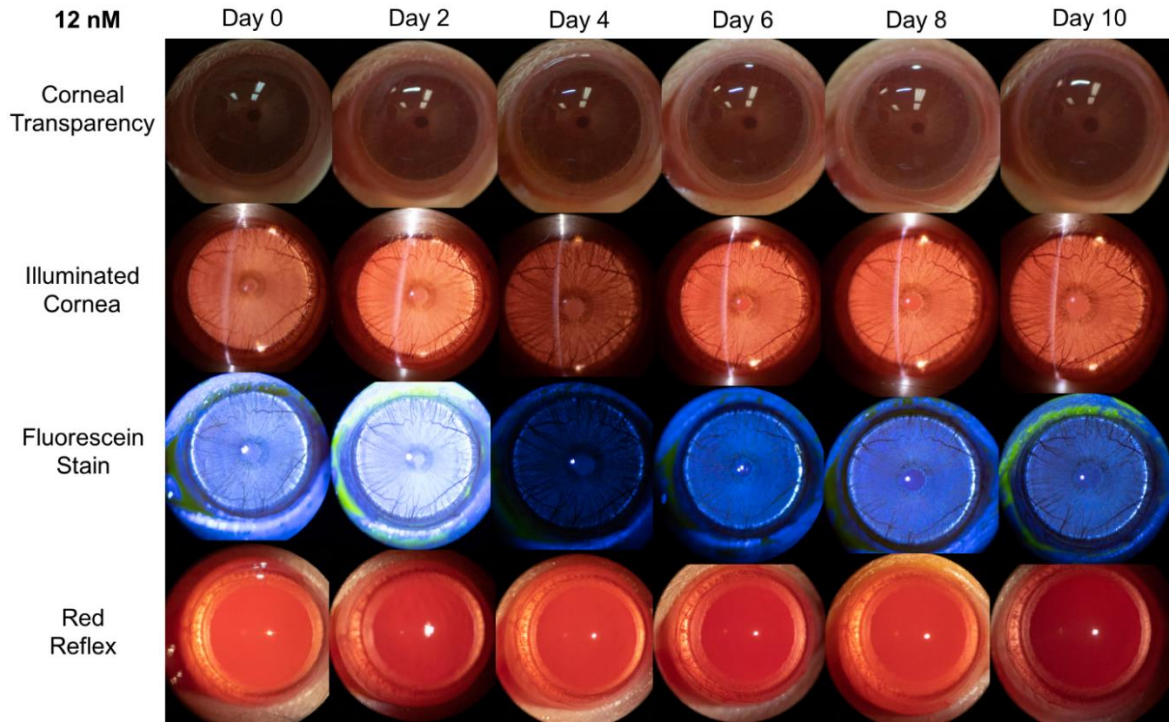

Figure 5.7 *In vivo* toxicity with KX2-4245 (12 nM)

5.4 Conclusion

The present study serves as a first attempt to investigate the efficacy of a newly developed FAK inhibitor for CNV treatment. First, we conducted a cytotoxicity assay to determine an optimal concentration using HUVEC and APRE19. The drug was topically applied to alkali-induced CNV model, which showed outstanding results. We further investigated the preliminary *in vivo* tolerability analysis and discovered that KX2-4245 was well-tolerated. No corneal epithelial damage can be observed even when the concentration was increased by 6-folds. However, the present work requires future *in vitro* analysis to further elucidate the protein expression after KX2-4245 treatment. Regardless, current *in vivo* data provided an encouraging result and served as evidence for its utility in ocular angiogenic diseases.

6 Conclusion and Future Perspective

Accurate diagnosis and effective treatment for ocular diseases are of the utmost importance in clinical settings. However, current clinical diagnosis and treatment options have distinct disadvantages that are yet to be improved. This thesis primarily addressed the issues in current conventional clinical examination modality, administration method and new drug discovery for ocular use.

First, the work in chapter three investigated and studied the potential utility of PAI for objective analysis in an experimental CNV disease model. Using PAI, the data provided a new aspect to present the disease progression through numerical representation. This method offers a few distinct advantages over images obtained from conventional slit-lamp, such as molecular information and non-invasive nature. Through the use of corresponding wavelengths, PAI allowed specific examination of a particular molecular species presented within the organ. Thus, PAI could provide molecular information regarding the disease status that conventional slit-lamp images fail to deliver. Moreover, disease diagnosis with slit-lamp could be subjective to a certain extent. The images quality captured during slit-lamp examination could have an impact on disease diagnosis. Apart from image quality, the corneal curvature makes it hard to capture all blood vessels in one single clear image. Thus, monitoring haemoglobin PA signals with PAI without using exogenous agents provides an objective analysis over conventional slit-lamp images. Therefore, PAI demonstrated detection of haemoglobin PA signals could bypass these obstacles and deliver a more objective analysis for CNV diagnosis. Furthermore, conventional blood vessel examination method requires intravenous injection of chemical dye, whereas PAI relies on natural haemoglobin signals. This reduces the risk of undesired side effects for patients with liver/renal dysfunction. Thus, the non-invasive nature of PAI stands out as a promising tool for future clinical use in the field of ophthalmology.

Secondly, a polymeric nanoparticle drug delivery system with enhanced permeability was developed for ocular drug administration. Topical administration is the most convenient way to administrate ocular drugs to anterior segment. However, the efficacy is generally hampered by the poor absorption profile due to the natural barriers of the cornea as well as other natural defence mechanisms.

Therefore, the work in chapter four developed a CPP-conjugated polymer NP system for CNV treatment. The NPs demonstrated sustained *in vitro* drug release pattern and enhanced cellular uptake. Quantitative analysis with PAI revealed that CPP conjugated NP with FK506 delivered better treatment outcomes compared to free FK506 eye drops. Furthermore, NP formulation also reduced dosing frequency to twice daily, where conventional topical administration requires three to four times daily. Therefore, NP drug delivery system with CPP surface decoration shows enormous potentials in the pharmaceutical industry.

Lastly, chapter five investigated a new drug candidate in CNV treatment through topical administration. The drug, KX2-4245, developed by Kinex Pharmaceuticals has shown outstanding effects in cancer treatment. It specifically targets FAK, which is an important kinase in regulating the angiogenic process. Experiment data showed its capability in demolishing and inhibiting CNV with a concentration of 2 nM. Furthermore, tolerability analysis showed that the KX2-4545 was well-tolerated when applied topically. Despite encouraging results, further experiments are warranted to yield more insights on the impact of KX2-4245 on ocular tissues.

6.1 Future Perspective

This dissertation only explored the surface of PAI technique and polymeric nanoparticle drug delivery system in the corneal angiogenesis model. The potentials underneath these technologies could deliver far more benefits to other ocular diseases, and these areas are yet to be determined. Future work shall focus on utilising PAI to construct a 3D image of corneal angiogenesis model. The PAI technique may also be applied to posterior diseases such as diabetic retinopathy and age-related macular degeneration. These diseases are sight-threatening and involve abnormal growth of blood vessels at the back of the eye where PAI may serve as a non-invasive diagnosis tool. Through 3D PAI image construction, the PAI may potentially map the blood network at the back of the eye. This could assist ophthalmologists to locate problematic area and deliver precise treatment.

Repetitive intraocular injection may be required for those suffer from diabetic retinopathy or age-related macular degeneration. Given the ability to suppress angiogenesis, the KX2-4245 may serve as

potential treatment for ocular diseases that involve pathological angiogenesis. Furthermore, with the current success of NP drug delivery system, future work shall investigate the possibility of encapsulating KX2-4245 into NP drug delivery system to achieve sustained release formulation for ocular diseases. Therefore, the frequency of intraocular injections can be reduced which avoids side effects such as endophthalmitis and cataract.

Finally, further studies are warranted to examine and confirm the molecular mechanism of KX2-4245 in ocular diseases.

7 References

1. Hornof M, Toropainen E, Urtti A. Cell culture models of the ocular barriers. *Eur J Pharm Biopharm*. 2005;60(2):207-225. doi:10.1016/J.EJPB.2005.01.009.

2. Willoughby CE, Ponzin D, Ferrari S, Lobo A, Landau K, Omidi Y. Anatomy and physiology of the human eye: Effects of mucopolysaccharidoses disease on structure and function - a review. *Clin Exp Ophthalmol*. 2010;38(SUPPL. 1):2-11. doi:10.1111/j.1442-9071.2010.02363.x.

3. Govindarajan B, Gipson IK. Membrane-tethered mucins have multiple functions on the ocular surface. *Exp Eye Res*. 2010;90(6):655-663. doi:10.1016/j.exer.2010.02.014.

4. Sridhar MS. Anatomy of cornea and ocular surface. *Indian J Ophthalmol*. 2018;66(2):190-194. doi:10.4103/IJO.IJO_646_17.

5. Hanna C, Bicknell DS, O'brien JE. Cell turnover in the adult human eye. *Arch Ophthalmol*. 1961;65(5):695-698. doi:10.1001/archopht.1961.01840020697016.

6. Wiley L, SundarRaj N, Sun TT, Thoft RA. Regional heterogeneity in human corneal and limbal epithelia: An immunohistochemical evaluation. *Investig Ophthalmol Vis Sci*. 1991;32(3):594-602.

7. Cholkar K, Dasari SR, Pal D, Mitra AK. Eye: anatomy, physiology and barriers to drug delivery. *Ocular Transporters and Receptors: Their Role in Drug Delivery* (2013) doi:10.1533/9781908818317.1.

8. Meek KM, Boote C. The organization of collagen in the corneal stroma. *Exp Eye Res*. 2004;78(3):503-512. doi:10.1016/j.exer.2003.07.003.

9. Anseth A. Studies on corneal polysaccharides: VIII. Changes in the glycosaminoglycans in some human corneal disorders. *Exp Eye Res*. 1969;8(4):438-441. doi:10.1016/S0014-4835(69)80010-2.

10. Mikami T, Kitagawa H. Sulfated glycosaminoglycans: their distinct roles in stem cell biology. *Glycoconj J*. 2017;34(6):725-735. doi:10.1007/s10719-016-9732-9.

11. Borcherding MS, Blacik LJ, Sittig RA, Bizzell JW, Breen M, Weinstein HG. Proteoglycans and collagen fibre organization in human corneoscleral tissue. *Exp Eye Res*. 1975;21(1):59-70. doi:10.1016/0014-4835(75)90057-3.

12. Funderburgh JL. Keratan sulfate: structure, biosynthesis, and function. *Glycobiology*. 2000;10(10):951-958. doi:10.1093/GLYCOB/10.10.951.

13. Puri S, Coulson-Thomas YM, Gesteira TF, Coulson-Thomas VJ. Distribution and function of glycosaminoglycans and proteoglycans in the development, homeostasis and pathology of the ocular surface. *Front Cell Dev Biol*. 2020;8(August). doi:10.3389/fcell.2020.00731.

14. Littlechild SL, Young RD, Caterson B, et al. Keratan sulfate phenotype in the β-1,3-N-acetylglucosaminyltransferase-7-null mouse cornea. *Invest Ophthalmol Vis Sci*. 2018;59(3):1641-1651. doi:10.1167/IOVS.17-22716.

15. Boote C, Dennis S, Newton RH, Puri H, Meek KM. Collagen fibrils appear more closely packed in the prepupillary cornea: Optical and biomechanical implications. *Investig Ophthalmol Vis Sci*. 2003;44(7):2941-2948. doi:10.1167/iovs.03-0131.

16. Saikia P, Medeiros CS, Thangavadivel S, Wilson SE. Basement membranes in the cornea and other organs that commonly develop fibrosis. *Cell Tissue Res*. 2018;374(3):439-453. doi:10.1007/S00441-018-2934-7.

17. Yurchenco P, Patton B. Developmental and pathogenic mechanisms of basement membrane assembly. *Curr Pharm Des*. 2009;15(12):1277-1294. doi:10.2174/138161209787846766.

18. Khoshnoodi J, Pedchenko V, Hudson BG. Mammalian collagen IV. *Microsc Res Tech*. 2008;71(5):357-370. doi:10.1002/JEMT.20564.

19. Miner JH, Yurchenco PD. Laminin functions in tissue morphogenesis. *Annu Rev Cell Dev*

Biol. 2004;20(M):255-284. doi:10.1146/annurev.cellbio.20.010403.094555.

20. Aumailley M, Bruckner-Tuderman L, Carter WG, et al. A simplified laminin nomenclature. *Matrix Biol*. 2005;24(5):326-332. doi:10.1016/j.matbio.2005.05.006.

21. Ho MSP, Böse K, Mokkapati S, Nischt R, Smyth N. Nidogens-extracellular matrix linker molecules. *Microsc Res Tech*. 2008;71(5):387-395. doi:10.1002/jemt.20567.

22. Ettner N, Göhring W, Sasaki T, Mann K, Timpl R. The N-terminal globular domain of the laminin α1 chain binds to α1β1 and α2β1 integrins and to the heparan sulfate-containing domains of perlecan. *FEBS Lett*. 1998;430(3):217-221. doi:10.1016/S0014-5793(98)00601-2.

23. Gordon SR. Fibronectin antibody labels corneal stromal collagen fibrils in situ along their length and circumference and demonstrates distinct staining along the cell and stromal interfaces of descemet's membrane. *Curr Eye Res*. 2014;39(3):312-316. doi:10.3109/02713683.2013.841260.

24. de Oliveira RC, Wilson SE. Descemet's membrane development, structure, function and regeneration. *Exp Eye Res*. 2020;197(February):108090. doi:10.1016/j.exer.2020.108090.

25. Bourne WM. Biology of the corneal endothelium in health and disease. *Eye*. 2003;17(8):912-918. doi:10.1038/sj.eye.6700559.

26. Eghrari AO, Riazuddin SA, Gottsch JD. Overview of the cornea: structure, function, and development. *Prog Mol Biol Transl Sci*. 2015;134:7-23. doi:10.1016/BS.PMBTS.2015.04.001.

27. Joyce NC, Navon SE, Roy S, Zieske JD. Expression of cell cycle-associated proteins in human and rabbit corneal endothelium in situ. *Investig Ophthalmol Vis Sci*. 1996;37(8):1566-1575.

28. Lee P, Wang CC, Adamis AP. Ocular neovascularization: an epidemiologic review. *Surv Ophthalmol*. 1998;43(3):245-269. doi:10.1016/S0039-6257(98)00035-6.

29. Roodhooft JM. Leading causes of blindness worldwide. *Bull Soc Belge Ophtalmol*. 2002;(283):19-25.

30. Feizi S, Azari AA, Safapour S. Therapeutic approaches for corneal neovascularization. *Eye Vis*. 2017;4(1):1-10. doi:10.1186/s40662-017-0094-6.

31. Niederkorn JY. Immune privilege and immune regulation in the eye. *Adv Immunol*. 1990;48:191-226. doi:10.1016/s0065-2776(08)60755-5.

32. Panda A, Vanathi M, Kumar A, Dash Y, Priya S. Corneal graft rejection. *Surv Ophthalmol*. 2007;52(4):375-396. doi:10.1016/j.survophthal.2007.04.008.

33. Faraj LA, Elalfy MS, Said DG, Dua HS. Fine needle diathermy occlusion of corneal vessels. *Br J Ophthalmol*. 2014;98(9):1287-1290. doi:10.1136/bjophthalmol-2014-304891.

34. Gupta D, Illingworth C. Treatments for corneal neovascularization: A review. *Cornea*. 2011;30(8):927-938. doi:10.1097/ICO.0b013e318201405a.

35. Folkman J, Shing Y. Angiogenesis. *J Biol Chem*. 1992;267(16):10931-10934. doi:10.1016/s0021-9258(19)49853-0.

36. Chang JH, Gabison EE, Kato T, Azar DT. Corneal neovascularization. *Curr Opin Ophthalmol*. 2001;12(4):242-249. doi:10.1097/00055735-200108000-00002.

37. Folkman J. Angiogenesis in cancer, vascular, rheumatoid and other disease. *Nat Med*. 1995;1(1):27-30. doi:10.1038/nm0195-27.

38. Kwitko S, Marinho D, Barcaro S, et al. Allograft conjunctival transplantation for bilateral ocular surface disorders. *Ophthalmology*. 1995;102(7):1020-1025. doi:10.1016/S0161-6420(95)30918-9.

39. Ben Ezra D. Neovasculogenesis. Triggering factors and possible mechanisms. *Surv Ophthalmol*. 1979;24(3):167-176. doi:10.1016/0039-6257(79)90020-1.

40. Neufeld G, Cohen T, Gengrinovitch S, Poltorak Z. Vascular endothelial growth factor (VEGF) and its receptors. *FASEB J*. 1999;13(1):9-22. doi:10.1096/FASEBJ.13.1.9.

41. Shibuya M. Vegf-vegfr signals in health and disease. *Biomol Ther*. 2014;22(1):1-9.

doi:10.4062/biomolther.2013.113.

42. Cursiefen C, Chen L, Borges LP, et al. VEGF-A stimulates lymphangiogenesis and hemangiogenesis in inflammatory neovascularization via macrophage recruitment. *J Clin Invest*. 2004;113(7):1040-1050. doi:10.1172/JCI20465.

43. Carmeliet P. VEGF as a key mediator of angiogenesis in cancer. *Oncology*. 2005;69(SUPPL. 3):4-10. doi:10.1159/000088478.

44. Cao Y, Linden P, Farnebo J, et al. Vascular endothelial growth factor C induces angiogenesis in vivo. *Proc Natl Acad Sci U S A*. 1998;95(24):14389-14394. doi:10.1073/pnas.95.24.14389.

45. Takahashi T, Ueno H, Shibuya M. VEGF activates protein kinase C-dependent, but Ras-independent Raf-MEK-MAP kinase pathway for DNA synthesis in primary endothelial cells. *Oncogene*. 1999;18(13):2221-2230. doi:10.1038/sj.onc.1202527.

46. Azar D. Corneal angiogenic privilege: angiogenic and antiangiogenic factors in corneal avascularity, vasculogenesis, and wound healing. *Trans Am Ophthalmol Soc*. 2006;104(2):264-302. http://www.ncbi.nlm.nih.gov/pmc/articles/PMC1809914/.

47. Amano S, Rohan R, Kuroki M, Tolentino M, Adamis AP. Requirement for vascular endothelial growth factor in wound- and inflammation-related corneal neovascularization. *Investig Ophthalmol Vis Sci*. 1998;39(1):18-22.

48. Kvanta A, Sarman S, Fagerholm P, Seregard S, Steen B. Expression of matrix metalloproteinase-2 (MMP-2) and vascular endothelial growth factor (VEGF) in inflammation-associated corneal neovascularization. *Exp Eye Res*. 2000;70(4):419-428. doi:10.1006/exer.1999.0790.

49. Mastyugin V, Mosaed S, Bonazzi A, Dunn MW, Schwartzman ML. Corneal epithelial VEGF and cytochrome P450 4B1 expression in a rabbit model of closed eye contact lens wear. *Curr Eye Res*. 2001;23(1):1-10. doi:10.1076/ceyr.23.1.1.5422.

50. Zheng M, Deshpande S, Lee S, Ferrara N, Rouse BT. Contribution of vascular endothelial growth factor in the neovascularization process during the pathogenesis of herpetic stromal keratitis. *J Virol*. 2001;75(20):9828-9835. doi:10.1128/jvi.75.20.9828-9835.2001.

51. Tammela T, Zarkada G, Wallgard E, et al. Blocking VEGFR-3 suppresses angiogenic sprouting and vascular network formation. *Nature*. 2008;454(7204):656-660. doi:10.1038/nature07083.

52. Cui N, Hu M, Khalil RA. Biochemical and biological attributes of matrix metalloproteinases. *Prog Mol Biol Transl Sci*. 2017;147:1-73. doi:10.1016/BS.PMBTS.2017.02.005.

53. Sivak JM, Fini ME. MMPs in the eye: Emerging roles for matrix metalloproteinases in ocular physiology. *Prog Retin Eye Res*. 2002;21(1):1-14. doi:10.1016/S1350-9462(01)00015-5.

54. Chang JH, Huang YH, Cunningham CM, et al. Matrix metalloproteinase 14 modulates signal transduction and angiogenesis in the cornea. *Surv Ophthalmol*. 2016;61(4):478-497. doi:10.1016/J.SURVOPHTHAL.2015.11.006.

55. Roshandel D, Eslani M, Baradaran-Rafii A, et al. Current and upcoming therapies for corneal neovascularization. *Ocul Surf*. 2018;16(4):398. doi:10.1016/J.JTOS.2018.06.004.

56. Pola R, Ling LE, Silver M, et al. The morphogen Sonic hedgehog is an indirect angiogenic agent upregulating two families of angiogenic growth factors. *Nat Med*. 2001;7(6):706-711. doi:10.1038/89083.

57. Kusano KF, Pola R, Murayama T, et al. Sonic hedgehog myocardial gene therapy: Tissue repair through transient reconstitution of embryonic signaling. *Nat Med*. 2005;11(11):1197-1204. doi:10.1038/nm1313.

58. Renault MA, Roncalli J, Tongers J, et al. Sonic hedgehog induces angiogenesis via Rho kinase-dependent signaling in endothelial cells. *J Mol Cell Cardiol*. 2010;49(3):490-498. doi:10.1016/j.yjmcc.2010.05.003.

59. Laronha H, Caldeira J. Structure and function of human matrix metalloproteinases. *Cells*. 2020;9(5). doi:10.3390/cells9051076.

60. Liu J, Khalil RA. Matrix metalloproteinase inhibitors as investigational and therapeutic tools in unrestrained tissue remodeling and pathological disorders. *Prog Mol Biol Transl Sci*. 2017;148:355-420. doi:10.1016/BS.PMBTS.2017.04.003.

61. Nagase H, Visse R, Murphy G. Structure and function of matrix metalloproteinases and TIMPs. *Cardiovasc Res*. 2006;69(3):562-573. doi:10.1016/j.cardiores.2005.12.002.

62. Amălinei C, Căruntu ID, Bălan RA. Biology of metalloproteinases. *Rom J Morphol Embryol*. 2007;48(4):323-334.

63. Maskos K. Crystal structures of MMPs in complex with physiological and pharmacological inhibitors. *Biochimie*. 2005;87(3-4 SPEC. ISS.):249-263. doi:10.1016/j.biochi.2004.11.019.

64. Tallant C, Marrero A, Gomis-rüth FX. Matrix metalloproteinases : Fold and function of their catalytic domains. *BBA - Mol Cell Res*. 2010;1803(1):20-28. doi:10.1016/j.bbamcr.2009.04.003.

65. Jacobsen JA, Jourden JLM, Miller MT, Cohen SM. To bind zinc or not to bind zinc : An examination of innovative approaches to improved metalloproteinase inhibition. *BBA - Mol Cell Res*. 2010;1803(1):72-94. doi:10.1016/j.bbamcr.2009.08.006.

66. Verma RP, Hansch C. Matrix metalloproteinases (MMPs): Chemical-biological functions and (Q)SARs. *Bioorganic Med Chem*. 2007;15(6):2223-2268. doi:10.1016/j.bmc.2007.01.011.

67. Al-Raawi D, Abu-El-Zahab H, El-Shinawi M, Mohamed MM. Membrane type-1 matrix metalloproteinase (MT1-MMP) correlates with the expression and activation of matrix metalloproteinase-2 (MMP-2) in inflammatory breast cancer. *Int J Clin Exp Med*. 2011;4(4):265-275.

68. Dean RA, Butler GS, Hamma-Kourbali Y, et al. Identification of candidate angiogenic

inhibitors processed by matrix metalloproteinase 2 (MMP-2) in cell-based proteomic Screens: disruption of vascular endothelial growth factor (VEGF)/heparin affin regulatory peptide (pleiotrophin) and VEGF/connective . *Mol Cell Biol*. 2007;27(24):8454-8465. doi:10.1128/mcb.00821-07.

69. Ebrahem Q, Chaurasia SS, Vasanji A, et al. Cross-talk between vascular endothelial growth factor and matrix metalloproteinases in the induction of neovascularization in vivo. *Am J Pathol*. 2010;176(1):496-503. doi:10.2353/AJPATH.2010.080642.

70. Maciag T, Mehlman T, Friesel R, Schreiber AB. Heparin binds endothelial cell growth factor, the principal endothelial cell mitogen in bovine brain. *Science (80-)*. 1984;225(4665):932-935. doi:10.1126/science.6382607.

71. Itoh N, Ornitz DM. Evolution of the Fgf and Fgfr gene families. *Trends Genet*. 2004;20(11):563-569. doi:10.1016/j.tig.2004.08.007.

72. Presta M, Dell'Era P, Mitola S, Moroni E, Ronca R, Rusnati M. Fibroblast growth factor/fibroblast growth factor receptor system in angiogenesis. *Cytokine Growth Factor Rev*. 2005;16(2 SPEC. ISS.):159-178. doi:10.1016/j.cytogfr.2005.01.004.

73. Klagsbrun M. The affinity of fibroblast growth factors (FGFs) for heparin; FGF-heparan sulfate interactions in cells and extracellular matrix. *Curr Opin Cell Biol*. 1990;2(5):857-863. doi:10.1016/0955-0674(90)90084-R.

74. Zhou W, Feng X, Wu Y, Benge J, Zhang Z, Chen Z. FGF-receptor substrate 2 functions as a molecular sensor integrating external regulatory signals into the FGF pathway. *Cell Res*. 2009;19(10):1165-1177. doi:10.1038/cr.2009.95.

75. Francavilla C, Rigbolt KTG, Emdal KB, et al. Functional proteomics defines the molecular switch underlying FGF receptor trafficking and cellular outputs. *Mol Cell*. 2013;51(6):707-722. doi:10.1016/j.molcel.2013.08.002.

76. Huang Z, Marsiglia WM, Roy UB, et al. Two FGF Receptor kinase molecules act in concert to

recruit and transphosphorylate phospholipase Cγ. *Mol Cell*. 2016;61(2):324. doi:10.1016/j.molcel.2016.01.007.

77. Chen M, Bao L, Zhao M, Cao J, Zheng H. Progress in research on the role of FGF in the formation and treatment of corneal neovascularization. *Front Pharmacol*. 2020;11(February):1-6. doi:10.3389/fphar.2020.00111.

78. Presta M, Maier JAM, Rusnati M, Ragnotti G. Basic fibroblast growth factor is released from endothelial extracellular matrix in a biologically active form. *J Cell Physiol*. 1989;140(1):68-74. doi:10.1002/jcp.1041400109.

79. Javerzat S, Auguste P, Bikfalvi A. The role of fibroblast growth factors in vascular development. *Trends Mol Med*. 2002;8(10):483-489. doi:10.1016/S1471-4914(02)02394-8.

80. and Dana RCJL. Inflammatory corneal neovascularization: Etiopathogenesis. *Semin Ophthalmol*. 2011;26(4-5):235-245. doi:10.3109/08820538.2011.588652.

81. Chung ES, Saban DR, Chauhan SK, Dana R. Regulation of blood vessel versus lymphatic vessel growth in the cornea. *Invest Ophthalmol Vis Sci*. 2009;50(4):1613. doi:10.1167/IOVS.08-2212.

82. Kanayama S, Nishida K, Yamato M, et al. Analysis of angiogenesis induced by cultured corneal and oral mucosal epithelial cell sheets in vitro. *Exp Eye Res*. 2007;85(6):772-781. doi:10.1016/j.exer.2007.08.011.

83. Moioli EK, Hong L, Guardado J, Clark PA, Mao JJ. Sustained release of TGFβ3 from PLGA microspheres and its effect on early osteogenic differentiation of human mesenchymal stem cells. *Tissue Eng*. 2006;12(3):537. doi:10.1089/TEN.2006.12.537.

84. Rao RC, Varani J, Soong HK. FGF Promotes corneal stromal fibroblast motility. *J Ocul Pharmacol*. 1992;8(1):77-81. doi:10.1089/jop.1992.8.77.

85. Jeong GL, Kay EDP. FGF-2-induced wound healing in corneal endothelial cells requires

Cdc42 activation and rho inactivation through the phosphatidylinositol 3-kinase pathway. *Investig Ophthalmol Vis Sci*. 2006;47(4):1376-1386. doi:10.1167/iovs.05-1223.

86. Zhu YT, Chen HC, Chen SY, Tseng SCG. Nuclear p120 catenin unlocks mitotic block of contactinhibited human corneal endothelial monolayers without disrupting adherent junctions. *J Cell Sci*. 2012;125(15):3636-3648. doi:10.1242/jcs.103267.

87. Gong L, Ji WK, Hu XH, et al. Sumoylation differentially regulates Sp1 to control cell differentiation. *Proc Natl Acad Sci U S A*. 2014;111(15):5574-5579. doi:10.1073/pnas.1315034111.

88. Xiao O, Xie Z lian, Lin B wu, Yin X fang, Pi R biao, Zhou S you. Minocycline inhibits alkali burn-induced corneal neovascularization in mice. *PLoS One*. 2012;7(7):1-9. doi:10.1371/journal.pone.0041858.

89. Soiberman U, Kambhampati SP, Wu T, et al. Subconjunctival injectable dendrimer-dexamethasone gel for the treatment of corneal inflammation. *Biomaterials*. 2017;125:38-53. doi:10.1016/j.biomaterials.2017.02.016.

90. Shahriary A, Sabzevari-Ghahfarokhi M, Jadidi K, Yazdani F, Aghamollaei H. The role of inflammatory cytokines in neovascularization of chemical ocular injury. *Ocul Immunol Inflamm*. 2021;0(0):1-13. doi:10.1080/09273948.2020.1870148.

91. Cade F, Paschalis EI, Regatieri C V., Vavvas DG, Dana R, Dohlman CH. Alkali burn to the eye: Protection using TNF-α inhibition. *Cornea*. 2014;33(4):382-389. doi:10.1097/ICO.0000000000000071.

92. Saika S, Miyamoto T, Yamanaka O, et al. Therapeutic effect of topical administration of SN50, an inhibitor of nuclear factor-κB, in treatment of corneal alkali burns in mice. *Am J Pathol*. 2005;166(5):1393-1403. doi:10.1016/S0002-9440(10)62357-7.

93. Verstrepen L, Bekaert T, Chau TL, Tavernier J, Chariot A, Beyaert R. TLR-4, IL-1R and TNF-R signaling to NF-kappaB: variations on a common theme. *Cell Mol Life Sci*.

2008;65(19):2964-2978. doi:10.1007/s00018-008-8064-8.

94. Vandenabeele P, Declercq W, Van Herreweghe F, Berghe T Vanden. The role of the kinases RIP1 and RIP3 in TNF-induced necrosis. *Sci Signal*. 2010;3(115). doi:10.1126/scisignal.3115re4.

95. Shimizu H, Sakimoto T, Yamagami S. Pro-inflammatory role of NLRP3 inflammasome in experimental sterile corneal inflammation. *Sci Rep*. 2019;9(1). doi:10.1038/s41598-019-46116-9.

96. Bian F, Xiao Y, Zaheer M, et al. Inhibition of NLRP3 inflammasome pathway by butyrate improves corneal wound healing in corneal alkali burn. *Int J Mol Sci*. 2017;18(3). doi:10.3390/ijms18030562.

97. Yamada J, Dana MR, Sotozono C, Kinoshita S. Local suppression of IL-1 by receptor antagonist in the rat model of corneal alkali injury. *Exp Eye Res*. 2003;76(2):161-167. doi:10.1016/S0014-4835(02)00293-2.

98. Dana MR, Zhu SN, Yamada J. Topical modulation of interleukin-1 activity in corneal neovascularization. *Cornea*. 1998;17(4):403-409. doi:10.1097/00003226-199807000-00011.

99. Nakao S, Hata Y, Miura M, et al. Dexamethasone inhibits interleukin-1β-induced corneal neovascularization: Role of nuclear factor-κB-activated stromal cells in inflammatory angiogenesis. *Am J Pathol*. 2007;171(3):1058-1065. doi:10.2353/ajpath.2007.070172.

100. Ebihara N, Matsuda A, Nakamura S, Matsuda H, Murakami A. Role of the IL-6 classic-and trans-signaling pathways in corneal sterile inflammation and wound healing. *Investig Ophthalmol Vis Sci*. 2011;52(12):8549-8557. doi:10.1167/iovs.11-7956.

101. Sakimoto T, Sugaya S, Ishimori A, Sawa M. Anti-inflammatory effect of IL-6 receptor blockade in corneal alkali burn. *Exp Eye Res*. 2012;97(1):98-104. doi:10.1016/j.exer.2012.02.015.

102. Balla MMS, Desai S, Purwar P, et al. Differential diagnosis of lung cancer, its metastasis and chronic obstructive pulmonary disease based on serum Vegf, Il-8 and MMP-9. *Sci Rep*. 2016;6(May):6-12. doi:10.1038/srep36065.

103. Wang Z, Yang Y, Yang H, et al. NF-κB feedback control of JNK1 activation modulates TRPV1- induced increases in IL-6 and IL-8 release by human corneal epithelial cells. *Mol Vis*. 2011;17:3137-3146.

104. Sharif Z, Sharif W. Corneal neovascularization: updates on pathophysiology, investigations & management. *Rom J Ophthalmol*. 2019;63(1):15-22.

105. Feizi S. Corneal angiogenesis: Etiologies, complications, and management. *Physiol Pathol Angiogenes - Signal Mech Target Ther*. 2017. doi:10.5772/66713.

106. Kim TI, Kim SW, Kim S, Kim T, Kim EK. Inhibition of experimental corneal neovascularization by using subconjunctival injection of bevacizumab (Avastin). *Cornea*. 2008;27(3):349-352. doi:10.1097/ICO.0b013e31815cf67d.

107. Kirwan RP, Zheng Y, Tey A, Anijeet D, Sueke H, Kaye SB. Quantifying changes in corneal neovascularization using fluorescein and indocyanine green angiography. *Am J Ophthalmol*. 2012;154(5):850-858.e2. doi:10.1016/j.ajo.2012.04.021.

108. Anijeet DR, Zheng Y, Tey A, Hodson M, Sueke H, Kaye SB. Imaging and evaluation of corneal vascularization using fluorescein and indocyanine green angiography. *Investig Ophthalmol Vis Sci*. 2012;53(2):650-658. doi:10.1167/iovs.11-8014.

109. Kwan ASL, Barry C, McAllister IL, Constable I. Fluorescein angiography and adverse drug reactions revisited: The Lions Eye experience. *Clin Exp Ophthalmol*. 2006;34(1):33-38. doi:10.1111/j.1442-9071.2006.01136.x.

110. Hope-Ross M, Yannuzzi LA, Gragoudas ES, et al. Adverse reactions due to indocyanine green. *Ophthalmology*. 1994;101(3):529-533. doi:10.1016/S0161-6420(94)31303-0.

111. Steger B, Romano V, Kaye SB. Corneal Indocyanine green angiography to guide medical and surgical management of corneal neovascularization. *Cornea*. 2016;35(1):41-45. doi:10.1097/ICO.0000000000000683.

112. Cursiefen C, Hofmann-Rummelt C, Küchle M, Schlötzer-Schrehardt U. Pericyte recruitment in human corneal angiogenesis: An ultrastructural study with clinicopathological correlation. *Br J Ophthalmol*. 2003;87(1):101-106. doi:10.1136/bjo.87.1.101.

113. Ahuja OP, Nema H V. Experimental corneal vascularization and its management. *Am J Ophthalmol*. 1966;62(4):707-710. doi:10.1016/0002-9394(66)92199-4.

114. Mahoney JM, Waterbury LD. Drug effects on the neovascularization response to silver nitrate cauterization of the rat cornea. *Curr Eye Res*. 1985;4(5):531-535. doi:10.3109/02713688508999984.

115. Jones IS, Meyer K. Inhibition of vascularization of the rabbit cornea by local application of cortisone. *Proc Soc Exp Biol Med*. 1950;74(1):102-104. doi:10.3181/00379727-74-17822.

116. Mcdonald PR, Leopold IH, Vogel AW, Mulberger RD. Hydrocortisone (compound F) in ophthalmology; clinical and experimental studies. *AMA Arch Ophthalmol*. 1953;49(4):400-412. doi:10.1001/ARCHOPHT.1953.00920020410004.

117. Michaelson IC, Gluecker L, Stieglitz E. Influence of low-voltage x-radiation on inhibition and prevention of new vessels in cornea; comparison with influence of cortisone. *AMA Arch Ophthalmol*. 1954;52(1):77-84. doi:10.1001/ARCHOPHT.1954.00920050079009.

118. Dana MR, Streilein JW. Loss and restoration of immune privilege in eyes with corneal neovascularization. *Investig Ophthalmol Vis Sci*. 1996;37(12):2485-2494.

119. Phillips K, Cintron C, Kenyon KR, et al. Effects of prednisolone and medroxyprogesterone on corneal wound healing, ulceration, and neovascularization. *Arch Ophthalmol*. 1983;101(4):640-643. doi:10.1001/archopht.1983.01040010640024.

120. Robin JB, Regis Pacheco LF, Kash RL, Schanzlin DJ. The histopathology of corneal neovascularization: Inhibitor effects. *Arch Ophthalmol*. 1985;103(2):284-287. doi:10.1001/archopht.1985.01050020136037.

121. Murata M, Shimizu S, Horiuchi S, Taira M. Inhibitory effect of triamcinolone acetonide on corneal neovascularization. *Graefes Arch Clin Exp Ophthalmol*. 2006;244(2):205-209. doi:10.1007/S00417-005-0036-1.

122. Fromer CH, Klintworth GK. An evaluation of the role of leukocytes in the pathogenesis of experimentally induced corneal vascularization. II. Studies on the effect of leukocytic elimination on corneal vascularization. *Am J Pathol*. 1975;81(3):531-544.

123. Schleimer RP, Freeland HS, Peters SP, Brown KE, Derse CP. An assessment of the effects of glucocorticoids on degranulation, chemotaxis, binding to vascular endothelium and formation of leukotriene B4 by purified human neutrophils. *J Pharmacol Exp Ther*. 1989;250(2).

124. Ebrabem Q, Minamoto A, Hoppe G, Anand-Apte B, Sears JE. Triamcinolone acetonide inhibits IL-6- and VEGF-induced angiogenesis downstream of the IL-6 and VEGF receptors. *Investig Ophthalmol Vis Sci*. 2006;47(11):4935-4941. doi:10.1167/iovs.05-1651.

125. Besedovsky H, Del Rey A, Sorkin E, Dinarello CA. Immunoregulatory feedback between interleukin-1 and glucocorticoid hormones. *Science*. 1986;233(4764):652-654. doi:10.1126/SCIENCE.3014662.

126. Beutler B, Krochin N, Milsark IW, Luedke C, Cerami A. Control of cachectin (tumor necrosis factor) synthesis: mechanisms of endotoxin resistance. *Science*. 1986;232(4753):977-980. doi:10.1126/SCIENCE.3754653.

127. Hori Y, Hu DE, Yasui K, Smither RL, Gresham GA, Fan TPD. Differential effects of angiostatic steroids and dexamethasone on angiogenesis and cytokine levels in rat sponge implants. *Br J Pharmacol*. 1996;118(7):1584-1591. doi:10.1111/j.1476-5381.1996.tb15578.x.

128. Snyder DS, Unanue ER. Corticosteroids inhibit murine macrophage Ia expression and

interleukin 1 production. *J Immunol*. 1982;129(5):1803-1805. http://www.ncbi.nlm.nih.gov/pubmed/6811653.

129. Waage A, Slupphaug G, Shalaby R. Glucocorticoids inhibit the production of IL 6 from monocytes, endothelial cells and fibroblasts. *Eur J Immunol*. 1990;20(11):2439-2443. doi:10.1002/eji.1830201112.

130. Aydin E, Kivilcim M, Peyman GA, Esfahani MR, Kazi AA, Sanders DR. Inhibition of experimental angiogenesis of cornea by various doses of doxycycline and combination of triamcinolone acetonide with low-molecular-weight heparin and doxycycline. *Cornea*. 2008;27(4):446-453. doi:10.1097/ICO.0B013E3181605FF9.

131. Folkman J, Weisz PB, Joullié MM, Li WW, Ewing WR. Control of angiogenesis with synthetic heparin substitutes. *Science (80-).* 1989;243(4897):1490-1493. doi:10.1126/science.2467380.

132. Lepri A, Benelli U, Bernardini N, et al. Effect of low molecular weight heparan sulphate on angiogenesis in the rat cornea after chemical cauterization. *J Ocul Pharmacol*. 1994;10(1):273-280. doi:10.1089/jop.1994.10.273.

133. Tommila P, Summanen P, Tervo T. Cortisone, heparin and argon laser in the treatment of corneal neovascularization. *Acta Ophthalmol*. 1987;65(182 S):89-92. doi:10.1111/j.1755-3768.1987.tb02600.x.

134. Li WW, Casey R, Gonzalez EM, Folkman J. Angiostatic steroids potentiated by sulfated cyclodextrins inhibit corneal neovascularization. *Investig Ophthalmol Vis Sci*. 1991;32(11):2898-2905.

135. Ingber DE, Madri JA, Folkman J. A possible mechanism for inhibition of angiogenesis by angiostatic steroids: Induction of capillary basement membrane dissolution. *Endocrinology*. 1986;119(4):1768-1775. doi:10.1210/endo-119-4-1768.

136. Blei F, Wilson EL, Mignatti P, Rifkin DB. Mechanism of action of angiostatic steroids:

Suppression of plasminogen activator activity via stimulation of plasminogen activator inhibitor synthesis. *J Cell Physiol*. 1993;155(3):568-578. doi:10.1002/jcp.1041550315.

137. Al-Torbak A, Al-Amri A, Wagoner MD. Deep corneal neovascularization after implantation with intrastromal corneal ring segments. *Am J Ophthalmol*. 2005;140(5):926-927. doi:10.1016/j.ajo.2005.05.020.

138. Masferrer JL, Koki A, Seibert K. COX-2 inhibitors. A new class of antiangiogenic agents. In: *Annals of the New York Academy of Sciences*. Vol 889. Ann N Y Acad Sci; 1999:84-86. doi:10.1111/j.1749-6632.1999.tb08726.x.

139. Yamada M, Kawai M, Kawai Y, Mashima Y. The effect of selective cyclooxygenase-2 inhibitor on corneal angiogenesis in the rat. *Curr Eye Res*. 1999;19(4):300-304. doi:10.1076/CEYR.19.4.300.5301.

140. Castro MR, Lutz D, Edelman JL. Effect of COX inhibitors on VEGF-induced retinal vascular leakage and experimental corneal and choroidal neovascularization. *Exp Eye Res*. 2004;79(2):275-285. doi:10.1016/J.EXER.2004.04.008.

141. Deutsch TA, Hughes WF. Suppressive effects of indomethacin on thermally induced neovascularization of rabbit corneas. *Am J Ophthalmol*. 1979;87(4):536-540. doi:10.1016/0002-9394(79)90245-9.

142. Takahashi K, Saishin Y, Saishin Y, et al. Topical nepafenac inhibits ocular neovascularization. *Invest Ophthalmol Vis Sci*. 2003;44(1):409-415. doi:10.1167/IOVS.02-0346.

143. BenEzra D. Neovasculogenic ability of prostaglandins, growth factors, and synthetic chemoattractants. *Am J Ophthalmol*. 1978;86(4):455-461. doi:10.1016/0002-9394(78)90289-1.

144. Frucht J, Zauberman H. Topical indomethacin effect on neovascularisation of the cornea and on prostaglandin E2 levels. *Br J Ophthalmol*. 1984;68(9):656-659. doi:10.1136/BJO.68.9.656.

145. Ueda M, Sugatani J, Unezaki S, et al. Involvement of prostaglandin E2 in rabbit corneal injury

by anterior segment ischaemia. *Prostaglandins Leukot Essent Fatty Acids*. 1997;57(3):285-291. doi:10.1016/S0952-3278(97)90546-9.

146. Duffin RM, Weissman BA, Glasser DB, Pettit TH. Flurbiprofen in the treatment of corneal neovascularization induced by contact lenses. *Am J Ophthalmol*. 1982;93(5):607-614. doi:10.1016/S0002-9394(14)77376-3.

147. Peyman GA, Kazi AA, Riazi-Esfahani M, Aydin E, Kivilcim M, Sanders DR. The effect of combinations of flurbiprofen, low molecular weight heparin, and doxycycline on the inhibition of corneal neovascularization. *Cornea*. 2006;25(5):582-585. doi:10.1097/01.ICO.0000220767.73660.3A.

148. Congdon NG, Schein OD, Von Kulajta P, Lubomski LH, Gilbert D, Katz J. Corneal complications associated with topical ophthalmic use of nonsteroidal antiinflammatory drugs. *J Cataract Refract Surg*. 2001;27(4):622-631. doi:10.1016/S0886-3350(01)00801-X.

149. Flach AJ, Lemp MA, Shine O. Corneal melts associated with topically applied nonsteroidal anti-inflammatory drugs. *Trans Am Ophthalmol Soc*. 2001;99:205. /pmc/articles/PMC1359011/?report=abstract. Accessed June 27, 2022.

150. Guidera AC, Luchs JI, Udell IJ. Keratitis, ulceration, and perforation associated with topical nonsteroidal anti-inflammatory drugs. *Ophthalmology*. 2001;108(5):936-944. doi:10.1016/S0161-6420(00)00538-8.

151. Nirankari VS, Baer JC. Corneal argon laser photocoagulation for neovascularization in penetrating keratoplasty. *Ophthalmology*. 1986;93(10):1304-1309. doi:10.1016/S0161-6420(86)33581-4.

152. Pytowski B, Goldman J, Persaud K, et al. Complete and specific inhibition of adult lymphatic regeneration by a novel VEGFR-3 neutralizing antibody. *J Natl Cancer Inst*. 2005;97(1):14-21. doi:10.1093/JNCI/DJI003.

153. Witte L, Hicklin DJ, Zhu Z, et al. Monoclonal antibodies targeting the VEGF receptor-2

(Flk1/KDR) as an anti-angiogenic therapeutic strategy. *Cancer Metastasis Rev*. 1998;17(2):155-161. doi:10.1023/A:1006094117427.

154. Aiello LP, Pierce EA, Foley ED, et al. Suppression of retinal neovascularization in vivo by inhibition of vascular endothelial growth factor (VEGF) using soluble VEGF-receptor chimeric proteins. *Proc Natl Acad Sci U S A*. 1995;92(23):10457-10461. doi:10.1073/PNAS.92.23.10457.

155. Chang JH, Garg NK, Lunde E, Han KY, Jain S, Azar DT. Corneal neovascularization: An anti-VEGF therapy review. *Surv Ophthalmol*. 2012;57(5):415. doi:10.1016/J.SURVOPHTHAL.2012.01.007.

156. Reed JW, Fromer C, Klintworth GK. Induced corneal vascularization remission with argon laser therapy. *Arch Ophthalmol (Chicago, Ill 1960)*. 1975;93(10):1017-1019. doi:10.1001/ARCHOPHT.1975.01010020797012.

157. Ferrara N, Hillan KJ, Novotny W. Bevacizumab (Avastin), a humanized anti-VEGF monoclonal antibody for cancer therapy. *Biochem Biophys Res Commun*. 2005;333(2):328-335. doi:10.1016/J.BBRC.2005.05.132.

158. Chévez-Barrios P. Are we getting closer to prevention and treatment of corneal neovascularization? *Clin Experiment Ophthalmol*. 2007;35(8):689-690. doi:10.1111/J.1442-9071.2007.01616.X.

159. Bock F, König Y, Kruse F, Baier M, Cursiefen C. Bevacizumab (Avastin) eye drops inhibit corneal neovascularization. *Graefes Arch Clin Exp Ophthalmol*. 2008;246(2):281-284. doi:10.1007/S00417-007-0684-4.

160. Dastjerdi MH, Al-Arfaj KM, Nallasamy N, et al. Topical bevacizumab in the treatment of corneal neovascularization: results of a prospective, open-label, noncomparative study. *Arch Ophthalmol (Chicago, Ill 1960)*. 2009;127(4):381-389. doi:10.1001/ARCHOPHTHALMOL.2009.18.

161. DeStafeno JJ, Kim T. Topical bevacizumab therapy for corneal neovascularization. *Arch Ophthalmol (Chicago, Ill 1960)*. 2007;125(6):834-836. doi:10.1001/ARCHOPHT.125.6.834.

162. Awadein A. Subconjunctival bevacizumab for vascularized rejected corneal grafts. *J Cataract Refract Surg*. 2007;33(11):1991-1993. doi:10.1016/J.JCRS.2007.07.012.

163. Carrasco MA. Subconjunctival bevacizumab for corneal neovascularization in herpetic stromal keratitis. *Cornea*. 2008;27(6):743-745. doi:10.1097/QAI.0B013E31815B833A.

164. You IC, Kang IS, Lee SH, Yoon KC. Therapeutic effect of subconjunctival injection of bevacizumab in the treatment of corneal neovascularization. *Acta Ophthalmol*. 2009;87(6):653-658. doi:10.1111/J.1755-3768.2008.01399.X.

165. MacKenzie SE, Tucker WR, Poole TRG. Bevacizumab (avastin) for corneal neovascularization--corneal light shield soaked application. *Cornea*. 2009;28(2):246-247. doi:10.1097/ICO.0B013E3181861CC9.

166. Bahar I, Kaiserman I, McAllum P, Rootman D, Slomovic A. Subconjunctival bevacizumab injection for corneal neovascularization in recurrent pterygium. *Curr Eye Res*. 2008;33(1):23-28. doi:10.1080/02713680701799101.

167. Yoeruek E, Spitzer MS, Tatar O, Aisenbrey S, Bartz-Schmidt KU, Szurman P. Safety profile of bevacizumab on cultured human corneal cells. *Cornea*. 2007;26(8):977-982. doi:10.1097/ICO.0B013E3180DE1D0A.

168. Jo N, Mailhos C, Ju M, et al. Inhibition of platelet-derived growth factor B signaling enhances the efficacy of anti-vascular endothelial growth factor therapy in multiple models of ocular neovascularization. *Am J Pathol*. 2006;168(6):2036-2053. doi:10.2353/AJPATH.2006.050588.

169. Mwaikambo BR, Sennlaub F, Ong H, Chemtob S, Hardy P. Activation of CD36 inhibits and induces regression of inflammatory corneal neovascularization. *Invest Ophthalmol Vis Sci*. 2006;47(10):4356-4364. doi:10.1167/IOVS.05-1656.

170. Fernando NH, Hurwitz HI. Targeted therapy of colorectal cancer: clinical experience with bevacizumab. *Oncologist*. 2004;9 Suppl 1(S1):11-18. doi:10.1634/THEONCOLOGIST.9-SUPPL_1-11.

171. Kabbinavar F, Hurwitz HI, Fehrenbacher L, et al. Phase II, randomized trial comparing bevacizumab plus fluorouracil (FU)/leucovorin (LV) with FU/LV alone in patients with metastatic colorectal cancer. *J Clin Oncol*. 2003;21(1):60-65. doi:10.1200/JCO.2003.10.066.

172. Hernández GL, Volpert O V., Íñiguez MA, et al. Selective inhibition of vascular endothelial growth factor-mediated angiogenesis by cyclosporin A: roles of the nuclear factor of activated T cells and cyclooxygenase 2. *J Exp Med*. 2001;193(5):607-620. doi:10.1084/JEM.193.5.607.

173. Bucak YY, Erdurmus M, Terzi EH, Kükner A, Çelebi S. Inhibitory effects of topical cyclosporine A 0.05% on immune-mediated corneal neovascularization in rabbits. *Graefes Arch Clin Exp Ophthalmol*. 2013;251(11):2555-2561. doi:10.1007/S00417-013-2467-4.

174. Baroja-Mazo A, Revilla-Nuin B, Ramírez P, Pons JA. Immunosuppressive potency of mechanistic target of rapamycin inhibitors in solid-organ transplantation. *World J Transplant*. 2016;6(1):183. doi:10.5500/WJT.V6.I1.183.

175. Gidfar S, Milani FY, Milani BY, et al. Rapamycin prolongs the survival of corneal epithelial cells in culture. *Sci Rep*. 2017;7. doi:10.1038/SREP40308.

176. Shin YJ, Hyon JY, Choi WS, et al. Chemical injury-induced corneal opacity and neovascularization reduced by rapamycin via TGF-β1/ERK pathways regulation. *Invest Ophthalmol Vis Sci*. 2013;54(7):4452-4458. doi:10.1167/IOVS.13-11684.

177. Çakmak H, Ergin K, Bozkurt G, Kocatürk T, Evliçoılu GE. The effects of topical everolimus and sunitinib on corneal neovascularization. *Cutan Ocul Toxicol*. 2016;35(2):97-103. doi:10.3109/15569527.2015.1034360.

178. Sari ES, Yazici A, Aksit H, et al. Inhibitory effect of sub-conjunctival tocilizumab on alkali burn induced corneal neovascularization in rats. *Curr Eye Res*. 2015;40(1):48-55.

doi:10.3109/02713683.2014.914541.

179. Marsh RJ. Argon laser treatment of lipid keratopathy. *Br J Ophthalmol*. 1988;72(12):900. doi:10.1136/BJO.72.12.900.

180. Peter J, Fraenkel G, Goggin M, Drew A. Fluorescein angiographic monitoring of corneal vascularization in lipid keratopathy. *Clin Experiment Ophthalmol*. 2004;32(1):78-80. doi:10.1046/J.1442-9071.2004.00764.X.

181. Gerten G. Bevacizumab (avastin) and argon laser to treat neovascularization in corneal transplant surgery. *Cornea*. 2008;27(10):1195-1199. doi:10.1097/ICO.0B013E318180E50F.

182. Sharma A, Samal A, Narang S, Gutpa A, Ram J, Gupta A. Frequency doubled Nd :YAG (532 nm) laser photocoagulation in corneal vascularisation : Efficacy and time sequenced changes. *Indian J Ophthalmol*. 2001;49(4):235.

183. Parsa CF, Temprano J, Wilson D, Green WR. Hemorrhage complicating YAG laser feeder vessel coagulation of cornea vascularization. *Cornea*. 1994;13(3):264-268. doi:10.1097/00003226-199405000-00013.

184. Pillai CT, Dua HS, Hossain P. Fine Needle Diathermy occlusion of corneal vessels. *Invest Ophthalmol Vis Sci*. 2000;41(8):2148-2153.

185. Koenig Y, Bock F, Kruse FE, Stock K, Cursiefen C. Angioregressive pretreatment of mature corneal blood vessels before keratoplasty: fine-needle vessel coagulation combined with anti-VEGFs. *Cornea*. 2012;31(8):887-892. doi:10.1097/ICO.0B013E31823F8F7A.

186. Xia J, Yao J, Wang L V. Photoacoustic tomography: principles and advances. *Electromagn waves (Cambridge, Mass)*. 2014;147:1. doi:10.2528/PIER14032303.

187. Lengenfelder B, Mehari F, Hohmann M, et al. Remote photoacoustic sensing using speckle-analysis. *Sci Reports*. 2019;9(1):1-11. doi:10.1038/s41598-018-38446-x.

188. Wang L V., Hu S. Photoacoustic tomography: In vivo imaging from organelles to organs.

Science. 2012;335(6075):1458-1462. doi:10.1126/SCIENCE.1216210.

189. Luke GP, Yeager D, Emelianov SY. Biomedical applications of photoacoustic imaging with exogenous contrast agents. *Ann Biomed Eng*. 2012;40(2):422-437. doi:10.1007/s10439-011-0449-4.

190. Wu D, Huang L, Jiang MS, Jiang H. Contrast agents for photoacoustic and thermoacoustic imaging: A review. *Int J Mol Sci*. 2014;15(12):23616-23639. doi:10.3390/IJMS151223616.

191. Weber J, Beard PC, Bohndiek SE. Contrast agents for molecular photoacoustic imaging. *Nat Publ Gr*. 2016;13(8):639-650. doi:10.1038/nmeth.3929.

192. Stoffels I, Morscher S, Helfrich I, et al. Metastatic status of sentinel lymph nodes in melanoma determined noninvasively with multispectral optoacoustic imaging. *Sci Transl Med*. 2015;7(317). doi:10.1126/SCITRANSLMED.AAD1278/SUPPL_FILE/AAD1278_MOVIE_S4.MPG.

193. Ho CJH, Balasundaram G, Driessen W, et al. Multifunctional photosensitizer-based contrast agents for photoacoustic imaging. *Sci Reports.* 2014;4(1):1-6. doi:10.1038/srep05342.

194. Meng-Lin Li, Jung-Taek Oh, Xueyi Xie, et al. Simultaneous molecular and hypoxia imaging of brain tumors in vivo using spectroscopic photoacoustic tomography. *Proc IEEE*. 2008;96(3):481-489. doi:10.1109/JPROC.2007.913515.

195. Hariri A, Wang J, Kim Y, et al. In vivo photoacoustic imaging of chorioretinal oxygen gradients. *J Biomed Opt*. 2018;23(3):36005. doi:10.1117/1.JBO.23.3.036005.

196. Rich LJ, Seshadri M. Photoacoustic monitoring of tumor and normal tissue response to radiation. *Sci Reports 2016 61*. 2016;6(1):1-10. doi:10.1038/srep21237.

197. Bray F, Ferlay J, Soerjomataram I, Siegel RL, Torre LA, Jemal A. Global cancer statistics 2018: GLOBOCAN estimates of incidence and mortality worldwide for 36 cancers in 185 countries. *CA Cancer J Clin*. 2018;68(6):394-424. doi:10.3322/CAAC.21492.

198. Heywang-Köbrunner SH, Hacker A, Sedlacek S. Advantages and disadvantages of mammography screening. *Breast Care*. 2011;6(3):199. doi:10.1159/000329005.

199. Piras D, Engh FM van den, Hespen JCG van, et al. Visualizing breast cancer using the Twente photoacoustic mammoscope: What do we learn from twelve new patient measurements? *Opt Express*. 2012;20(11):11582-11597. doi:10.1364/OE.20.011582.

200. Geisel J, Raghu M, Hooley R. The role of ultrasound in breast cancer screening: The case for and against ultrasound. *Semin Ultrasound, CT MRI*. 2018;39(1):25-34. doi:10.1053/J.SULT.2017.09.006.

201. Longatto Filho A, Lopes JM, Schmitt FC. Angiogenesis and breast cancer. *J Oncol*. 2010. doi:10.1155/2010/576384.

202. Di Leo G, Trimboli RM, Sella T, Sardanelli F. Optical imaging of the breast: Basic principles and clinical applications. *Am J Roentgenol*. 2017;209(1):230-238. doi:10.2214/AJR.16.17220.

203. Lin L, Hu P, Shi J, et al. Single-breath-hold photoacoustic computed tomography of the breast. *Nat Commun 2018 91*. 2018;9(1):1-9. doi:10.1038/s41467-018-04576-z.

204. Toi M, Asao Y, Matsumoto Y, et al. Visualization of tumor-related blood vessels in human breast by photoacoustic imaging system with a hemispherical detector array. *Sci Reports 2017 71*. 2017;7(1):1-11. doi:10.1038/srep41970.

205. Heijblom M, Piras D, Brinkhuis M, et al. Photoacoustic image patterns of breast carcinoma and comparisons with magnetic resonance imaging and vascular stained histopathology. *Sci Reports 2015 51*. 2015;5(1):1-16. doi:10.1038/srep11778.

206. Heijblom M, Piras D, van den Engh FM, et al. The state of the art in breast imaging using the Twente Photoacoustic Mammoscope: results from 31 measurements on malignancies. *Eur Radiol*. 2016;26(11):3874-3887. doi:10.1007/S00330-016-4240-7/FIGURES/4.

207. Razansky D, Deán-Ben XL. Portable spherical array probe for volumetric real-time

optoacoustic imaging at centimeter-scale depths. *Opt Express, Vol 21, Issue 23, pp 28062-28071*. 2013;21(23):28062-28071. doi:10.1364/OE.21.028062.

208. Deán-Ben XL, Fehm TF, Gostic M, Razansky D. Volumetric hand-held optoacoustic angiography as a tool for real-time screening of dense breast. *J Biophotonics*. 2016;9(3):253-259. doi:10.1002/JBIO.201500008.

209. Aguirre J, Schwarz M, Garzorz N, et al. Precision assessment of label-free psoriasis biomarkers with ultra-broadband optoacoustic mesoscopy. *Nat Biomed Eng 2017 15*. 2017;1(5):1-8. doi:10.1038/s41551-017-0068.

210. Zabihian B, Weingast J, Liu M, et al. In vivo dual-modality photoacoustic and optical coherence tomography imaging of human dermatological pathologies. *Biomed Opt Express*. 2015;6(9):3163. doi:10.1364/BOE.6.003163.

211. Korenbrot JI. Speed, sensitivity, and stability of the light response in rod and cone photoreceptors: Facts and models. *Prog Retin Eye Res*. 2012;31(5):442-466. doi:10.1016/J.PRETEYERES.2012.05.002.

212. Pierrot-Deseilligny C, Milea D, Müri RM. Eye movement control by the cerebral cortex. *Curr Opin Neurol*. 2004;17(1):17-25. doi:10.1097/00019052-200402000-00005.

213. Guidelines on limits of exposure to broad-band incoherent optical radiation (0.38 to 3 microM). International Commission on Non-Ionizing Radiation Protection - PubMed. *Heal Phys*. 1997;73:539-545.

214. American National Standard for safe use of lasers. *ANSI*. 2014;136.1. https://blog.ansi.org/ansi-z136-1-2014-safe-use-of-lasers/#gref.

215. Delori FC, Webb RH, Sliney DH. Maximum permissible exposures for ocular safety (ANSI 2000), with emphasis on ophthalmic devices. *J Opt Soc Am A Opt Image Sci Vis*. 2007;24(5):1250. doi:10.1364/JOSAA.24.001250.

216. Organisciak DT, Vaughan DK. Retinal light damage: mechanisms and protection. *Prog Retin Eye Res*. 2010;29(2):113-134. doi:10.1016/J.PRETEYERES.2009.11.004.

217. Nabili A, Duncan DD, Kandimalla H, et al. Measurement of oxygen saturation in the retina with a spectroscopic sensitive multi aperture camera. *Opt Express, Vol 16, Issue 9, pp 6170-6182*. 2008;16(9):6170-6182. doi:10.1364/OE.16.006170.

218. Harris A, Dinn RB, Kagemann L, Rechtman E. A review of methods for human retinal oximetry. *Ophthalmic Surg Lasers Imaging*. 2003;34(2):152-164. doi:10.3928/1542-8877-20030301-16.

219. Schweitzer D, Hammer M, Kraft J, Thamm E, Königsdörffer E, Strobel J. In vivo measurement of the oxygen saturation of retinal vessels in healthy volunteers. *IEEE Trans Biomed Eng*. 1999;46(12):1454-1465. doi:10.1109/10.804573.

220. Liu W, Jiao S, Zhang HF. Accuracy of retinal oximetry: a Monte carlo investigation. *J Biomed Opt*. 2013;18(6):66003. doi:10.1117/1.JBO.18.6.066003.

221. Shonat RD, Kight AC. Oxygen tension imaging in the mouse retina. *Ann Biomed Eng*. 2003;31(9):1084-1096. doi:10.1114/1.1603256.

222. Wangsa-Wirawan ND, Linsenmeier RA. Retinal oxygen: fundamental and clinical aspects. *Arch Ophthalmol (Chicago, Ill 1960)*. 2003;121(4):547-557. doi:10.1001/ARCHOPHT.121.4.547.

223. Yi J, Wei Q, Liu W, Backman V, Zhang HF. Visible-light optical coherence tomography for retinal oximetry. *Opt Lett*. 2013;38(11):1796. doi:10.1364/OL.38.001796.

224. Zhang HF, Yi J, Chen S. Measuring oxygen saturation in retinal and choroidal circulations in rats using visible light optical coherence tomography angiography. *Biomed Opt Express, Vol 6, Issue 8, pp 2840-2853*. 2015;6(8):2840-2853. doi:10.1364/BOE.6.002840.

225. Leahy C, Merkle CW, Radhakrishnan H, Chong SP, Srinivasan VJ. Quantitative microvascular

hemoglobin mapping using visible light spectroscopic Optical Coherence Tomography. *Biomed Opt Express, Vol 6, Issue 4, pp 1429-1450*. 2015;6(4):1429-1450. doi:10.1364/BOE.6.001429.

226. Kanis MJ, Berendschot TTJM, van Norren D. Influence of macular pigment and melanin on incident early AMD in a white population. *Graefes Arch Clin Exp Ophthalmol*. 2007;245(6):767-773. doi:10.1007/S00417-006-0478-0.

227. Berendschot TTJM, Willemse-Assink JJM, Bastiaanse M, De Jong PTVM, Van Norren D. Macular pigment and melanin in age-related maculopathy in a general population. *Investig Ophthalmol Vis Sci*. 2002;43(6):1928-1932.

228. Keilhauer CN, Delori FC. Near-infrared autofluorescence imaging of the fundus: Visualization of ocular melanin. *Invest Ophthalmol Vis Sci*. 2006;47(8):3556-3564. doi:10.1167/IOVS.06-0122.

229. W. Song, Q. Wei, R. Zhang, H.F. Zhang. In vivo photoacoustic chorioretinal vascular imaging in albino mouse. *Chin Opt Lett*. 2014;12:51704.

230. Liu W, Schultz KM, Zhang K, et al. In vivo corneal neovascularization imaging by optical-resolution photoacoustic microscopy. *Photoacoustics*. 2014;2(2):81-86. doi:10.1016/j.pacs.2014.04.003.

231. Jeon S, Song HB, Kim J, et al. In Vivo Photoacoustic imaging of anterior ocular vasculature: A random sample consensus approach. *Sci Rep*. 2017;7(1):4318. doi:10.1038/s41598-017-04334-z.

232. Jiao S, Jiang M, Hu J, et al. Photoacoustic ophthalmoscopy for in vivo retinal imaging. *Opt Express*. 2010;18(4):3967. doi:10.1364/oe.18.003967.

233. Song W, Wei Q, Feng L, et al. Multimodal photoacoustic ophthalmoscopy in mouse. *J Biophotonics*. 2013;6(6-7):505-512. doi:10.1002/JBIO.201200061.

234. Liu T, Li H, Song W, Jiao S, Zhang HF. Fundus camera guided photoacoustic pphthalmoscopy. *Curr Eye Res*. 2013;38(12):1229-1234. doi:10.3109/02713683.2013.815219.

235. Wei Q, Liu T, Jiao S, Zhang HF. Image chorioretinal vasculature in albino rats using photoacoustic ophthalmoscopy. *J Mod Opt*. 2011;58(21):1997-2001. doi:10.1080/09500340.2011.601331.

236. Liu X, Liu T, Wen R, et al. Optical coherence photoacoustic microscopy for in vivo multimodal retinal imaging. *Opt Lett*. 2015;40(7):1370. doi:10.1364/OL.40.001370.

237. Liu T, Wei Q, Song W, Burke JM, Jiao S, Zhang HF. Near-infrared light photoacoustic ophthalmoscopy. *Biomed Opt Express*. 2012;3(4):792. doi:10.1364/BOE.3.000792.

238. Patel A, Kishore C, Agrahari V, Mitra AK. Ocular drug delivery systems: An overview. *World J Pharmacol*. 2013;2(2):47. doi:10.5497/wjp.v2.i2.47.

239. Sánchez-López E, Espina M, Doktorovova S, Souto EB, García ML. Lipid nanoparticles (SLN, NLC): Overcoming the anatomical and physiological barriers of the eye - Part I - Barriers and determining factors in ocular delivery. *Eur J Pharm Biopharm*. 2017;110:70-75. doi:10.1016/J.EJPB.2016.10.009.

240. Destruel PL, Zeng N, Maury M, Mignet N, Boudy V. In vitro and in vivo evaluation of in situ gelling systems for sustained topical ophthalmic delivery: state of the art and beyond. *Drug Discov Today*. 2017;22(4):638-651. doi:10.1016/J.DRUDIS.2016.12.008.

241. Gorantla S, Rapalli VK, Waghule T, et al. Nanocarriers for ocular drug delivery: Current status and translational opportunity. *RSC Adv*. 2020;10(46):27835-27855. doi:10.1039/d0ra04971a.

242. Mannermaa E, Vellonen KS, Urtti A. Drug transport in corneal epithelium and blood-retina barrier: emerging role of transporters in ocular pharmacokinetics. *Adv Drug Deliv Rev*. 2006;58(11):1136-1163. doi:10.1016/J.ADDR.2006.07.024.

243. Cholkar K, Patel SP, Vadlapudi AD, Mitra AK. Novel strategies for anterior segment ocular

drug delivery. *J Ocul Pharmacol Ther*. 2013;29(2):106-123. doi:10.1089/jop.2012.0200.

244. Vadlapatla R, Vadlapudi A, Pal D, Mitra A. Role of membrane transporters and metabolizing enzymes in ocular drug delivery. *Curr Drug Metab*. 2014;15(7):680-693. doi:10.2174/1389200215666140926152459.

245. Amrite AC, Kompella UB. Size-dependent disposition of nanoparticles and microparticles following subconjunctival administration. *J Pharm Pharmacol*. 2005;57(12):1555-1563. doi:10.1211/JPP.57.12.0005.

246. Urtti A. Challenges and obstacles of ocular pharmacokinetics and drug delivery. *Adv Drug Deliv Rev*. 2006;58(11):1131-1135. doi:10.1016/J.ADDR.2006.07.027.

247. Addo RT. Ocular drug delivery: Advances, challenges and applications. *Springer International Publishing*. 2016. doi:10.1007/978-3-319-47691-9.

248. Kwatra D, Mitra AK. Drug delivery in ocular diseases: Barriers and strategies. *World J Pharmacol*. 2013;2(4):78-83. doi:10.5497/WJP.V2.I4.78.

249. Nayak K, Misra M. A review on recent drug delivery systems for posterior segment of eye. *Biomed Pharmacother*. 2018;107:1564-1582. doi:10.1016/J.BIOPHA.2018.08.138.

250. Girdhar V, Patil S, Banerjee S, Singhvi G. Nanocarriers for drug delivery: Mini review. *Curr Nanomedicine*. 2018;8(2):88-99. doi:10.2174/2468187308666180501092519.

251. Singhvi G, Patil S, Girdhar V, Dubey SK. Nanocarriers for topical drug delivery: Approaches and advancements. *Nanosci Nanotechnology-Asia*. 2018;9(3):329-336. doi:10.2174/2210681208666180320122534.

252. Lee BK, Yun YH, Park K. Smart nanoparticles for drug delivery: Boundaries and opportunities. *Chem Eng Sci*. 2015;125:164. doi:10.1016/J.CES.2014.06.042.

253. Naahidi S, Jafari M, Edalat F, Raymond K, Khademhosseini A, Chen P. Biocompatibility of engineered nanoparticles for drug delivery. *J Control Release*. 2013;166(2):182-194.

doi:10.1016/J.JCONREL.2012.12.013.

254. Wilczewska AZ, Niemirowicz K, Markiewicz KH, Car H. Nanoparticles as drug delivery systems. *Pharmacol Reports*. 2012;64(5):1020-1037. doi:10.1016/S1734-1140(12)70901-5.

255. Cooper ER. Nanoparticles: A personal experience for formulating poorly water soluble drugs. *J Control Release*. 2010;141(3):300-302. doi:10.1016/j.jconrel.2009.10.006.

256. Lai P, Daear W, Löbenberg R, Prenner EJ. Overview of the preparation of organic polymeric nanoparticles for drug delivery based on gelatine, chitosan, poly(d,l-lactide-co-glycolic acid) and polyalkylcyanoacrylate. *Colloids Surfaces B Biointerfaces*. 2014;118:154-163. doi:10.1016/J.COLSURFB.2014.03.017.

257. Ali A, Ahmed S. A review on chitosan and its nanocomposites in drug delivery. *Int J Biol Macromol*. 2018;109:273-286. doi:10.1016/J.IJBIOMAC.2017.12.078.

258. Jana S, Kumar Sen K, Gandhi A. Alginate based nanocarriers for drug delivery applications. *Curr Pharm Des*. 2016;22(22):3399-3410. doi:10.2174/1381612822666160510125718.

259. Mundargi RC, Babu VR, Rangaswamy V, Patel P, Aminabhavi TM. Nano/micro technologies for delivering macromolecular therapeutics using poly(D,L-lactide-co-glycolide) and its derivatives. *J Control Release*. 2008;125(3):193-209. doi:10.1016/J.JCONREL.2007.09.013.

260. Makadia HK, Siegel SJ. Poly Lactic-co-Glycolic Acid (PLGA) as biodegradable controlled drug delivery carrier. *Polymers (Basel)*. 2011;3(3):1377-1397. doi:10.3390/POLYM3031377.

261. Zhang Y, Chan HF, Leong KW. Advanced materials and processing for drug delivery: the past and the future. *Adv Drug Deliv Rev*. 2013;65(1):104-120. doi:10.1016/J.ADDR.2012.10.003.

262. Ospina-Villa JD, Gómez-Hoyos C, Zuluaga-Gallego R, Triana-Chávez O. Encapsulation of proteins from Leishmania panamensis into PLGA particles by a single emulsion-solvent evaporation method. *J Microbiol Methods*. 2019;162:1-7. doi:10.1016/J.MIMET.2019.05.004.

263. Patel A, Patel M, Yang X, Mitra AK. Recent advances in protein and peptide drug delivery: A

special emphasis on polymeric nanoparticles. *Protein Pept Lett*. 2014;21(11):1102. doi:10.2174/09298665216661408071142 40.

264. Haggag YA, Faheem AM, Tambuwala MM, et al. Effect of poly(ethylene glycol) content and formulation parameters on particulate properties and intraperitoneal delivery of insulin from PLGA nanoparticles prepared using the double-emulsion evaporation procedure. *Pharm Dev Technol*. 2018;23(4):370-381. doi:10.1080/10837450.2017.1295066.

265. Van De Weert M, Hoechstetter J, Hennink WE, Crommelin DJA. The effect of a water/organic solvent interface on the structural stability of lysozyme. *J Control Release*. 2000;68(3):351-359. doi:10.1016/S0168-3659(00)00277-7.

266. Varshochian R, Jeddi-Tehrani M, Mahmoudi AR, et al. The protective effect of albumin on bevacizumab activity and stability in PLGA nanoparticles intended for retinal and choroidal neovascularization treatments. *Eur J Pharm Sci*. 2013;50(3-4):341-352. doi:10.1016/J.EJPS.2013.07.014.

267. Stanwick JC, Baumann MD, Shoichet MS. Enhanced neurotrophin-3 bioactivity and release from a nanoparticle-loaded composite hydrogel. *J Control Release*. 2012;160(3):666-675. doi:10.1016/J.JCONREL.2012.03.024.

268. Son S, Lee WR, Joung YK, Kwon MH, Kim YS, Park KD. Optimized stability retention of a monoclonal antibody in the PLGA nanoparticles. *Int J Pharm*. 2009;368(1-2):178-185. doi:10.1016/J.IJPHARM.2008.09.061.

269. Leon RAL, Somasundar A, Badruddoza AZM, Khan SA. Microfluidic fabrication of multi-drug-loaded polymeric microparticles for topical glaucoma therapy. *Part Part Syst Charact*. 2015;32(5):567-572. doi:10.1002/PPSC.201400229.

270. Allahyari M, Mohit E. Peptide/protein vaccine delivery system based on PLGA particles. *Hum Vaccin Immunother*. 2016;12(3):806. doi:10.1080/21645515.2015.1102804.

271. Araújo J, Vega E, Lopes C, Egea MA, Garcia ML, Souto EB. Effect of polymer viscosity on

physicochemical properties and ocular tolerance of FB-loaded PLGA nanospheres. *Colloids Surfaces B Biointerfaces*. 2009;72(1):48-56. doi:10.1016/J.COLSURFB.2009.03.028.

272. Cañadas C, Alvarado H, Calpena AC, et al. In vitro, ex vivo and in vivo characterization of PLGA nanoparticles loading pranoprofen for ocular administration. *Int J Pharm*. 2016;511(2):719-727. doi:10.1016/J.IJPHARM.2016.07.055.

273. Sánchez-López E, Egea MA, Cano A, et al. PEGylated PLGA nanospheres optimized by design of experiments for ocular administration of dexibuprofen—in vitro, ex vivo and in vivo characterization. *Colloids Surfaces B Biointerfaces*. 2016;145:241-250. doi:10.1016/J.COLSURFB.2016.04.054.

274. Sánchez-López E, Egea MA, Davis BM, et al. Memantine-loaded PEGylated biodegradable nanoparticles for the treatment of glaucoma. *Small*. 2018;14(2):1701808. doi:10.1002/SMLL.201701808.

275. Sánchez-López E, Ettcheto M, Egea MA, et al. Memantine loaded PLGA PEGylated nanoparticles for Alzheimer's disease: In vitro and in vivo characterization. *J Nanobiotechnology*. 2018;16(1):1-16. doi:10.1186/S12951-018-0356-Z/FIGURES/9.

276. Ding D, Zhu Q. Recent advances of PLGA micro/nanoparticles for the delivery of biomacromolecular therapeutics. *Mater Sci Eng C*. 2018;92:1041-1060. doi:10.1016/J.MSEC.2017.12.036.

277. Zielinska A, Carreiró F, Oliveira AM, et al. Polymeric nanoparticles: Production, characterization, toxicology and ecotoxicology. *Molecules*. 2020;25(16):3731. doi:10.3390/MOLECULES25163731.

278. Wang Y, Li P, Tran TTD, Zhang J, Kong L. Manufacturing techniques and surface engineering of polymer based nanoparticles for targeted drug delivery to cancer. *Nanomater*. 2016;6(2):26. doi:10.3390/NANO6020026.

279. Bilati U, Allémann E, Doelker E. Nanoprecipitation versus emulsion-based techniques for the

encapsulation of proteins into biodegradable nanoparticles and process-related stability issues. *AAPS PharmSciTech*. 2005;6(4):E594. doi:10.1208/PT060474.

280. Fessi H, Puisieux F, Devissaguet JP, Ammoury N, Benita S. Nanocapsule formation by interfacial polymer deposition following solvent displacement. *Int J Pharm*. 1989;55(1):R1-R4. doi:10.1016/0378-5173(89)90281-0.

281. Guterres SS, Alves MP, Pohlmann AR. Polymeric nanoparticles, nanospheres and nanocapsules for cutaneous applications. *Drug Target Insights*. 2007;2(1):147-157. doi:10.33393/DTI.2007.1300.

282. Salatin S, Barar J, Barzegar-Jalali M, Adibkia K, Kiafar F, Jelvehgari M. Development of a nanoprecipitation method for the entrapment of a very water soluble drug into Eudragit RL nanoparticles. *Res Pharm Sci*. 2017;12(1):1. doi:10.4103/1735-5362.199041.

283. Martínez Rivas CJ, Tarhini M, Badri W, et al. Nanoprecipitation process: From encapsulation to drug delivery. *Int J Pharm*. 2017;532(1):66-81. doi:10.1016/J.IJPHARM.2017.08.064.

284. Oz UC, Küçüktürkmen B, Devrim B, Saka OM, Bozkir A. Development and optimization of alendronate sodium loaded PLGA nanoparticles by central composite design. *Macromol Res.* 2019;27(9):857-866. doi:10.1007/S13233-019-7119-Z.

285. Zhang M, He J, Zhang W, Liu J. Fabrication of TPGS-stabilized liposome-PLGA hybrid nanoparticle via a new modified nanoprecipitation approach: In vitro and in vivo evaluation. *Pharm Res*. 2018;35(11):1-13. doi:10.1007/S11095-018-2485-3/FIGURES/7.

286. Schrurs F, Lison D. Join the dialogue. *Nat Nanotechnol 2012 79*. 2012;7(9):545-545. doi:10.1038/nnano.2012.150.

287. Manning G, Whyte DB, Martinez R, Hunter T, Sudarsanam S. The protein kinase complement of the human genome. *Science*. 2002;298(5600):1912-1934. doi:10.1126/SCIENCE.1075762.

288. Schlessinger J. Cell signaling by receptor tyrosine kinases. *Cell*. 2000;103(2):211-225.

doi:10.1016/S0092-8674(00)00114-8.

289. Pawson T. Specificity in signal transduction: from phosphotyrosine-SH2 domain interactions to complex cellular systems. *Cell*. 2004;116(2):191-203. doi:10.1016/S0092-8674(03)01077-8.

290. Takahashi T, Yamaguchi S, Chida K, Shibuya M. A single autophosphorylation site on KDR/Flk-1 is essential for VEGF-A-dependent activation of PLC-γ and DNA synthesis in vascular endothelial cells. *EMBO J*. 2001;20(11):2768. doi:10.1093/EMBOJ/20.11.2768.

291. Kowanetz M, Ferrara N. Vascular endothelial growth factor signaling pathways: therapeutic perspective. *Clin Cancer Res*. 2006;12(17):5018-5022. doi:10.1158/1078-0432.CCR-06-1520.

292. Zachary I, Gliki G. Signaling transduction mechanisms mediating biological actions of the vascular endothelial growth factor family. *Cardiovasc Res*. 2001;49(3):568-581. doi:10.1016/S0008-6363(00)00268-6.

293. Gotink KJ, Verheul HMW. Anti-angiogenic tyrosine kinase inhibitors: What is their mechanism of action? *Angiogenesis*. 2010;13(1):1-14. doi:10.1007/S10456-009-9160-6/FIGURES/4.

294. Sun L, Liang C, Shirazian S, et al. Discovery of 5-[5-fluoro-2-oxo-1,2-dihydroindol-(3Z)-ylidenemethyl]-2, 4-dimethyl-1H-pyrrole-3-carboxylic acid (2-diethylaminoethyl)amide, a novel tyrosine kinase inhibitor targeting vascular endothelial and platelet-derived growth factor receptor tyrosine kinase. *J Med Chem*. 2003;46(7):1116-1119. doi:10.1021/JM0204183/SUPPL_FILE/JM0204183_S.PDF.

295. Goodman VL, Rock EP, Dagher R, et al. Approval summary: sunitinib for the treatment of imatinib refractory or intolerant gastrointestinal stromal tumors and advanced renal cell carcinoma. *Clin Cancer Res*. 2007;13(5):1367-1373. doi:10.1158/1078-0432.CCR-06-2328.

296. Detry B, Blacher S, Erpicum C, et al. Sunitinib inhibits inflammatory corneal lymphangiogenesis. *Invest Ophthalmol Vis Sci*. 2013;54(5):3082-3093. doi:10.1167/IOVS.12-10856.

297. Pérez-Santonja JJ, Campos-Mollo E, Lledó-Riquelme M, Javaloy J, Alió JL. Inhibition of corneal neovascularization by topical bevacizumab (Anti-VEGF) and Sunitinib (Anti-VEGF and Anti-PDGF) in an animal model. *Am J Ophthalmol*. 2010;150(4). doi:10.1016/J.AJO.2010.04.024.

298. Bayyoud T, Hofmann J, Spitzer M, Bartz-Schmidt KU, Yoeruek E. Cytotoxic properties of sunitinib and sorafenib on human corneal epithelial cells. *Curr Eye Res*. 2014;39(2):149-154. doi:10.3109/02713683.2013.833629.

299. Wilhelm SM, Carter C, Tang LY, et al. BAY 43-9006 exhibits broad spectrum oral antitumor activity and targets the RAF/MEK/ERK pathway and receptor tyrosine kinases involved in tumor progression and angiogenesis. *Cancer Res*. 2004;64(19):7099-7109. doi:10.1158/0008-5472.CAN-04-1443.

300. Seo JW, Chung SH, Choi JS, Joo CK. Inhibition of corneal neovascularization in rats by systemic administration of sorafenib. *Cornea*. 2012;31(8):907-912. doi:10.1097/ICO.0B013E31823F8B9C.

301. den Hollander P, Savage MI, Brown PH. Targeted therapy for breast cancer prevention. *Front Oncol*. 2013;3. doi:10.3389/FONC.2013.00250.

302. Kaya MK, Demir T, Bulut H, Akpolat N, Turgut B. Effects of lapatinib and trastuzumab on vascular endothelial growth factor in experimental corneal neovascularization. *Clin Experiment Ophthalmol*. 2015;43(5):449-457. doi:10.1111/CEO.12500.

303. Liu W, Schultz KM, Zhang K, et al. In vivo corneal neovascularization imaging by optical-resolution photoacoustic microscopy. *Photoacoustics*. 2014;2(2):81. doi:10.1016/J.PACS.2014.04.003.

304. Anijeet DR, Zheng Y, Tey A, Hodson M, Sueke H, Kaye SB. Imaging and evaluation of corneal vascularization using fluorescein and indocyanine green angiography. *Invest Ophthalmol Vis Sci*. 2012;53(2):650-658. doi:10.1167/iovs.11-8014.

305. Spiteri N, Romano V, Zheng Y, et al. Corneal angiography for guiding and evaluating fine-needle diathermy treatment of corneal neovascularization. *Ophthalmology*. 2015;122(6):1079-1084. doi:10.1016/j.ophtha.2015.02.012.

306. Olsen TW. Anaphylactic shock following indocyanine green angiography. *Arch Ophthalmol*. 1996;114(1):97. doi:10.1001/archopht.1996.01100130093018.

307. Kim C, Favazza C, Wang L V. In vivo photoacoustic tomography of chemicals: High-resolution functional and molecular optical imaging at new depths. *Chem Rev*. 2010;110(5):2756-2782. doi:10.1021/cr900266s.

308. Weber J, Beard PC, Bohndiek SE. Contrast agents for molecular photoacoustic imaging. *Nat Methods 2016 138*. 2016;13(8):639-650. doi:10.1038/nmeth.3929.

309. Liu W, Zhang HF. Photoacoustic imaging of the eye: A mini review. *Photoacoustics*. 2016;4(3):112-123.

310. Qu H, Yang X. Metformin Inhibits Angiogenesis induced by interaction of hepatocellular carcinoma with hepatic stellate cells. *Cell Biochem Biophys*. 2015;71(2):931-936. doi:10.1007/s12013-014-0287-8.

311. Yang Y, Jin G, Liu H, et al. Metformin inhibits esophageal squamous cell carcinoma-induced angiogenesis by suppressing JAK/STAT3 signaling pathway. *Oncotarget*. 2017;8(43):74673-74687. doi:10.18632/oncotarget.20341.

312. Rattan R, Graham RP, Maguire JL, Giri S, Shridhar V. Metformin suppresses ovarian cancer growth and metastasis with enhancement of cisplatin. *Neoplasia*. 2011;13(5):483-491. doi:10.1593/neo.11148.

313. Wang J, Sun X, Ma Q, et al. Metformin's antitumour and anti-angiogenic activities are mediated by skewing macrophage polarization. *J Cell Mol Med*. 2018;22(8):3825-3836. doi:10.1111/jcmm.13655.

314. Wang J, Li G, Wang Y, et al. Suppression of tumor angiogenesis by metformin treatment via a mechanism linked to targeting of HER2/HIF-1α/VEGF secretion axis. *Oncotarget*. 2015;6(42):44579-44592. doi:10.18632/oncotarget.6373.

315. Orecchioni S, Reggiani F, Talarico G, et al. The biguanides metformin and phenformin inhibit angiogenesis, local and metastatic growth of breast cancer by targeting both neoplastic and microenvironment cells. *Int J Cancer*. 2015;136(6):534-545. doi:10.1002/ijc.29193.

316. Joe SG, Yoon YH, Choi JA, Koh J. Anti-angiogenic effect of metformin in mouse oxygen-induced retinopathy is mediated by reducing levels of the vascular endothelial growth factor receptor Flk-1. *PLoS One*. 2015;10(3):1-14. doi:10.1371/journal.pone.0119708.

317. Ying Y, Ueta T, Jiang S, et al. Metformin inhibits ALK1-mediated angiogenesis via activation of AMPK. *Oncotarget*. 2017;8(20):32794-32806. doi:10.18632/oncotarget.15825.

318. Zhang Y, Chen F, Wang L. Metformin inhibits development of diabetic retinopathy through microRNA-497a-5p. *Am J Transl Res*. 2017;9(12):5558-5566. http://www.ncbi.nlm.nih.gov/pubmed/29312507.

319. Han J, Li Y, Liu X, et al. Metformin suppresses retinal angiogenesis and inflammation in vitro and in vivo. *PLoS One*. 2018;13(3):1-16. doi:10.1371/journal.pone.0193031.

320. Liu D, Wu Q, Zhu Y, et al. Co-delivery of metformin and levofloxacin hydrochloride using biodegradable thermosensitive hydrogel for the treatment of corneal neovascularization. *Drug Deliv*. 2019;26(1):522-531. doi:10.1080/10717544.2019.1609623.

321. Faraj LA, Said DG, Dua HS. Evaluation of corneal neovascularisation. *Br J Ophthalmol*. 2011;95(10):1343-1344. doi:10.1136/bjophthalmol-2011-300856.

322. Gaudana R, Ananthula HK, Parenky A, Mitra AK. Ocular drug delivery. *AAPS J*. 2010;12(3):348-360. doi:10.1208/s12248-010-9183-3.

323. Whitcher JP, Srinivasan M, Upadhyay MP. Corneal blindness: a global perspective. *Bull*

World Heal Organ . 2001;79(3):214-221.

324. Gain P, Jullienne R, He Z, et al. Global survey of corneal transplantation and eye banking. *JAMA Ophthalmol*. 2016;134(2):167-173. doi:10.1001/JAMAOPHTHALMOL.2015.4776.

325. Vyas SP, Mysore N, Jaitely V, Venkatesan N. Discoidal niosome based controlled ocular delivery of timolol maleate. *Pharmazie*. 1998;53(7):466-469. https://europepmc.org/article/med/9742041. Accessed June 30, 2022.

326. Kang H, Rho S, Stiles WR, et al. Size-dependent EPR effect of polymeric nanoparticles on tumor targeting. *Adv Healthc Mater*. 2020;9(1):1901223. doi:10.1002/ADHM.201901223.

327. Fan X, Jiang S, Li Z, Loh XJ. Conjugation of poly(ethylene glycol) to poly(lactide)-based polyelectrolytes: An effective method to modulate cytotoxicity in gene delivery. *Mater Sci Eng C*. 2017;73:275-284. doi:10.1016/J.MSEC.2016.12.029.

328. Li Z, Loh XJ. Recent advances of using polyhydroxyalkanoate-based nanovehicles as therapeutic delivery carriers. *Wiley Interdiscip Rev Nanomed Nanobiotechnol*. 2017;9(3). doi:10.1002/WNAN.1429.

329. Pack DW, Hoffman AS, Pun S, Stayton PS. Design and development of polymers for gene delivery. *Nat Rev Drug Discov 2005 47*. 2005;4(7):581-593. doi:10.1038/nrd1775.

330. Grigsby CL, Leong KW. Balancing protection and release of DNA: tools to address a bottleneck of non-viral gene delivery. *J R Soc Interface*. 2010;7(Suppl 1):S67. doi:10.1098/RSIF.2009.0260.

331. Putney SD, Burke PA. Improving protein therapeutics with sustained-release formulations. *Nat Biotechnol*. 1998;16(2):153. doi:10.1038/NBT0298-153.

332. Lerch S, Dass M, Musyanovych A, Landfester K, Mailänder V. Polymeric nanoparticles of different sizes overcome the cell membrane barrier. *Eur J Pharm Biopharm*. 2013;84(2):265-274. doi:10.1016/J.EJPB.2013.01.024.

333. Lorenz MR, Holzapfel V, Musyanovych A, et al. Uptake of functionalized, fluorescent-labeled polymeric particles in different cell lines and stem cells. *Biomaterials*. 2006;27(14):2820-2828. doi:10.1016/J.BIOMATERIALS.2005.12.022.

334. Wohlfart S, Gelperina S, Kreuter J. Transport of drugs across the blood-brain barrier by nanoparticles. *J Control Release*. 2012;161(2):264-273. doi:10.1016/J.JCONREL.2011.08.017.

335. Wang D, Wu LP. Nanomaterials for delivery of nucleic acid to the central nervous system (CNS). *Mater Sci Eng C*. 2017;70:1039-1046. doi:10.1016/J.MSEC.2016.04.011.

336. Wu F, Jin T. Polymer-based sustained-release dosage forms for protein drugs, challenges, and recent advances. *AAPS PharmSciTech*. 2008;9(4):1218. doi:10.1208/S12249-008-9148-3.

337. Masood F. Polymeric nanoparticles for targeted drug delivery system for cancer therapy. *Mater Sci Eng C Mater Biol Appl*. 2016;60:569-578. doi:10.1016/J.MSEC.2015.11.067.

338. Qodratnama R, Serino LP, Cox HC, Qutachi O, White LJ. Formulations for modulation of protein release from large-size PLGA microparticles for tissue engineering. *Mater Sci Eng C Mater Biol Appl*. 2015;47:230-236. doi:10.1016/J.MSEC.2014.11.003.

339. Kumari A, Yadav SK, Yadav SC. Biodegradable polymeric nanoparticles based drug delivery systems. *Colloids Surf B Biointerfaces*. 2010;75(1):1-18. doi:10.1016/J.COLSURFB.2009.09.001.

340. Moradian H, Keshvari H, Fasehee H, Dinarvand R, Faghihi S. Combining NT3-overexpressing MSCs and PLGA microcarriers for brain tissue engineering: A potential tool for treatment of Parkinson's disease. *Mater Sci Eng C*. 2017;76:934-943. doi:10.1016/J.MSEC.2017.02.178.

341. Li Z, Liu X, Chen X, Chua MX, Wu YL. Targeted delivery of Bcl-2 conversion gene by MPEG-PCL-PEI-FA cationic copolymer to combat therapeutic resistant cancer. *Mater Sci Eng C*. 2017;76:66-72. doi:10.1016/J.MSEC.2017.02.163.

342. Dechy-Cabaret O, Martin-Vaca B, Bourissou D. Controlled ring-opening polymerization of lactide and glycolide. *Chem Rev*. 2004;104(12):6147-6176. doi:10.1021/CR040002S/ASSET/CR040002S.FP.PNG_V03.

343. Conn J, Oyasu R, Welsh M, Beal JM. Vicryl (polyglactin 910) synthetic absorbable sutures. *Am J Surg*. 1974;128(1):19-23. doi:10.1016/0002-9610(74)90228-1.

344. Huh BK, Kim BH, Kim SN, et al. Surgical suture braided with a diclofenac-loaded strand of poly(lactic-co-glycolic acid) for local, sustained pain mitigation. *Mater Sci Eng C Mater Biol Appl*. 2017;79:209-215. doi:10.1016/J.MSEC.2017.05.024.

345. Dai Z, Yu X, Hong J, Liu X, Sun J, Sun X. Development of a novel CsA-PLGA drug delivery system based on a glaucoma drainage device for the prevention of postoperative fibrosis. *Mater Sci Eng C Mater Biol Appl*. 2016;66:206-214. doi:10.1016/J.MSEC.2016.04.077.

346. Jaidev LR, Krishnan UM, Sethuraman S. Gemcitabine loaded biodegradable PLGA nanospheres for in vitro pancreatic cancer therapy. *Mater Sci Eng C Mater Biol Appl*. 2015;47:40-47. doi:10.1016/J.MSEC.2014.11.027.

347. Kamaly N, Yameen B, Wu J, Farokhzad OC. Degradable controlled-release polymers and polymeric nanoparticles: Mechanisms of controlling drug release. *Chem Rev*. 2016;116(4):2602-2663. doi:10.1021/ACS.CHEMREV.5B00346/ASSET/IMAGES/ACS.CHEMREV.5B00346.SOCIAL.JPEG_V03.

348. Dinarvand R, Sepehri N, Manoochehri S, Rouhani H, Atyabi F. Polylactide-co-glycolide nanoparticles for controlled delivery of anticancer agents. *Int J Nanomedicine*. 2011;6:877-895. doi:10.2147/IJN.S18905.

349. Kawashima Y, Yamamoto H, Takeuchi H, Fujioka S, Hino T. Pulmonary delivery of insulin with nebulized DL-lactide/glycolide copolymer (PLGA) nanospheres to prolong hypoglycemic effect. *J Control Release*. 1999;62(1-2):279-287. doi:10.1016/S0168-3659(99)00048-6.

350. Yandrapu SK, Upadhyay AK, Petrash JM, Kompella UB. Nanoparticles in porous microparticles prepared by supercritical infusion and pressure quench technology for sustained delivery of bevacizumab. *Mol Pharm*. 2013;10(12):4676-4686. doi:10.1021/MP400487F.

351. Chumakova O V., Liopo A V., Andreev VG, et al. Composition of PLGA and PEI/DNA nanoparticles improves ultrasound-mediated gene delivery in solid tumors in vivo. *Cancer Lett*. 2008;261(2):215-225. doi:10.1016/J.CANLET.2007.11.023.

352. Lundberg P, Langel Ü. A brief introduction to cell-penetrating peptides. *J Mol Recognit*. 2003;16(5):227-233. doi:10.1002/JMR.630.

353. Temsamani J, Vidal P. The use of cell-penetrating peptides for drug delivery. *Drug Discov Today*. 2004;9(23):1012-1019. doi:10.1016/S1359-6446(04)03279-9.

354. Frankel AD, Pabo CO. Cellular uptake of the tat protein from human immunodeficiency virus. *Cell*. 1988;55(6):1189-1193. doi:10.1016/0092-8674(88)90263-2.

355. Futaki S, Suzuki T, Ohashi W, et al. Arginine-rich Peptides: an abundant source of membrane-permeable peptides having potential as carriers for intracellular protein delivery. *J Biol Chem*. 2001;276(8):5836-5840. doi:10.1074/JBC.M007540200.

356. Park D, Lee JY, Cho HK, et al. Cell-penetrating peptide-patchy deformable polymeric nanovehicles with enhanced cellular uptake and transdermal delivery. *Biomacromolecules*. 2018;19(7):2682-2690. doi:10.1021/ACS.BIOMAC.8B00292/SUPPL_FILE/BM8B00292_SI_001.PDF.

357. Jiang T, Zhang Z, Zhang Y, et al. Dual-functional liposomes based on pH-responsive cell-penetrating peptide and hyaluronic acid for tumor-targeted anticancer drug delivery. *Biomaterials*. 2012;33(36):9246-9258. doi:10.1016/J.BIOMATERIALS.2012.09.027.

358. Wei G, Wang Y, Huang X, Hou H, Zhou S. Peptide-based nanocarriers for cancer therapy. *Small Methods*. 2018;2(9):1700358. doi:10.1002/SMTD.201700358.

359. Bartlett RL, Sharma S, Panitch A. Cell-penetrating peptides released from thermosensitive nanoparticles suppress pro-inflammatory cytokine response by specifically targeting inflamed cartilage explants. *Nanomedicine*. 2013;9(3):419-427. doi:10.1016/J.NANO.2012.09.003.

360. Li S, Lui KH, Li X, et al. pH-Triggered poly(ethylene glycol)-poly(lactic acid/glycolic acid)/croconaine nanoparticles-assisted multiplexed photoacoustic imaging and enhanced photothermal cancer therapy. *ACS Appl Bio Mater*. 2021;4(5):4152-4164. doi:10.1021/acsabm.0c01578.

361. Knoll GA, Bell RC. Tacrolimus versus cyclosporin for immunosuppression in renal transplantation: meta-analysis of randomised trials. *BMJ Br Med J*. 1999;318(7191):1104. doi:10.1136/BMJ.318.7191.1104.

362. Crespo-Leiro MG. Tacrolimus in heart transplantation. *Transplant Proc*. 2003;35(5):1981-1983. doi:10.1016/S0041-1345(03)00566-9.

363. Bhorade SM, Jordan A, Villanueva J, et al. Comparison of three tacrolimus-based immunosuppressive regimens in lung transplantation. *Am J Transplant*. 2003;3(12):1570-1575. doi:10.1046/J.1600-6135.2003.00260.X.

364. Mills RA, Jones DB, Winkler CR, Wallace GW, Wilhelmus KR. Topical FK506 prevents experimental corneal allograft rejection. *Cornea*. 1995;14(2):157-160. doi:10.1097/00003226-199503000-00008.

365. Hikita N, Lapez JS, Chan CC, Mochizuki M, Nussenblatt RB, De Smet MD. Use of topical FK506 in a corneal graft rejection model in Lewis rats. *Investig Ophthalmol Vis Sci*. 1997;38(5):901-909. https://iovs.arvojournals.org/article.aspx?articleid=2161681. Accessed June 30, 2022.

366. Benelli U, Lepri A, Del Tacca M, Nardi M. FK506 delays corneal graft rejection in a model of corneal xenotransplantation. *J Ocul Pharmacol Ther*. 1996;12(4):425-431. doi:10.1089/JOP.1996.12.425.

367. Minamoto A, Sakata H, Okada K, Fujihara M. Suppression of corneal graft rejection by subconjunctival injection of FK-506 in a rat model of penetrating keratoplasty. *Jpn J Ophthalmol*. 1995;39(1):12-19. https://pubmed.ncbi.nlm.nih.gov/7543958/. Accessed June 30, 2022.

368. Liu D, Wu Q, Chen W, et al. A novel FK506 loaded nanomicelles consisting of amino-terminated poly(ethylene glycol)-block-poly(D,L)-lactic acid and hydroxypropyl methylcellulose for ocular drug delivery. *Int J Pharm*. 2019;562:1-10. doi:10.1016/J.IJPHARM.2019.03.022.

369. Ahmed OAA, Badr-Eldin SM. Biodegradable self-assembled nanoparticles of PEG-PLGA amphiphilic diblock copolymer as a promising stealth system for augmented vinpocetine brain delivery. *Int J Pharm*. 2020;588:119778. doi:10.1016/J.IJPHARM.2020.119778.

370. Gessner I, Neundorf I. Nanoparticles modified with cell-penetrating peptides: conjugation mechanisms, physicochemical properties, and application in cancer diagnosis and therapy. *Int J Mol Sci*. 2020;21(7). doi:10.3390/IJMS21072536.

371. Juang V, Chang CH, Wang CS, Wang HE, Lo YL. pH-Responsive PEG-shedding and targeting peptide-modified nanoparticles for dual-delivery of irinotecan and microRNA to enhance tumor-specific therapy. *Small*. 2019;15(49). doi:10.1002/SMLL.201903296.

372. Lin T, Zhao P, Jiang Y, et al. Blood-brain-barrier-penetrating albumin nanoparticles for niomimetic drug delivery via albumin-binding protein pathways for antiglioma therapy. *ACS Nano*. 2016;10(11):9999-10012. doi:10.1021/ACSNANO.6B04268.

373. Ma P, Yu H, Zhang X, et al. Increased active tumor targeting by an αvβ3-targeting and cell-penetrating bifunctional peptide-mediated dendrimer-based conjugate. *Pharm Res*. 2017;34(1):121-135. doi:10.1007/S11095-016-2045-7.

374. Silva S, Almeida AJ, Vale N. Combination of cell-penetrating peptides with nanoparticles for therapeutic application: A review. *Biomolecules*. 2019;9(1). doi:10.3390/BIOM9010022.

375. Hong S, Leroueil PR, Janus EK, et al. Interaction of polycationic polymers with supported lipid bilayers and cells: nanoscale hole formation and enhanced membrane permeability. *Bioconjug Chem*. 2006;17(3):728-734. doi:10.1021/BC060077Y.

376. Foroozandeh P, Aziz AA. Insight into Cellular Uptake and intracellular trafficking of nanoparticles. *Nanoscale Res Lett*. 2018;13(1). doi:10.1186/S11671-018-2728-6.

377. Leroueil PR, Hong S, Mecke A, Baker JR, Orr BG, Holl MMB. Nanoparticle interaction with biological membranes: does nanotechnology present a Janus face? *Acc Chem Res*. 2007;40(5):335-342. doi:10.1021/AR600012Y.

378. Yesenia K, Hern´hernández-Giottonini H, Rodríguezrodríguez-C´ Ordova RJ, et al. PLGA nanoparticle preparations by emulsification and nanoprecipitation techniques: effects of formulation parameters. *RSC Adv*. 2020;10(8):4218-4231. doi:10.1039/C9RA10857B.

379. Zweers MLT, Grijpma DW, Engbers GHM, Feijen J. The preparation of monodisperse biodegradable polyester nanoparticles with a controlled size. *J Biomed Mater Res B Appl Biomater*. 2003;66(2):559-566. doi:10.1002/JBM.B.10046.

380. Duxfield L, Sultana R, Wang R, et al. Development of gatifloxacin-loaded cationic polymeric nanoparticles for ocular drug delivery. *Pharm Dev Technol*. 2016;21(2):172-179. doi:10.3109/10837450.2015.1091839.

381. Yin Win K, Feng SS. Effects of particle size and surface coating on cellular uptake of polymeric nanoparticles for oral delivery of anticancer drugs. *Biomaterials*. 2005;26(15):2713-2722. doi:10.1016/J.BIOMATERIALS.2004.07.050.

382. Chen G, Shi X, Wang B, et al. Unimolecular micelle-based hybrid system for perivascular drug delivery produces long-term efficacy for neointima attenuation in rats. *Biomacromolecules*. 2017;18(7):2205-2213. doi:10.1021/ACS.BIOMAC.7B00617.

383. Siepmann J, Elkharraz K, Siepmann F, Klose D. How autocatalysis accelerates drug release from PLGA-based microparticles: A quantitative treatment. *Biomacromolecules*.

2005;6(4):2312-2319. doi:10.1021/BM050228K.

384. Fredenberg S, Wahlgren M, Reslow M, Axelsson A. The mechanisms of drug release in poly(lactic-co-glycolic acid)-based drug delivery systems—A review. *Int J Pharm*. 2011;415(1-2):34-52. doi:10.1016/J.IJPHARM.2011.05.049.

385. Han B, Gao SZ, Zhang XH, Tian HB, Wang HT, Shang ZH. Preparation of aclarubicin PLGA nanospheres and related in vitro/in vivo studies. *J Appl Polym Sci*. 2010;117(5):2754-2761. doi:10.1002/APP.31464.

386. Bae SE, Son JS, Park K, Han DK. Fabrication of covered porous PLGA microspheres using hydrogen peroxide for controlled drug delivery and regenerative medicine. *J Control Release*. 2009;133(1):37-43. doi:10.1016/J.JCONREL.2008.09.006.

387. Saini V, Jain V, Sudheesh MS, Jaganathan KS, Murthy PK, Kohli D V. Comparison of humoral and cell-mediated immune responses to cationic PLGA microspheres containing recombinant hepatitis B antigen. *Int J Pharm*. 2011;408(1-2):50-57. doi:10.1016/J.IJPHARM.2011.01.045.

388. Park TG. Degradation of poly(lactic-co-glycolic acid) microspheres: effect of copolymer composition. *Biomaterials*. 1995;16(15):1123-1130. doi:10.1016/0142-9612(95)93575-X.

389. Sinha VR, Trehan A. Biodegradable microspheres for protein delivery. *J Control Release*. 2003;90(3):261-280. doi:10.1016/S0168-3659(03)00194-9.

390. El-Sayed A, Khalil IA, Kogure K, Futaki S, Harashima H. Octaarginine- and octalysine-modified nanoparticles have different modes of endosomal escape. *J Biol Chem*. 2008;283(34):23450-23461. doi:10.1074/JBC.M709387200.

391. Chen L, Zhong J, Li S, et al. The long-term effect of tacrolimus on alkali burn-induced corneal neovascularization and inflammation surpasses that of anti-vascular endothelial growth factor. *Drug Des Devel Ther*. 2018;12:2959. doi:10.2147/DDDT.S175297.

392. Sun S, Wu HJ, Guan JL. Nuclear FAK and its kinase activity regulate VEGFR2 transcription in angiogenesis of adult mice. *Sci Rep*. 2018;8(1):1-11. doi:10.1038/s41598-018-20930-z.

393. Holmes K, Roberts OL, Thomas AM, Cross MJ. Vascular endothelial growth factor receptor-2: Structure, function, intracellular signalling and therapeutic inhibition. *Cell Signal*. 2007;19(10):2003-2012. doi:10.1016/J.CELLSIG.2007.05.013.

394. Wary KK, Kohler EE, Chatterjee I. Focal adhesion kinase regulation of neovascularization. *Microvasc Res*. 2012;83(1):64-70. doi:10.1016/j.mvr.2011.05.002.

395. Orr AW, Murphy-Ullrich JE. Regulation of endothelial cell function by FAK and Pyk2. *Front Biosci*. 2004;9:1254-1266. doi:10.2741/1239.

396. Vadali K, Cai X, Schaller MD. Focal adhesion kinase: An essential kinase in the regulation of cardiovascular functions. *IUBMB Life*. 2007;59(11):709-716. doi:10.1080/15216540701694245.

397. Zhao J, Guan JL. Signal transduction by focal adhesion kinase in cancer. *Cancer Metastasis Rev*. 2009;28(1-2):35-49. doi:10.1007/s10555-008-9165-4.

398. Schaller MD, Borgman CA, Parsons JT. Autonomous expression of a noncatalytic domain of the focal adhesion-associated protein tyrosine kinase pp125FAK. *Mol Cell Biol*. 1993;13(2):785-791. doi:10.1128/MCB.13.2.785-791.1993.

399. Schaller MD, Hildebrand JD, Shannon JD, Fox JW, Vines RR, Parsons JT. Autophosphorylation of the focal adhesion kinase, pp125FAK, directs SH2-dependent binding of pp60src. *Mol Cell Biol*. 1994;14(3):1680-1688. doi:10.1128/mcb.14.3.1680-1688.1994.

400. Schlaepfer DD, Broome MA, Hunter T. Fibronectin-stimulated signaling from a focal adhesion kinase-c-Src complex: involvement of the Grb2, p130cas, and Nck adaptor proteins. *Mol Cell Biol*. 1997;17(3):1702-1713. doi:10.1128/mcb.17.3.1702.

401. Risau W. Mechanisms of angiogenesis. *Nature*. 1997;386(6626):671-674.

doi:10.1038/386671A0.

402. Cursiefen C, Küchle M, Naumann GOH. Angiogenesis in corneal diseases: histopathologic evaluation of 254 human corneal buttons with neovascularization. *Cornea*. 1998;17(6):611-613. doi:10.1097/00003226-199811000-00008.

403. Cursiefen C, Cao J, Chen L, et al. Inhibition of hemangiogenesis and lymphangiogenesis after normal-risk corneal transplantation by neutralizing VEGF promotes graft survival. *Invest Ophthalmol Vis Sci*. 2004;45(8):2666-2673. doi:10.1167/IOVS.03-1380.

404. Watson BD, Huang AJW, Hernandez E, Tseng SCG. Photothrombosis of corneal neovascularization by intravenous rose bengal and argon laser irradiation. *Arch Ophthalmol (Chicago, Ill 1960)*. 1988;106(5):680-685. doi:10.1001/ARCHOPHT.1988.01060130742036.

405. Primbs GB, Casey R, Wamser K, Snyder W., Crean D. Photodynamic therapy for corneal neovascularization. *Ophthalmic Surg Lasers*. 1998;29:832-838. doi: 10.3928/1542-8877-19981001-09

406. Andreoli CM, Miller JW. Anti-vascular endothelial growth factor therapy for ocular neovascular disease. *Curr Opin Ophthalmol*. 2007;18(6):502-508. doi:10.1097/ICU.0B013E3282F0CA54.

407. Chan WM, Lai TYY, Liu DTL, Lam DSC. Intravitreal bevacizumab (Avastin) for myopic choroidal neovascularization: six-month results of a prospective pilot study. *Ophthalmology*. 2007;114(12). doi:10.1016/J.OPHTHA.2007.03.043.

408. Manzano RPA, Peyman GA, Khan P, et al. Inhibition of experimental corneal neovascularisation by bevacizumab (Avastin). *Br J Ophthalmol*. 2007;91(6):804-807. doi:10.1136/BJO.2006.107912.

409. Erdurmus M, Totan Y. Subconjunctival bevacizumab for corneal neovascularization. *Graefes Arch Clin Exp Ophthalmol*. 2007;245(10):1577-1579. doi:10.1007/S00417-007-0587-4.